NASA Contractor Report 165674

GENERATION OF OPTIMUM VERTICAL PROFILES FOR AN ADVANCED FLIGHT MANAGEMENT SYSTEM

John A. Sorensen and Mark H. Waters

Contract NAS1-15497
March 1981

NASA

NASA Contractor Report 165674

GENERATION OF OPTIMUM VERTICAL PROFILES FOR AN ADVANCED FLIGHT MANAGEMENT SYSTEM

John A. Sorensen and Mark H. Waters

Analytical Mechanics Associates, Inc.
Mountain View, California

Prepared for
Langley Research Center
under Contract NAS1-15497

National Aeronautics and
Space Administration

Langley Research Center
Hampton, Virginia 23665

March 1981

FOREWORD

This effort for development of concepts for generating optimum vertical flight profiles that minimize fuel or direct operating costs was supported under NASA Contract No. NAS1-15497, by Langley Research Center, Hampton, Virginia. The project Technical Monitor at Langley Research Center was Robert E. Shanks. Technical discussion and suggestions from Mr. Shanks and Samuel A. Morello, Charles E. Knox, and Kathy Samms of Langley Research Center and Heinz Erzberger of NASA Ames Research Center are gratefully acknowledged.

GENERATION OF OPTIMUM VERTICAL PROFILES FOR AN ADVANCED FLIGHT MANAGEMENT SYSTEM

John A. Sorensen
Mark H. Waters

Analytical Mechanics Associates, Inc.
Mountain View, California 94043

SUMMARY

The objective of this project is to develop and evaluate one or more algorithms and flight management concepts for the on-board minimization of fuel or direct operating costs. These concepts are to be used for steering a CTOL aircraft in the vertical plane between fixed origin and destination airports along a given horizontal path.

In this report, algorithms for generating minimum fuel or minimum cost vertical profiles are derived and examined. The option for fixing the time of flight is included in the concepts developed. These algorithms form the basis for the design of an advanced on-board flight management system. The variations in the optimum vertical profiles (resulting from these concepts) due to variations in wind, takeoff mass, and range-to-destination are next presented. Fuel savings due to optimum climb, free cruise altitude, and absorbing delays enroute are examined. Finally, the results are summarized, and recommendations are made for further work.

Five appendices are included which give technical details of optimum trajectory design, steering requirements for following these trajectories, modeling the aircraft, and off-line computer programs for testing the concepts. The two computer programs developed are called OPTIM and TRAGEN, and they are available from the Computer Software Management Information Center, Barrow Hall, University of Georgia, Athens, Georgia 30601.

TABLE OF CONTENTS

LIST OF FIGURES

LIST OF FIGURES (Con't)

LIST OF FIGURES (Con't)

LIST OF TABLES

SYMBOLS

a	-	speed of sound (m/s)
$b_1 - b_5$	-	coefficients in empirical equation to compute cruise range
C_D	-	total drag coefficient
$C_{D_{BASIC}}$	-	basic component of drag coefficient
$C_{D_{GEAR}}$	-	component of drag coefficient due to landing gear
C_d	-	direct operating cost DOC ($/hr)
C_f	-	cost of fuel ($/kg or $/lb)
C_L	-	total lift coefficient
$C_{L_{BASIC}}$	-	basic component of lift coefficient
C_{L_0}	-	basic lift component at $\alpha = 0°$
C_t	-	cost of time ($/hr)
C_{tmin}	-	minimum value of C_t ($/hr)
c, c_d	-	unit direct operating cost ($/hr)
$c_1 - c_3$	-	coefficient in emperical equation to compute landing weight
D, D_c	-	drag (N)
DOC	-	direct operating cost combining fuel and time costs ($/hr)
d_c	-	cruise distance (n.mi.)
d_{e_c}	-	error command computed by control law
d_f	-	total distance traveled (n.mi.)
d_{up}, d_{dn}	-	climb and descent range (n.mi.)
E, E_p	-	specific energy (m)
E_c, E_{ci}, E_{cf}	-	specific energy in cruise, initially, and finally (m)
E_{copt}	-	optimum value of specific energy during cruise at the optimum altitude (m)
E_{to}	-	initial specific energy (m)
EPR	-	engine pressure ratio
F	-	fuel burned (kg)
F_n	-	net thrust (N)

F_{up}, F_c, F_{dn}	-	fuel burned during climb, cruise, and descent (kg)
f	-	differential state equation
$f_1 - f_5$	-	function evaluated by subroutines
G_B, G_C	-	constants in the transfer functions relating perturbations in γ and V_a to perturbations in α
g	-	acceleration due to gravity (m/s^2)
H, H_c	-	Hamiltonian used for optimization ($/m)
H_{up}, H_{dn}	-	Hamiltonian during climb and descent ($/m)
J	-	flight cost function to be minimized ($)
KIAS	-	indicated airspeed (kt)
$K_1 - K_4$	-	control law gains
K_c	-	fuel flow correction factor
L	-	lift (N)
L(x,u,t)	-	cost per unit time along a trajectory ($/hr)
M	-	Mach number
M3	-	reference Mach number for handbook profile
m	-	aircraft mass (kg)
P	-	ratio of cruise cost ψ (or λ) to optimum cruise cost ψ_{copt}
p	-	air pressure (N/m^2)
p1,2	-	origin and destination points on flight path
pamb	-	ambient pressure (N/m^2)
q	-	pitch rate (°/s)
R_{min}, R_{max}	-	values of range where P = 1.5 and 1.01 on optimum profiles (n.mi.)
RPM	-	revolutions per minute of engine
S	-	reference area (m^2)
S_{FC}	-	specific fuel consumption (kg/hr)/N
s	-	Laplace transform operator
T, Th	-	thrust (N)
T_o	-	time-of-arrival (length of flight) for a minimum fuel profile (s)
$T_{1,2}$	-	alternate times-of-arrival (s)
T_o	-	atmospheric temperature (°K)
T_{T2}	-	stagnation pressure at compressor inlet (°K)

t	-	time (s)
t_{ci}, t_{cf}	-	time at beginning and end of cruise (s)
t_{fd}	-	desired arrival time (s)
t_o, t_f	-	initial and final times of trajectory (s)
t_{fmax}	-	maximum flight time obtained at minimum cruise speed (s)
u	-	control variables
V, V_a, V_c	-	airspeed, command airspeed (kt)
V_{cmin}	-	cruise speed where fuel flow rate is minimized (kt)
V_{IAS}	-	indicated airspeed (kt)
VIAS1, VIAS2	-	reference indicated airspeeds for handbook profile (kt)
V_T, V_{TP}	-	desired value of true airspeed (kt)
V_{up}, V_{dn}	-	airspeed during climb and descent (kt)
V_w	-	longitudinal component of wind speed (kt)
V_{wup}, V_{wdn}	-	wind speed during climb and descent (kt)
W, W_i, W_o, W_f, W_b	-	mass of the aircraft; initial and final mass (kg)
W_c, W_{ci}, W_{cf}	-	mass during cruise; initial and final cruise mass (kg)
W_{ref}	-	reference mass (kg)
$\dot{w}$	-	fuel flow (kg/hr)
W_{fCL}	-	fuel burned during climb (kg)
x	-	range traveled (n.mi.)
x_{up}, x_{dn}	-	components of range traveled during climb and descent (n.mi.)

GREEK SYMBOLS

α	-	angle-of-attack (°)
γ, γ_c	-	flight path angle with respect to airmass; command value (°)
γ_I, γ_{Ic}	-	inertial flight path angle; command value (°)
$\Delta C_{D_{GEAR}}$	-	drag coefficient due to landing gear
$\Delta C_{L_{GEAR}}$	-	lift coefficient due to landing gear
ΔE	-	change in specific energy (m)
Δh	-	incremental altitude (m)
ΔR, Δx	-	incremental range (n.mi.)
Δt	-	incremental time (s)
ΔW	-	incremental weight (kg)
δ_{amb}	-	ambient pressure ratio
δ_T	-	throttle setting (%)
ε	-	small distance
λ, λ_{min}	-	cruise cost per unit distance ($/n.mi.) also, adjoint variable or costate used for optimization
π	-	thrust control setting (throttle, EPR, or RPM)
π_{up}, π_{dn}	-	throttle setting during climb and descent
ρ	-	atmospheric density (kg/m^3)
ζ	-	damping term in transfer function
τ	-	time-to-go (s)
τ_B, τ_c	-	constants in the transfer functions relating perturbations in γ and V_a to perturbations in α (s)
ϕ	-	terminal cost function ($/n.mi.)
ψ, ψ_c	-	cost per unit distance of cruise (same as λ or H_c) ($/n.mi.)
ω	-	natural frequency in transfer function (s^{-1})
σ	-	specific fuel consumption (same as S_{FC}). (kg/hr)/N

SUBSCRIPTS AND NOTATION

amb - ambient
b - value computed on previous cycle
c - value during cruise or command value
d - desired value
idle - value during idle thrust
max - maximum value
min - minimum value
n - nominal value
opt - optimum value
STD - standard day value
$(\dot{})$ - first derivative with respect to time
$(\ddot{})$ - second derivative with respect to time
$\partial(\ )$ - partial of indicated variable
$\Delta(\ )$ - change in value

UNITS

In this report, the common British units used by U S. aircraft manufacturers are given in parentheses after a numerical value is first presented in mks units. Note that pounds mass and pounds force are both used rather than using slugs as a measure of mass. Here, the common definition of one pound mass equals (1/32.2) times one slug mass (1 slug = 32.2 lb sec^2/ft.) is used.

I

INTRODUCTION

Virtually every segment of civilization is being affected by the energy crisis, and we are awakening to the fact that we live in a system with finite resources. Our natural supplies of hydrocarbon fuels are being rapidly consumed, so that it has become mandatory that we seek to develop every feasible means to conserve fuel. The energy crisis and its effect on developing technology is especially impacting the air transportation industry which accounts for about 4 percent of our national petroleum consumption [1].

The current motivating factor for our air transportation industry to conserve fuel is the escalating cost of jet fuel. To the commercial air carrier, reduction in fuel usage means reduction in operating costs and an increased profit margin [2]. For military air operations, fuel reduction also implies increased aircraft range, greater payloads, more missions, and an enhanced defense reserve [3,4]. The U.S. Air Force has an annual fuel usage of over 15 billion liters (4 billion gallons) [3], while our domestic commercial fleet used about 38 billion liters (10 billion gallons) in 1978 [1,2].

Figures 1 and 2, taken from Ref. 2, illustrate the dilemma that exists for commercial aviation - increasing air transportation demand versus decreasing production capacity. Figure 2 also illustrates that accelerated technological advancements can potentially reduce future usage of fuel for air transportation by more than 30%. One of these advancements is developing the ability to fly each aircraft along profiles which minimize total fuel consumption.

Increasing labor costs and penalties on air travel time make it desirable to minimize both fuel usage and the flight time. These factors motivate the search for a flexible procedure for generating a reference flight profile which can minimize the total cost of an operation between two airports.

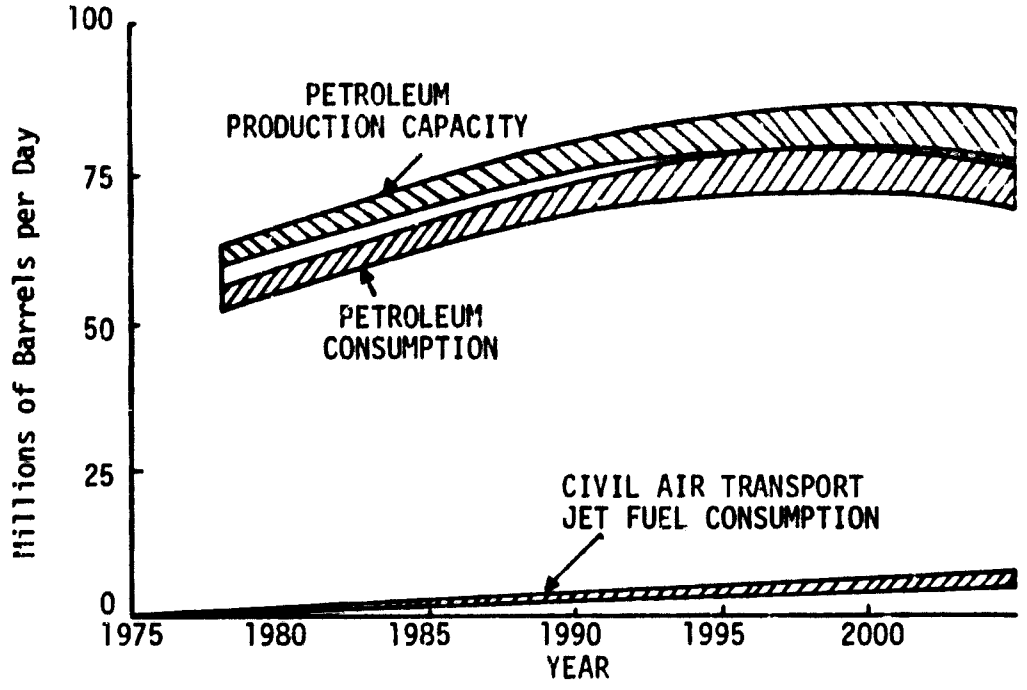

Figure 1. Projected Free World Petroleum Production Capacity vs Consumption [2].

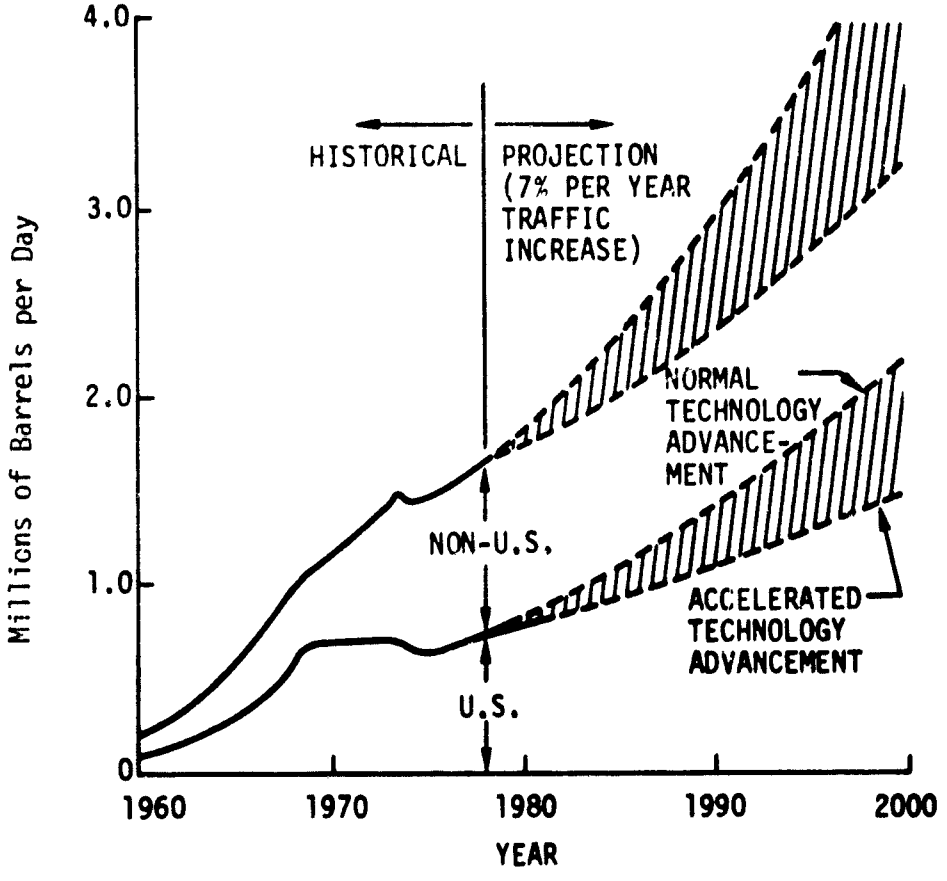

Figure 2. Free World Air Carrier Jet Fuel Consumption Projection [2].

Commercial airline flight profiles are presently generated using pseudo-optimization procedures. Given a reasonable knowledge of the jet stream, computer programs based on dynamic programming techniques test a series of horizontal paths between the departure and destination points to find the one providing minimum cost. The horizontal paths tested are predetermined, and they typically consist of a series of interconnected segments between VOR/DME and TACAN stations. The vertical path then consists of a fixed Mach number/indicated airspeed profile for climb and descent combined with a series of step changes in altitude during cruise. The altitude step changes are governed by predetermined fuel burnoff rates and air traffic control (ATC) considerations. This report is focused on various aspects of computing improved vertical profiles.

This computational procedure should be capable of minimizing fuel usage, flight time, or a combination of these variables (direct operating cost - DOC). Furthermore, it should be computationally efficient and implemented so that it can be used by the pilot while airborne to change the flight profile in case of change in weather conditions, final destination, or desired arrival time. Finally, this procedure should serve as a means of automatically driving the aircraft control surfaces and engine throttle settings. One element of the work summarized in this report is the development of a procedure that can be mechanized on-board to achieve the near-optimum path.

Before continuing with specifics, it is important to mention some relevant background concerning the control of flight time. Jet transport aircraft and their associated flight schedules have traditionally been designed to move passengers and cargo rapidly, and cruise speeds have been kept near the maximum design values. Because of air transportation's efficiency, this industry has enjoyed a rapid growth even though airport and terminal area congestion is becoming a critical problem. Terminal area congestion can produce significant time delays and requirements for aircraft holding patterns to absorb these delays. Thus, we have the condition where aircraft fly at high speeds to terminal areas where they then may have to hold for over 30 minutes or even divert to an alternate airport because of congestion. In 1975, average arrival delay was from

2.9 - 4-6 minutes at 91 of the busiest U.S. airports [5]. It is projected that with the present system, this delay will grow to an average of 8.4 minutes by 1990. These delays can easily consume any fuel saved from flying a minimim fuel profile to the terminal area [6].

Consider also that to reduce operating costs, the air transport industry has been gradually changing flight path characteristics from ones that emphasize speed (fast service; minimum time - dependent costs) to ones that tend to minimize a combination of time-of-flight and fuel. As fuel prices continue to climb, it is expected that the nominal flight path characteristics will eventually approach those of minimum fuel trajectories (which take a longer time). A host of flight management avionic systems are now appearing which may enable automatic or manual guidance along reduced DOC flight paths (e.g., [7]).

Another element which is affecting the evolution of our air transportation system is the technological advancement taking place in communications capability and digital computer equipment on the ground. The ATC management is taking advantage of these advancements to upgrade their system through further uses of automation [8]. This includes the eventual development of algorithms and software to command flight profiles which (a) minimize fuel, (b) provide orderly metered traffic in and out of terminal areas, and (c) are conflict free. Thus, the ATC system will be able to anticipate congestion and inform the pilot of what his delay will be before he reaches the terminal area (i.e., the controller will assign the pilot a desired time-of-arrival that is conflict free).

A second important element of this effort has been the extension of the optimization procedure to include the fixed time-of-arrival constraint. This extension is based on three assumptions:

a) that aircraft will soon be nominally flown along minimum fuel vertical flight paths,

b) that delays of variable length will occur at destination terminal areas because of congestion, and

c) the ATC system will be able to predict delay, inform the pilot of the magnitude of this delay while he is enroute, and give him credit for absorbing the delay enroute.

This study evaluates the benefit of absorbing delays enroute.

Previous significant work in generating optimum vertical flight paths that minimize fuel or direct operating costs are summarized in Refs. 9 and 10. Schultz and Zagalsky developed mathematical solutions of the minimum fuel-fixed range-fixed time problem [11]. Erwin developed the concept of strategic control [5, 12] in which control of arrival time can be used to reduce excess fuel that results from delays. Also, the previous time based metering work of the NASA Langley staff for flight testing profile descents on the Terminal Configured Vehicle (TCV) aircraft demonstrated the practicality of these solutions [13]. These tests verified previous simulation studies conducted by NASA and FAA personnel [14].

The NASA TCV aircraft provides a vital link in testing the feasibility and verifying the expected performance of both the advanced airborne flight management and ATC automation systems. The objective of this project has been to provide both profile optimization concepts and working models to be a part of an advanced flight management system design. This design may eventually be flight tested on the TCV aircraft.

This report is organized as follows:

a). In Chapter II, algorithms of methods for generating optimum vertical profiles are derived. These methods have many options including the ability to fix the time of flight (i.e., the time-of-arrival). These procedures also form the basis for specifying on-board mechanization requirements. The algorithms have been coded into a computer program called OPTIM.

b). In Chapter III, a presentation is made of an evaluation of the optimum vertical profiles using OPTIM and a program called TRAGEN. TRAGEN simulates an aircraft following a given vertical path (optimum or otherwise). Sensitivity results are presented of the variation in the optimum profile as a function of variations in wind, takeoff mass, and range-to-destination. Advantages of using free cruise altitude and fixed time-of-arrival options are also presented.

c). Chapter IV summarizes the study. It also makes recommendations regarding further work required to upgrade the computer programs and to mechanize the optimization techniques as part of an advanced flight management system.

Appendices A through E are presented to give technical details of trajectory optimization, modeling details of turbojet engine performance, medium range twin-jet transport aircraft dynamics, and climb fuel burn estimation, and steering requirements for following a reference vertical flight profile.

II

COMPUTATION OF THE OPTIMUM VERTICAL PROFILE

The primary subject addressed here is how to fly the aircraft in the vertical plane after the horizontal path has been specified. That is, the origin, destination, horizontal route, starting and ending altitudes and airspeeds, and takeoff mass are fixed. The problem then is to choose the vertical flight profile (altitude, airspeed, thrust, and flight path angle time histories) to minimize cost.

In this chapter, an algorithm is first derived which serves as the basis for generating an optimum vertical profile. This profile can either be generated before flight or as a background computation while in flight. This derivation is based on trajectory optimization principles which are outlined in the first part of Appendix A.

After the method of generating optimum profiles is explained, example climb and descent profiles are presented for two classes of aircraft. Then, modifications to the optimization algorithms are described which allow the user to fix the time length of the flight.

Derivation of the Optimization Algorithm

A set of nonlinear differential equations describing a point mass model of the aircraft longitudinal motion is adequate to describe the vertical motion of the aircraft for optimization purposes [16]. This model is, for no wind,

$$\begin{aligned} m\dot{V}_a &= T\cos\alpha - D - mg\sin\gamma, \\ mV_a\dot{\gamma} &= T\sin\alpha + L - mg\cos\gamma, \\ \dot{h} &= V_a\sin\gamma, \\ \dot{x} &= V_a\cos\gamma, \\ \dot{m} &= -\dot{w}. \end{aligned} \tag{1}$$

Here, the state variables are the true airspeed V_a, flight path angle γ, altitude h, horizontal range x, and mass m. The control variables are the thrust T and angle-of-attack α which are both amplitude limited. The variables lift L and drag D are functions of h, V_a, and α. The fuel flow $\dot{w}$ is a function of h, V_a, and T. These equations are analogous to Eqs. (A.1) in Appendix A. The cost function to be minimized is of the form,

$$J = \int_{t_o}^{t_f} (C_f \dot{w} + C_t) dt \quad , \tag{2}$$

where C_f and C_t are the unit costs of fuel ($/kg($/lb)) and time ($/hr). At this point, the final time t_f is free. The problem is to choose the sequence of controls (T and α) that drive Eqs. (1), satisfy the initial and final constraints, and minimize the cost of the flight, as governed by Eq. (2).

For general trajectory shaping, the flight path angle dynamics can be neglected, and it can be assumed that the angle-of-attack α is small. Then, the equations of motion of the aircraft in the longitudinal plane are

$$\begin{aligned} \dot{V}_a &= (T-D)/m - g \sin \gamma \ , \\ \dot{h} &= V_a \sin \gamma \ , \\ \dot{x} &= V_a \cos \gamma + V_w \ , \end{aligned} \tag{3}$$

where the longitudinal component of the wind velocity is included.

An early attempt at obtaining simplified solutions to the minimum time-to-climb and minimum fuel-to-climb problems was made by Rutowski [15] using graphical methods. He also suggested that the aircraft could adequately be represented in such a problem by its specific energy state,

$$E = h + V_a^2/2g \quad . \tag{4}$$

The use of this state assumes that kinetic and potential energy can be instantaneously interchanged.

Bryson, Desai, and Hoffman [16] used the energy state approximation and differentiated Eq. (4) to obtain

$$\dot{E} = V_a(T - D)/mg \tag{5}$$

as the single equation of motion. This assumed that lift L balanced weight mg, and true airspeed V_a was treated as a control variable.

Now, based on the previous researchers' experience, the specific energy and its derivative are defined according to Eqs. (4) and (5). The first and second of Eqs. (3) are replaced with Eq. (5).

Consider again the cost function of Eq. (2). What is actually desired is to minimize the cost in flying from origin p_1 to destination p_2, where the time of flight t_f is considered for now to be free. The cost function can be changed to have range as the independent variable by dividing Eq. (2) by the expression for range rate, or

$$J = \int_{p_1}^{p_2} \frac{(C_f \dot{w} + C_t)}{V_a \cos \gamma + V_w} dx \triangleq \int_{p_1}^{p_2} \frac{dc}{dx} dx \quad . \tag{6}$$

The remaining state equation (Eq. (5)) also is changed as

$$\frac{dE}{dx} = \frac{dE}{dt} / \frac{dx}{dt} \quad ,$$

$$= \frac{(T-D)}{mg} \left(\frac{V_a}{V_a \cos \gamma + V_w} \right) \quad . \tag{7}$$

This neglects fuel flow as a function of distance. Practical experience [17] has shown that as long as the current value of aircraft weight (mg) is used in Eq. (7), this simplification is appropriate.

Equations (6) and (7) are combined, using the procedures outlined in Appendix A to form the Hamiltonian,

$$H = \frac{dc}{dx} + \lambda \frac{dE}{dx} \quad , \tag{8}$$

$$= \frac{C_f \dot{w} + C_t + \lambda V_a (T-D)/mg}{V_a \cos \gamma + V_w} \quad .$$

As can be seen, this Hamiltonian allows for penalizing of time, it assumes no particular form for the fuel flow $\dot{w}$, and it takes into account the horizontal component of the wind V_w.

Note, again however, that none of the terms in Eq. (8) are explicit functions of the independent variable x. Then, according to the arguments associated with Eq. (A.12) in Appendix A, this Hamiltonian is a constant. This greatly facilitates obtaining the optimum profile solution.

Again, assume that the thrust T is a function of the engine pressure ratio (EPR) setting π. The two control variables can then be considered to be π and true airspeed V_a for this simplified dynamic model. (These arguments can be extended so that the conventional controls - throttle and elevator deflection - are used). Both π and V_a have upper and lower bounds. By following Eq. (A.11), the Hamiltonian H is minimized according to

$$\frac{\partial H}{\partial \pi} \delta\pi \geq 0 \quad , \tag{9a}$$

$$\frac{\partial H}{\partial V_a} \delta V_a \geq 0 \quad , \tag{9b}$$

for all admissible values of π and V_a. For an assumed constant value for H, Eqs. (8) and (9) constitute three equations with three unknowns - π, V_a, and λ at every point along the optimum trajectory.

Using the arguments of Refs. 17-20, assume that the vertical flight profile consists of three phases:

(a) a climb portion where both altitude and energy are monotonically increasing with range;

(b) an essentially equilibrium cruise portion where thrust equals drag and lift equals weight; and

(c) a descent portion where both altitude and energy are monotonically decreasing as range-to-go decreases.

For the cruise portion, the Hamiltonian can then be written as,

$$H_c = \frac{C_f \dot{w} + C_t}{V_a + V_w} \quad . \tag{10}$$

For a given cruise altitude and mass, the EPR setting and airspeed are found by numerical search techniques such that the value of this expression is minimized. This value of the Hamiltonian is then the constant value used to climb to and descend from this altitude. It also represents the minimum cost per unit distance traveled along the cruise path. (This implies that the cruise altitude and mass are known. These issues are also discussed later.)

The constant value of H_c can be substituted into Eq. (8), and Eq. (8) can be solved for the negative value of the unknown costate:

$$-\lambda = \frac{C_f \dot{w} + C_t - H_c (V_a \cos\gamma + V_w)}{V_a (T-D)/mg} \quad . \tag{11}$$

Thus, to minimize the cost function expressed by Eq. (8) requires that values of π and V be chosen such that Eq. (11) is minimized at every point along the climb and descent path. Equation (11) is the key algorithm to both offline and on-board computation of the optimum trajectory that minimizes direct operating cost.

The work of Erzberger et al [17-19, 21] has been based on an alternate approach to this problem. He used specific energy E as the independent variable with the assumption that it always increases monotonically during climb and that it decreases monotonically during descent. Thus, the remaining state variable is the last of Eqs. (3), and Eq. (8) is replaced by

$$\begin{aligned} H &= \frac{dc}{dE} + \lambda \frac{dx}{dE} \quad , \\ &= \frac{C_f \dot{w} + C_t + \lambda (V_a \cos\gamma + V_w)}{V_a (T-D)/mg} \quad . \end{aligned} \tag{12}$$

Equation (12) can be compared to Eq. (11), and it can be seen that the Hamiltonian H and the costate variable λ have reversed roles. Thus, these two solutions are duals of one another. For energy as the state variable, Erzberger shows, using transversality conditions, that λ is constant and is equal to the negative value of the cruise cost. In this case, the Hamiltonian varies in magnitude because variables within Eq. (12) vary with the magnitude of the specific energy (the independent variable).

Generation of Nominal Optimum Trajectories

Because Eqs. (11) and (12) are essentially identical in character and concept, it was convenient to make use of the computer program previously developed by Erzberger and Lee [21] to procede with generating optimum profiles. This program is based on the use of Eq. (12). To avoid confusion, the following description refers to minimizing the Hamiltonian of Eq. (12) with the costate variable λ treated as the constant. The computer program uses principles described in Ref. 21, and it is summarized in the second part of Appendix A. This program (referred to as OPTIM), which generates an optimum profile between origin and destination points, was extended to have additional desired features, and its specific characteristics (from a programming point of view) have been documented in a companion users' guide [22] to this report. It is instructive here, to present in general terms, the elements and steps required to generate an optimum trajectory.

The following quantities must be input to the program for generating points on the optimum profile:

a) The aircraft initial takeoff altitude, airspeed, and mass,

b) The final desired aircraft altitude and airspeed,

c) The range and heading to be followed by the aircraft from the origin to the destination points,

d) The wind velocity (if non-zero) and temperature profiles (if other than standard day) as functions of altitude, and

e) The values of the constants C_f and C_t in the cost function.

The program must have access to numerical data (either tables or polynomials) which produce values of lift and drag coefficients C_L and C_D, thrust T, and fuel flow $\dot{w}$ as functions of altitude, true airspeed, temperature, and EPR setting. Also, for the particular aircraft being used, the program must have the following two sets of empirical equations:

a). A method of guessing the approximate initial cruise mass based on initial takeoff mass and the values of fuel and time cost; and

b). A method of guessing the approximate landing mass based on the final cruise mass

Finally, the program must have an efficient procedure which can be used to find the minimum value of the Hamiltonian (Eq. (12)) at each energy level by varying one or more variables (here, η and V) over their admissible regions. For the OPTIM program, the Fibonacci search technique is used. (See Ref. 22)

It must be mentioned that for some cases, there is no cruise section of flight, as is explained in Appendix A. In this case, the constant value of the costate variable refers to what would be the cruise cost at the highest point on the trajectory where the profile transitions from climb to descent.

The basic steps that the optimum profile generation program follows are:

1). The minimum value of cruise cost (λ or H_c in Eq. (13)) is evaluated for various cruise masses and with altitude varying from sea level to ceiling height. The results are tabulated in a "cruise table". A typical example of cruise cost as a function of altitude is shown in Fig. A.7.

2). Based on initial mass and values of C_f and C_t, the amount of fuel required for the climb is approximated (See Eq. (A.38) and Fig. A.8). This produces cruise mass which is used to determine the optimum cruise cost and altitude from the cruise table. The cruise cost (λ in Eq. (12); $-\lambda(E_c)$ in Appendix A) is required for minimization of Eq. (13). Also, choosing the cruise cost from the cruise table also produces the associated maximum values of energy E_c where the climb portion of flight ends.

3). The next step is to minimize the Hamiltonian (Eq. (12)) at each point along the climb trajectory. This begins at the computed initial energy and stops with the precomputed final climb energy. The numerical procedure procedes as follows:

a). A step is made in specific energy ($E_n = E_{n-1} + \Delta E$), where the step size is held constant.

b). The range of acceptable values of V_a and π are computed for this energy value.

c). Over these ranges, the Hamiltonian (Eq. (12)) is minimized (using the Fibonacci technuique) with γ assumed to be small ($\cos \gamma \approx 1$). This, then specifies the values of airspeed, lift, drag, thrust, altitude, fuel flow, and energy rate (Eq. (5)).

d). The time required to make this step is computed as

$$\Delta t = \Delta E/\dot{E} \quad . \tag{13}$$

e). The flight path angle is then computed as

$$\gamma = \sin^{-1} (\Delta h/\Delta t)/V_a \quad . \tag{14}$$

f). The value of range is increased by Δx, where

$$\Delta x = (V_a \cos \gamma + V_w(h))\Delta t. \tag{15}$$

g). The aircraft mass is decreased by ΔW, where

$$\Delta W = \dot{w} \Delta t. \tag{16}$$

It is assumed that final climb energy and initial cruise energy are equal. The above procedure is repeated until the initial cruise energy level is reached. This produces an accurate measure of the fuel burned during climb and the range traveled during climb.

4). A final approach (or landing) mass is approximated by estimating the cruise range, cruise fuel, and other related quantities (See Eqs. (A.42) - (A.46)). This procedure also produces an estimate of the final cruise altitude, energy, and cruise cost.

5). The procedures for generating the descent profile are now followed using the same sequence as for Step (3) but by going backwards in time and constraining the energy rate to be negative. This is continued until the estimated final cruise energy level is reached. This produces an accurate estimate of the fuel burned during descent and the range traveled during descent.

6). The cruise distance is now recomputed by subtracting the climb and descent ranges from the total required. This cruise distance is used to compute the final cruise mass and the final approach (landing) mass,

7). With the revised final approach mass, the descent trajectory is recomputed using Step (5). This also provides refinement of the cruise distance, the total fuel burned, and time required to travel from origin to destination airports.

The above description is somewhat simplified in that profiles of short range flights (e.g., less than 250 n.mi.) require special computations. Figures A.4 and A.5 in Appendix A depict the shapes of the trajectories for short range for two types of control strategies. (Erzberger explains why these two distinct shapes occur in Ref. 17). If both V_a and π are used as controls, the trajectories have the shapes depicted in Fig. A.5. For this case with short range, there is no cruise segment, and an iterative process is required to obtain the constant value of λ and the maximum energy state used to compute the climb and descent profiles.

If only airspeed is used as the control variable, then thrust is set at maximum climb value for climb and idle value for descent. For the tri-jet aircraft model used in this study, this could increase the cost of the typical short-range profile by about 1%. However, it simplifies mechanization and it reduces the time required to compute the profile. Trajectories for this case have the characteristics depicted in Fig. A.4. That is, they have cruise segments, but these segments occur at altitude and energy levels lower than the optimal value E_{copt}. Again, the program must iterate on the correct value of λ, and Eq. (A.48) in Appendix A is used to compute the corresponding length of the cruise segment.

The OPTIM program has been constructed and extended so that various options can be exercised:

1). No wind or arbitrary input wind,
2). Optimize with V_a and π or V_a only,
3). Arbitrary cost terms C_f and C_t,
4). Fixed or free cruise altitude,
5). Twin-jet or tri-jet medium range transport aircraft models,
6). Fixed or free time of flight (discussed later),
7). With or without a speed constraint of 250 kt below 3048 m (10,000 ft.),

8). Start in cruise or after takeoff. For starting in cruise, the cruise altitude can be set to a fixed value, or the program can compute the best altitude associated with the given cruise mass.

In addition to generating optimum nominal profiles, OPTIM can be used to examine the sensitivities in trip cost due to variations in wind, range, takeoff mass, and the cost terms C_f and C_t. Examples of these variations are given in the next chapter.

The computations that take place in OPTIM for off-line generation of optimum vertical profiles are also the same as would be used by an on-board flight management system. For the on-board mechanization, the flight engineer would enter initial and final altitude and airspeed, initial mass, range, and heading. Wind and temperature profiles and aircraft mass estimates would be updated during flight. The seven basic steps listed earlier would be recomputed every few minutes to provide a current reference trajectory to be followed.

The basic OPTIM program was based on using a medium range tri-jet, transport aircraft model. It is desirable to extend this program to model all major classes of transport aircraft so that the program can serve as a flight planning tool for the airlines and others concerned with fuel conservation. A first step in this extension was to add the capability of generating optimum profiles for a medium range twin-jet transport aircraft. Logic was added throughout the program to account for differences in behavior and characteristics of the two aircraft.

More details on modeling the aircraft engine are presented in Appendix B. The modeling of aerodynamic characteristics of the twin-jet model is described in Appendix C. Climb mass estimation procedures are summarized in Appendix D.

Example Optimum Trajectories

Figures 3 and 4 show plots of various state variables as functions of time (or time-to-go) for optimum climb and descent of a tri-jet aircraft model traveling 200 n.mi. in range. For this example, the indicated airspeed was constrained below 250 kt below 3048 m (10,000 ft). Also, optimiza-

tion was done by varying V_a only, with π set to the maximum value for climb and idle value for descent. The cost constants were \$0.265 kg (\$0.12/lb) for fuel and \$600.00/hr. As can be seen, when 3048 m (10,000 ft) is reached, the aircraft levels off and accelerates before continuing to climb. The opposite is true for the descent profile. Note also that on both the climb or descent profile, Mach number is generally not constant (contrary to profiles that are specified in aircraft handbooks and normally flown). Small segments of constant Mach number in Figs. 3 and 4 are due to thrust and drag data specified in tabular form at given Mach numbers. This is discussed further later.

Figures 5 and 6 show plots of various state variables as functions of time (or time-to-go) for optimum climb and descent of the twin-jet aircraft traveling 750 n.mi. in range. For this example, the indicated airspeed was also constrained to be less than 250 kt below 3048 m (10,000 ft) altitude. Optimization was done by varying V_a and π, so the thrust could deviate from the maximum and idle values for climb and descent, respectively. The cost constants were \$0.33 kg (\$0.15/lb) for fuel and \$600.00/hr. Again, when 3048 m (10,000 ft) altitude is reached, the aircraft levels off and accelerates before continuing to climb.

By comparing Figs. 5 and 6 with Figs. 3 and 4, it is seen that the twin-jet aircraft profiles are similar in character to those of the tri-jet. One exception is that the twin-jet optimum climb profile has a relatively large portion where Mach number is held constant. (Again, it is expected that this is due to the tabular aerodynamic and engine data.) Also, for these paths, the flight path angle is rough because of the inherent assumption in the optimization theory that either altitude, airspeed, or both can be abruptly changed to obtain a change in energy. The flight path angle can either (a) be smoothed after it is generated to provide a more flyable path, or (b) the optimization process can be constrained by allowing only small changes in flight path angle between energy steps. Converting the aerodynamic and engine input data to polynominal form may also remove this problem.

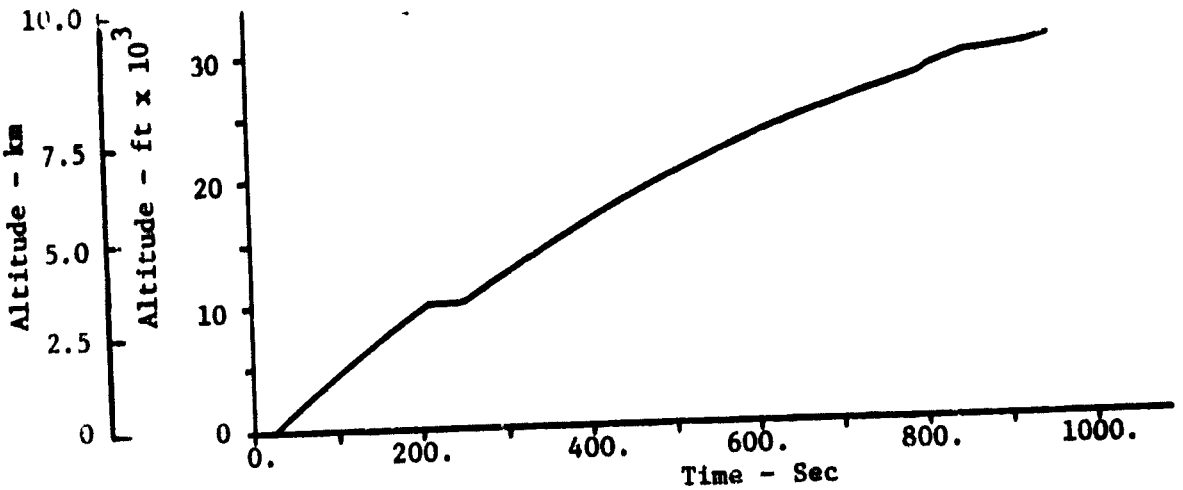

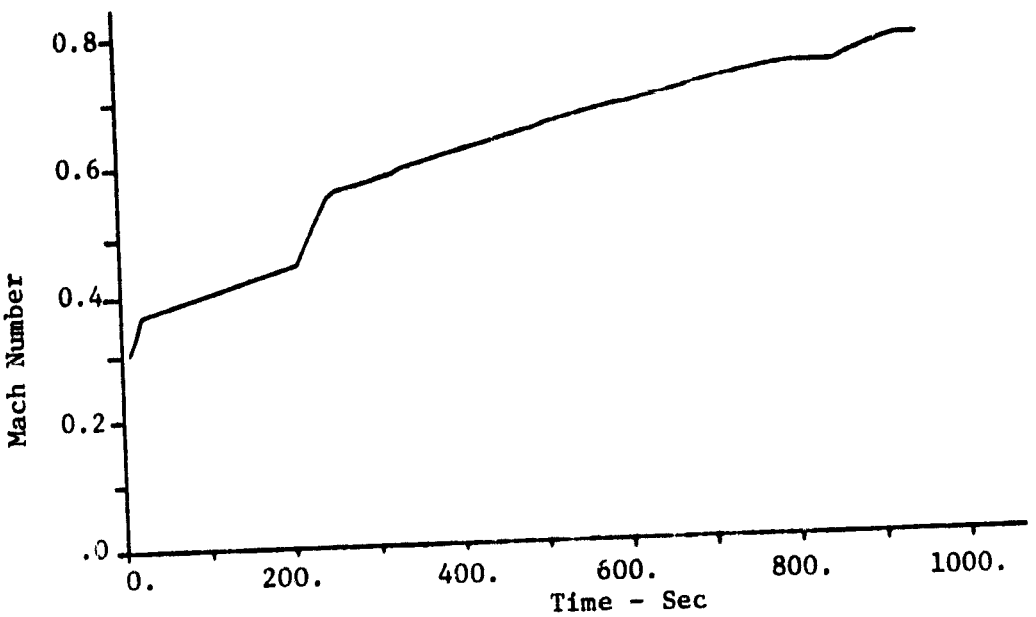

Figure 3. State Variables for an Optimum Climb Profile of a Medium-Range Tri-jet Aircraft on a 200 n.mi. Range Flight.

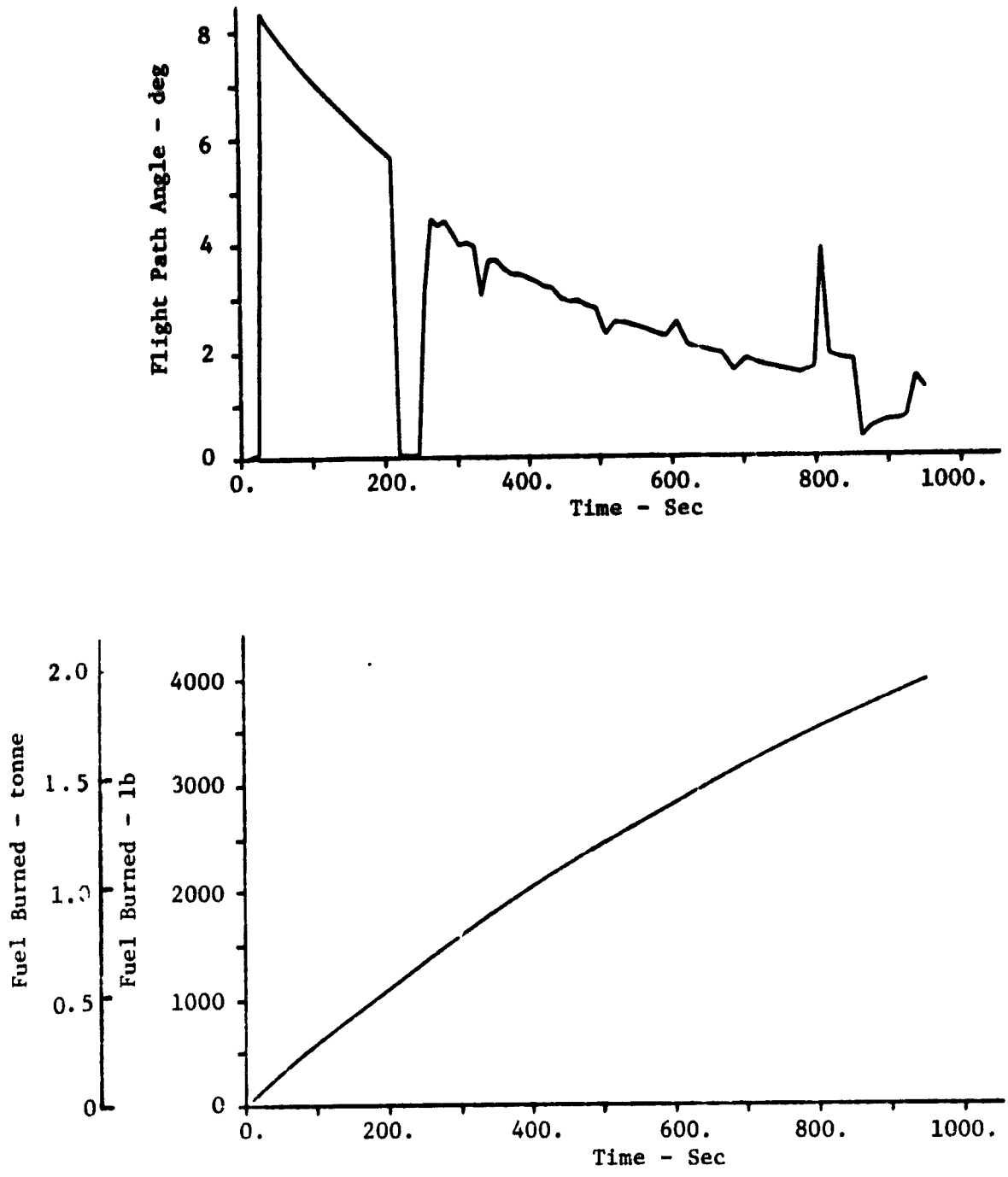

Figure 3. Concluded

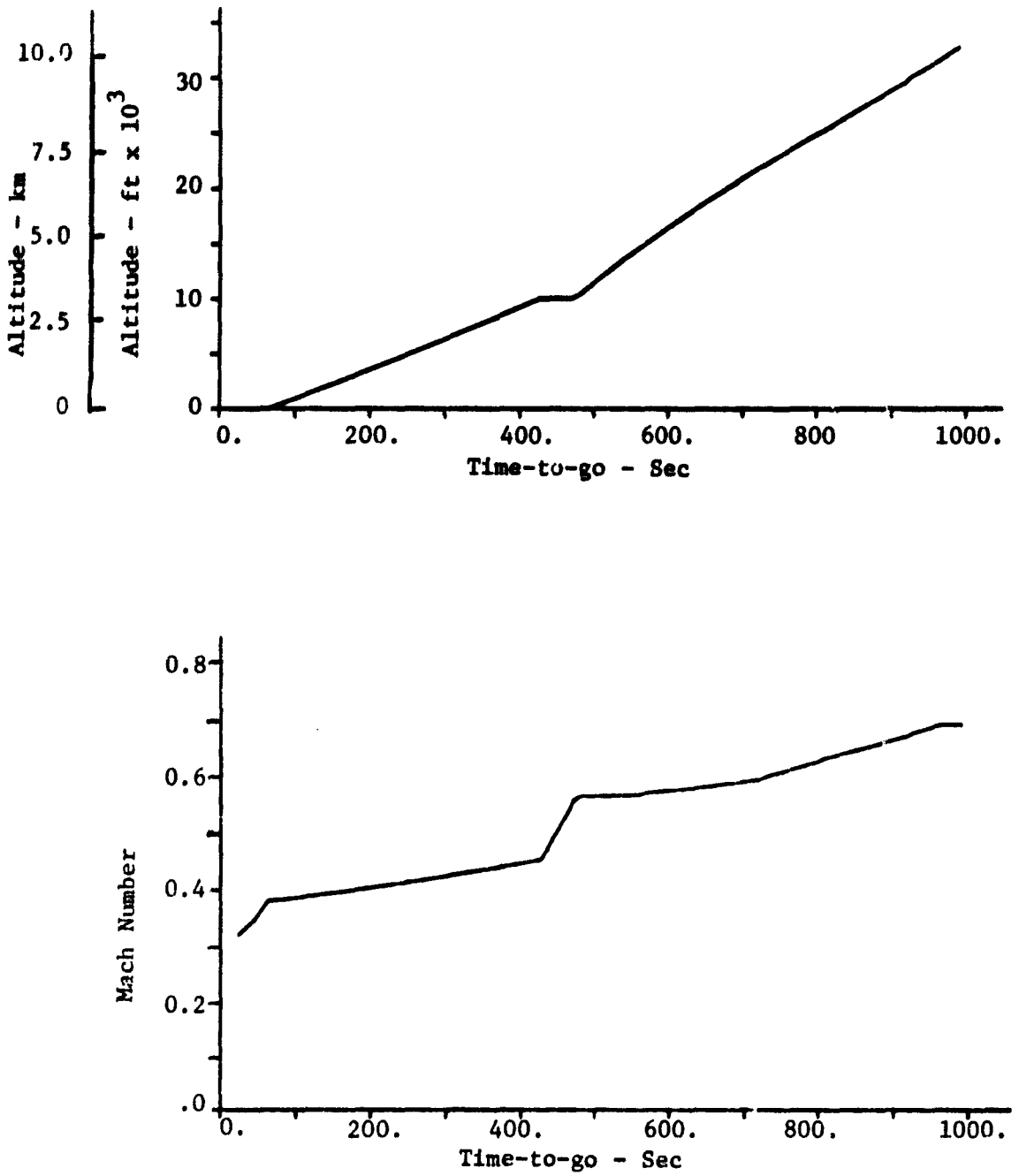

Figure 4. State Variables for an Optimum Descent Profile of a Medium Range Tri-jet Aircraft on a 200 n.mi. Range Flight.

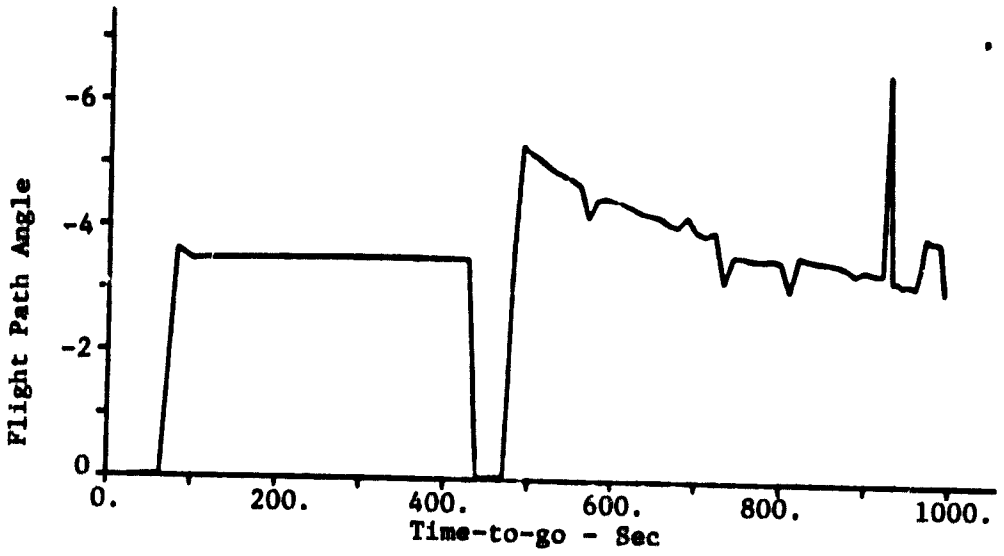

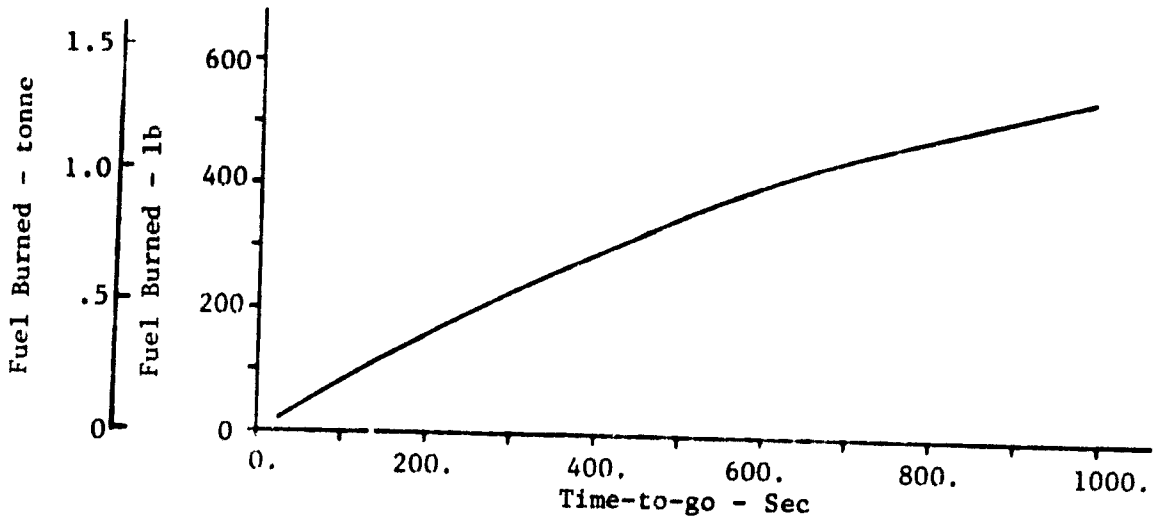

Figure 4. Concluded

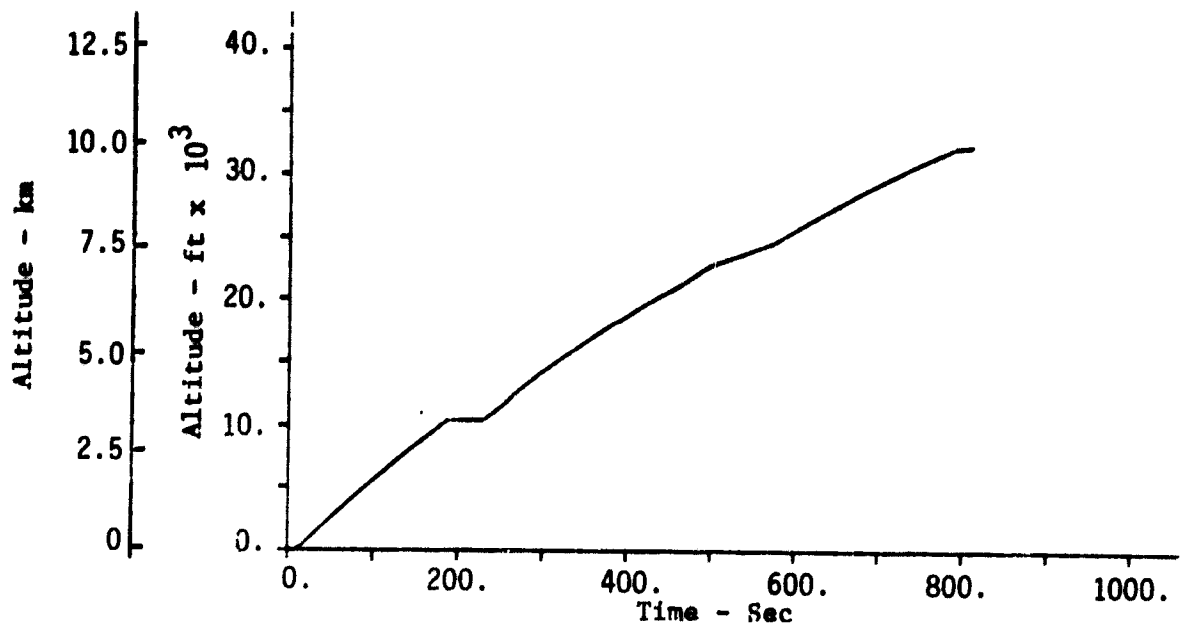

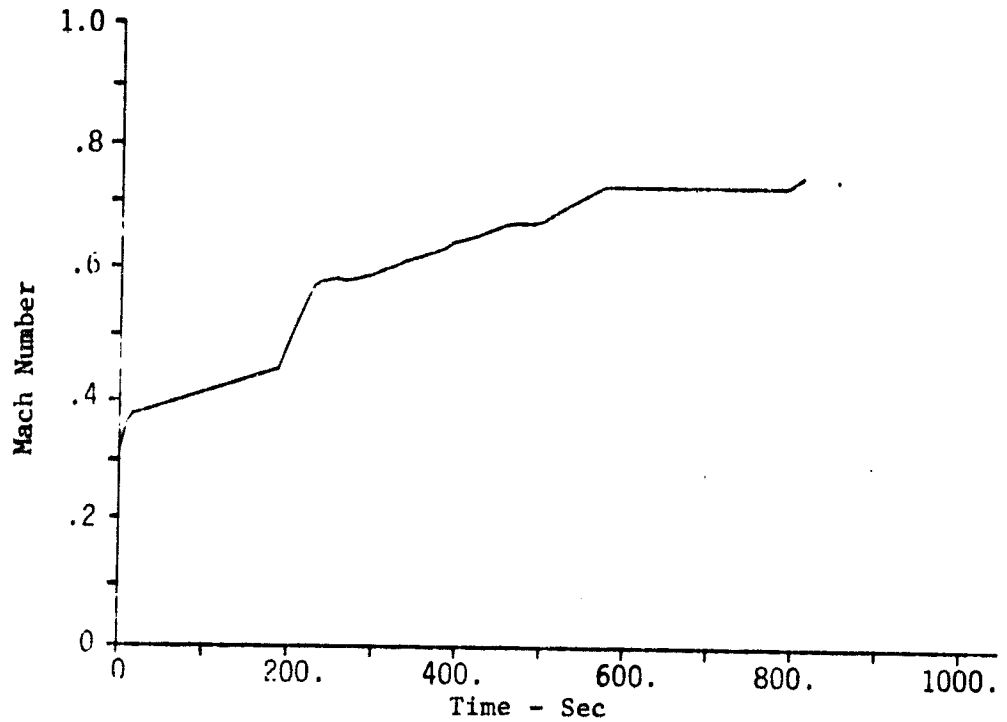

Figure 5. State Variables for an Optimum Climb Profile of the Twin-Jet Aircraft Traveling 750 n.mi.

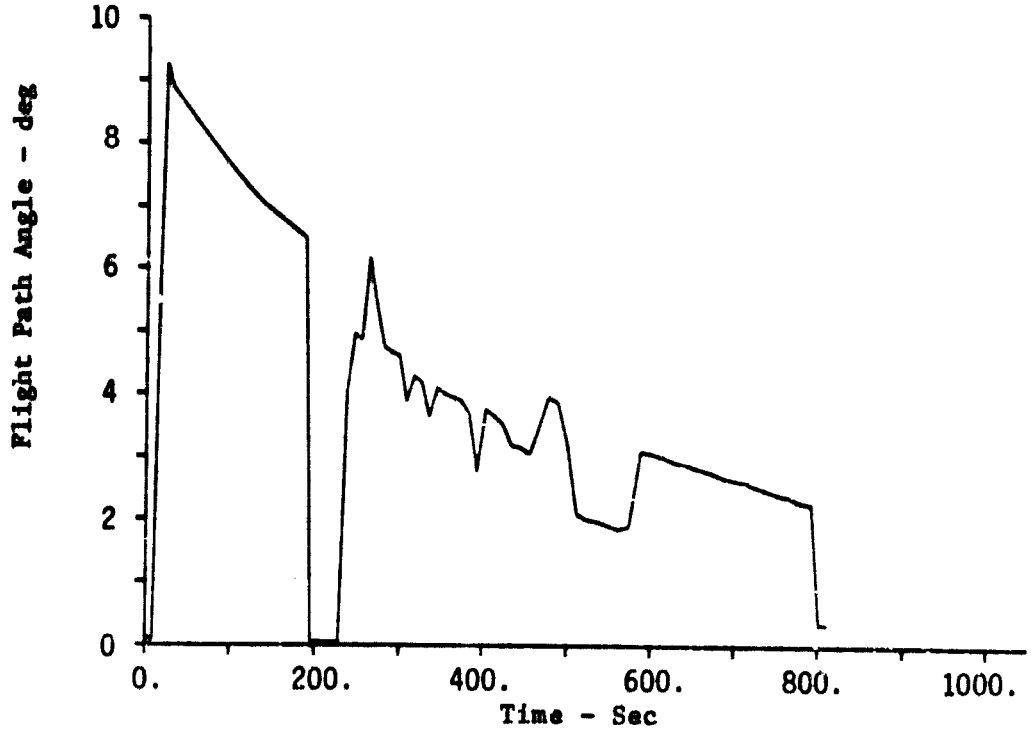

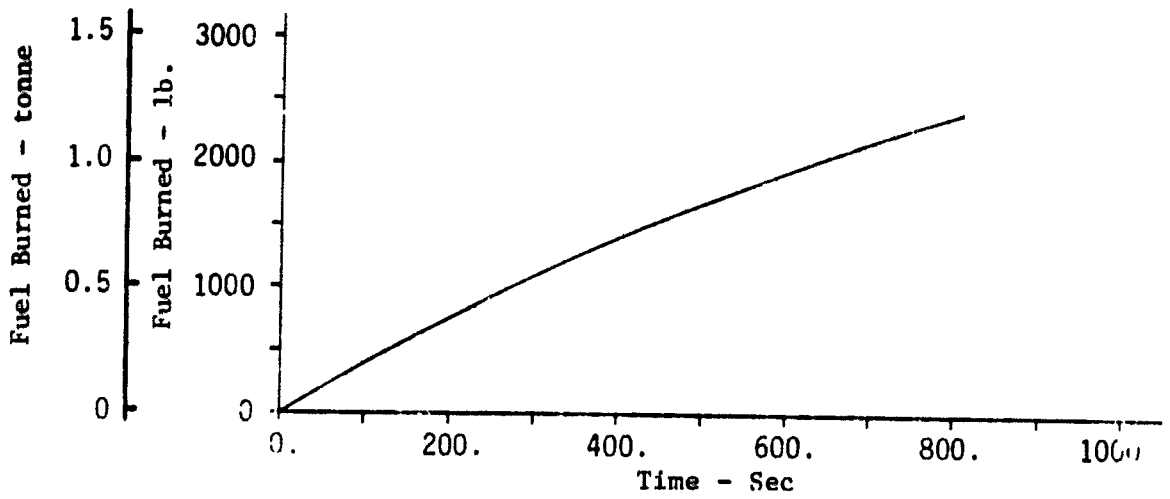

Figure 5. Concluded.

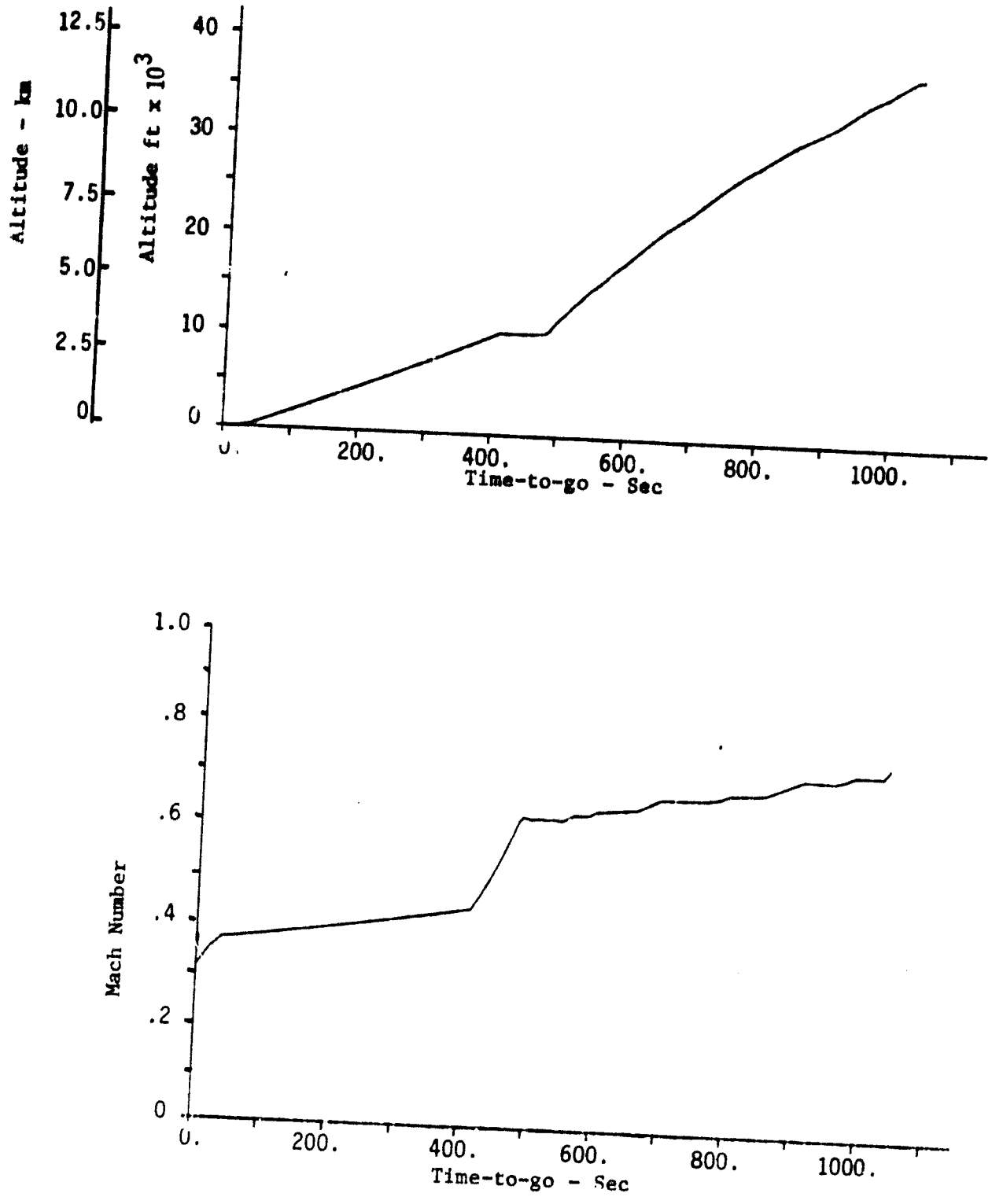

Figure 6. State Variables for an Optimum Descent Profile of the Twin-Jet Aircraft Traveling 750 n.mi.

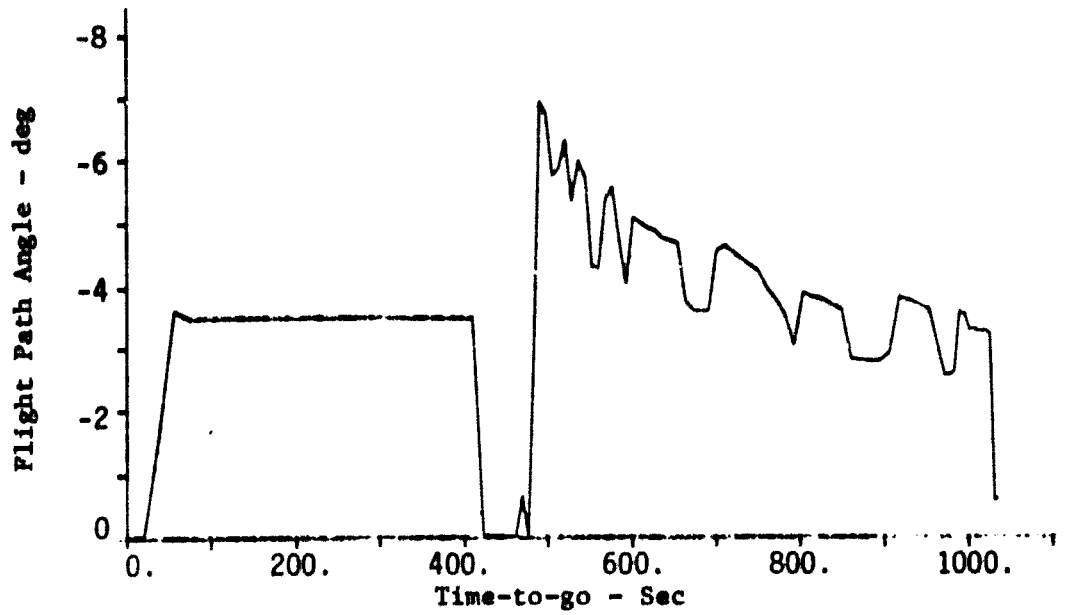

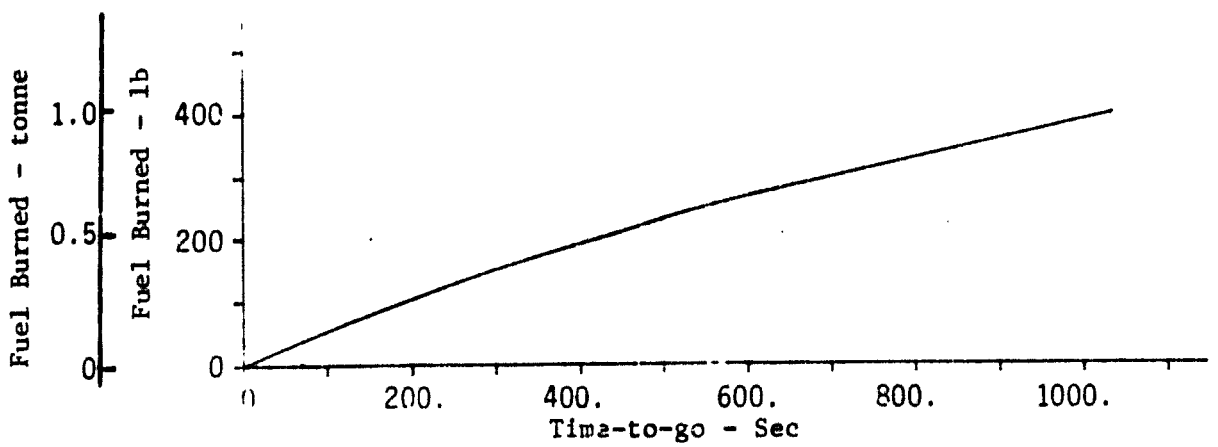

Figure 6. Concluded

Figure 7 compares the altitude vs. range profiles for three cases of the tri-jet aircraft traveling 200 n.mi. For these, both V_a and π were varied. However, a head wind and tail wind were added in two of the cases to produce the differences. The wind magnitude profile is also shown in Fig. 7, and it is representative of the Denver wind measured during August, 1977. (This wind is generally from the west.)

Table 1 makes various range and cost comparisons of the three profiles shown in Fig. 7, based on values of C_f of \$0.138/kg (\$0.0628/lb) and C_t of \$500.00/hr. It is seen that the head wind caused a total cost increase of \$24.95 (or 4.3%) while the tail wind decreased the cost \$23.59 (or 4.1%) compared to the no wind optimum case. Data, such as presented in Table 1, are printed for each run of OPTIM so that the trajectory costs and other characteristics can be readily evaluated (again, see Ref. 22).

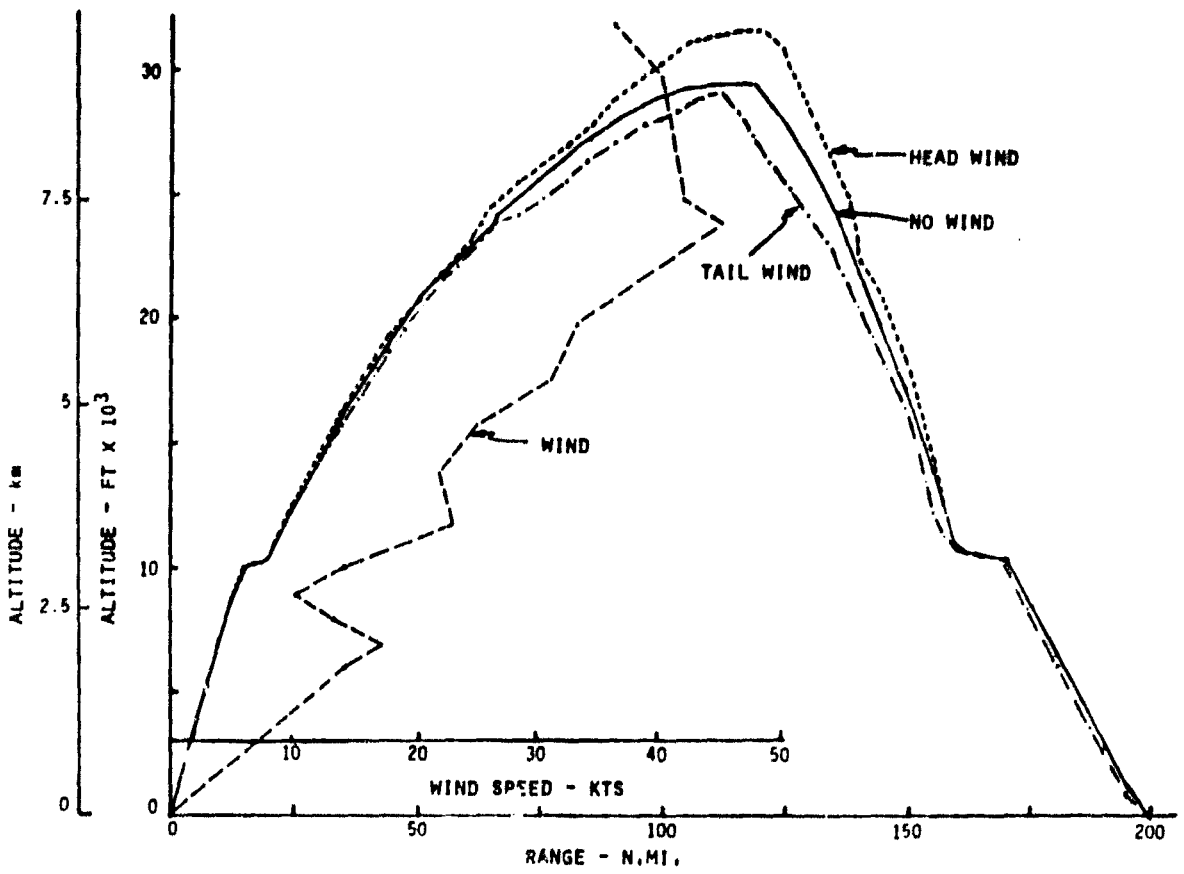

Figure 7. Comparison of Minimum Direct-Operating-Cost Flight Profiles for the Tri-jet Aircraft Model.

Table 1. Comparison of Flight Costs for 200 n.mi. Range with Varying Wind Conditions

	Case		
	No Wind	Head Wind	Tail Wind
Fuel Used (kg (lb))			
Climb	1945.8 (4289.60)	2013.0 (4437.82)	1805.2 (3979.66)
Descent	272.2 (600.19)	295.1 (650.57)	284.7 (628.13)
Total	2218.0 (4889.79)	2308.1 (5088.39)	2090.1 (4607.80)
Range (n.mi.)			
Climb	115.51	115.90	107.36
Descent	85.24	85.78	94.60
Total	200.75	201.68	201.96
Time (min:sec)			
Climb	17:31	18:33	15:41
Descent	15:05	15:33	16:11
Total	32:36	34:06	31:53
Cost ($)			
Climb	414.51	432.40	379.91
Descent	163.29	170.35	174.30
Total	577.80	602.75	554.21
Cost/Distance ($/n.mi.)			
Climb	3.59	3.73	3.54
Descent	1.92	1.99	1.84
Total	2.88	2.99	2.74

Fixed Time-of-Arrival

One of the problems associated with increased use of air travel and air transportation of cargo is the increased congestion that is occuring at the major hub airport terminal areas. Aircraft arrive in the terminal area on a somewhat random basis. If the aircraft arrive in too great a number, in a short period of time, they are currently placed in holding patterns by ATC. Then, they are instructed to land so that airport arrivals are at an acceptable rate. The holding pattern approach to regulating the landing rate has several shortcomings:

1. The holding pattern is expensive to the airlines in terms of increased fuel requirements, excess wear on the aircraft, and increased crew flying time.
2. The holding pattern delays the passenger, possibly causing missed connections.
3. The risk of collision is increased by holding aircraft in the already crowded terminal areas.
4. Maintaining several aircraft in safe holding patterns increases the air traffic controller's work load substantially.

One solution to this problem is to regulate the time of arrival of each aircraft such that they do not arrive in random groups but rather at a systematic acceptable rate. This is the ultimate goal of the FAA's metering, spacing, and flow control projects. This requires that the aircraft have the means to compute and regulate the flight profile so that the desired time-of-arrival is met.

The airlines also like to fly their aircraft with a scheduled, predetermined trip time. This time is selected to produce acceptable operating costs and desired service to the airline customers. Thus, there is a need to control the time length of a particular flight. With these motivations, OPTIM was modified to include this capability.

If time-of-arrival t_f is fixed, then the objective is to minimize the total fuel burned in traveling from p_1 to p_2 in time t_f. This is equivalent to minimizing the function

$$J = \int_0^{t_f} C_f \dot{w} \, dt \tag{17}$$

with the additional constraint that the range traveled is fixed.

The technique used in OPTIM to compute the profile that produces fixed range and fixed time-of-arrival is to fix C_f and to iterate on the value of C_t. For each value of C_t chosen, a given time-of-arrival t_f results.

As C_t is increased, the value of t_f decreases, and vice versa. Thus, an outer loop has been added to the OPTIM logic to adjust C_t to produce the desired t_f.

One constraint that had to be built into the program is the range that the variable C_t could span. As C_t increases, the emphasis is placed on achieving minimum time. As fuel prices increase however, this is not practical. On the other hand, as C_t decreases, the time-of-arrival increases. This is accompanied by a slowing down in cruise speed. A practical lower bound on cruise speed is that value (V_{cmin}) where fuel rate $\dot{w}$ is minimized. If more time is required in cruise to reach the destination at some desired time t_{fd}, then the aircraft should make up the difference by path stretching at the cruise speed V_{cmin}.

This posed the question of what should the lowest value of C_t be such that the resultant optimum cruise speed is V_{cmin}. This value was determined as follows.

The cost of flight during cruise is expressed by setting the Hamiltainion value H_c in Eq. (10) to the coefficient λ, or

$$\lambda = \frac{C_f \dot{w} + C_t}{V_a + V_w} \tag{18}$$

Mathematically, the question is what value of C_t will provide a trimmed cruise condition such that the trimmed cruise speed V_a will equal V_{cmin}?

At optimum cruise speed, the cruise cost λ is minimum, or

$$\frac{\partial \lambda}{\partial V_a} = 0. \tag{19}$$

If this is also the speed where fuel rate is minimum, then

$$\frac{\partial \dot{w}}{\partial V_a} = 0 \tag{20}$$

at this speed. Applying Eq. (19) to Eq. (18) yields

$$\frac{\partial \lambda}{\partial V_a} = \frac{C_f}{V_a + V_w} \frac{\partial \dot{w}}{\partial V_a} - \frac{C_f \dot{w} + C_t}{(V_a + V_w)^2} = 0, \tag{21}$$

By substituting Eq. (20) into Eq. (21), we get

$$C_f \dot{w} + C_t = 0,$$

or

$$C_{tmin} = - C_f \dot{w}_{min} . \tag{22}$$

Note, that at this value, from Eq. (18),

$$\lambda_{min} = 0. \tag{23}$$

Mathematically, this means that there is no cost to cruise at this condition.

Figure 8 shows the minimum fuel rate $\dot{w}$ for the tri-jet as a function of cruise altitude and cruise mass. As can be seen, flying at minimum fuel rate causes a large variation in optimum cruise altitude as cruise mass is varied. Figure 9 illustrates how optimum altitude and cruise airspeed vary as functions of cruise mass for the minimum fuel rate condition.

The results of Figs. 8 and 9 are used to compute the value of C_{tmin} and the associated cruise altitude in OPTIM. For example, for the tri-jet with a cruise mass of 54.43 tonne (120,000 lb) and a C_f of \$.33/kg (\$.15/lb), $\dot{w}_{min}$ is 2.585 tonne/hr (5686 lb/hr). This produces a C_{tmin} of -\$852.90/hr at an altitude of 9.25 km (30300 ft). The range on C_{tmin} for this aircraft is -\$777.60 to -\$1042.50 for cruise mass varying from 50 - 66 tonne (110,000 lb to 145,000 lb.)

Figures 10 and 11 illustrate how time-of-arrival and fuel used vary as C_t varies between +\$300/hr and -\$900/hr., for various combinations of initial mass and range-to-go for the tri-jet. In these example plots, cruise altitude

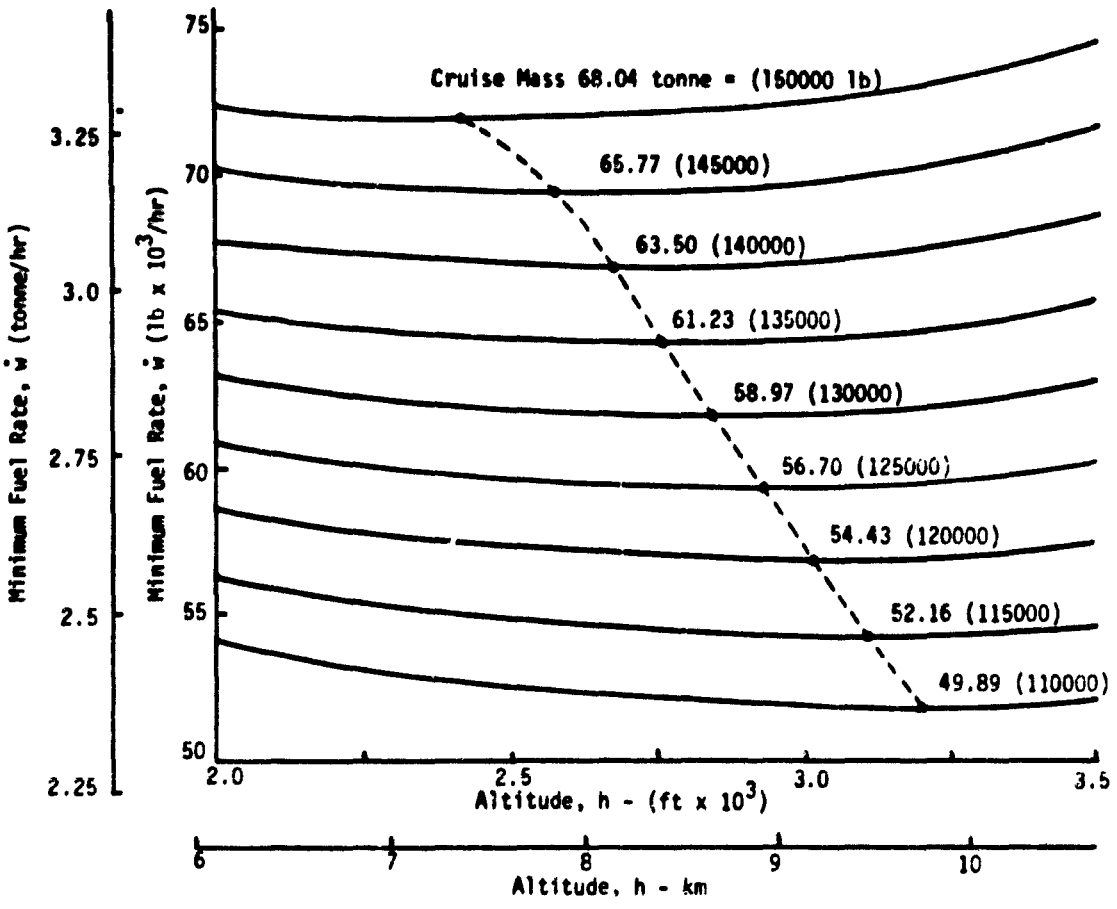

Figure 8. Minimum Fuel Rate for the Tri-Jet Model as a Function of Cruise Altitude and Mass.

is fixed at 10 km (33000 ft). The cost of fuel is set at \$.33/kg (\$.15/lb). Note that in Fig. 10, the time-of-arrival has a non-parabolic shape; this is different than would be expected. This indicates the presence of a convergence problem in OPTIM which is discussed shortly.

The fixed time-of-arrival option requires repeated generation of new cruise conditions associated with each successive value of time cost C_t tried. Thus, the OPTIM logic was set up so that this process was as efficient as possible. No short range flights were assumed so that cruise altitude was always reached. The table representing cruise conditions (the cruise table), spanned altitudes from 6 km - 12 km (20,000 ft - 40,000 ft). If a fixed cruise altitude was chosen, only that altitude was used in generating the cruise table.

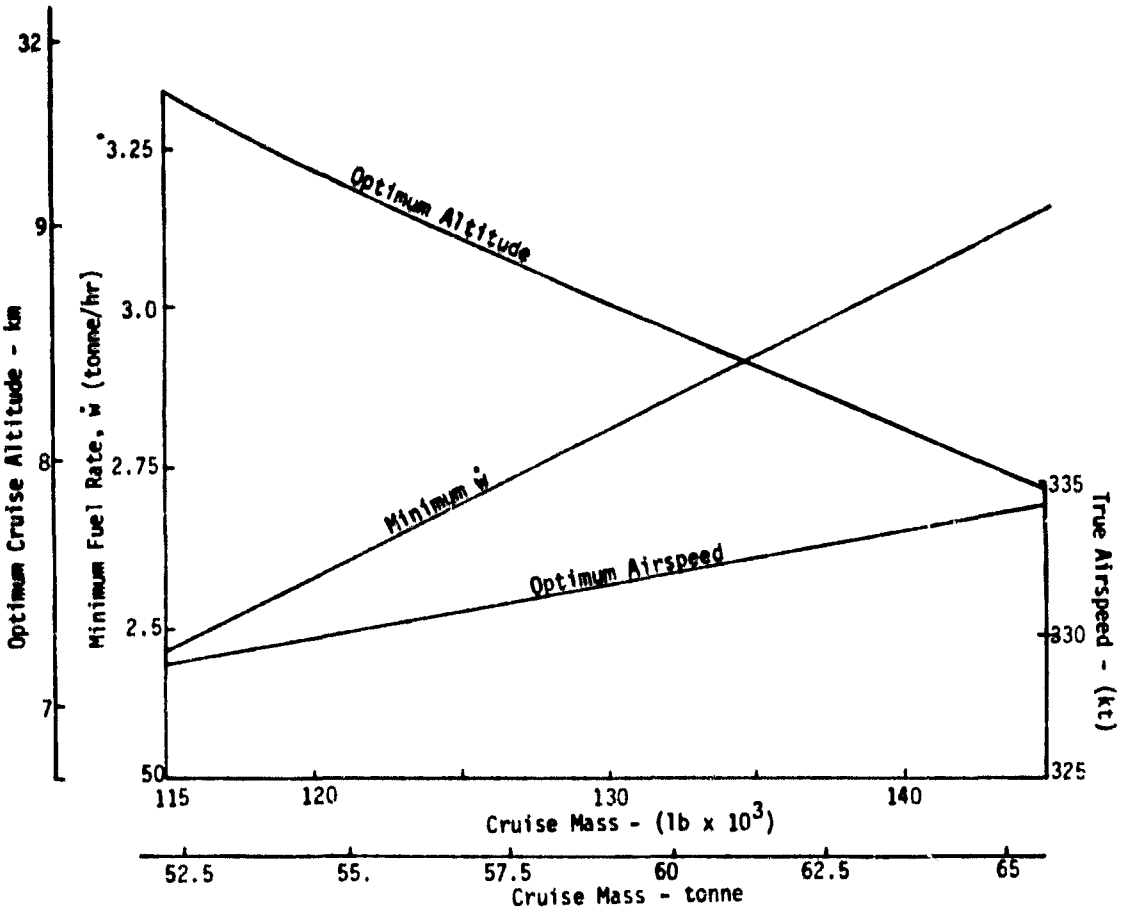

Figure 9. Optimum Cruise Altitude and Airspeed for a Tri-Jet Aircraft Flying at Minimum Fuel Rate as Functions of Cruise Mass.

The cruise table consists of two parts:

1. The cruise speed setting which minimizes λ, as defined by Eq. (18), and
2. The cruise speed setting which minimizes $\dot{w}$.

The second part of this table is generated only once at the beginning of the run because the $\dot{w}_{min}$ conditions do not depend on a particular C_t setting.

The program first sets C_t to zero. (This corresponds to the minimum fuel profile.) The resulting time-of-arrival T_o is then compared to the desired arrival time t_{fd}. If T_o is larger than t_{fd}, then flight is too slow. In this case, C_t must be positive. Next, trial values of C_t of \$300/hr and \$600/hr are used to obtain arrival times of T_1 and T_2. A

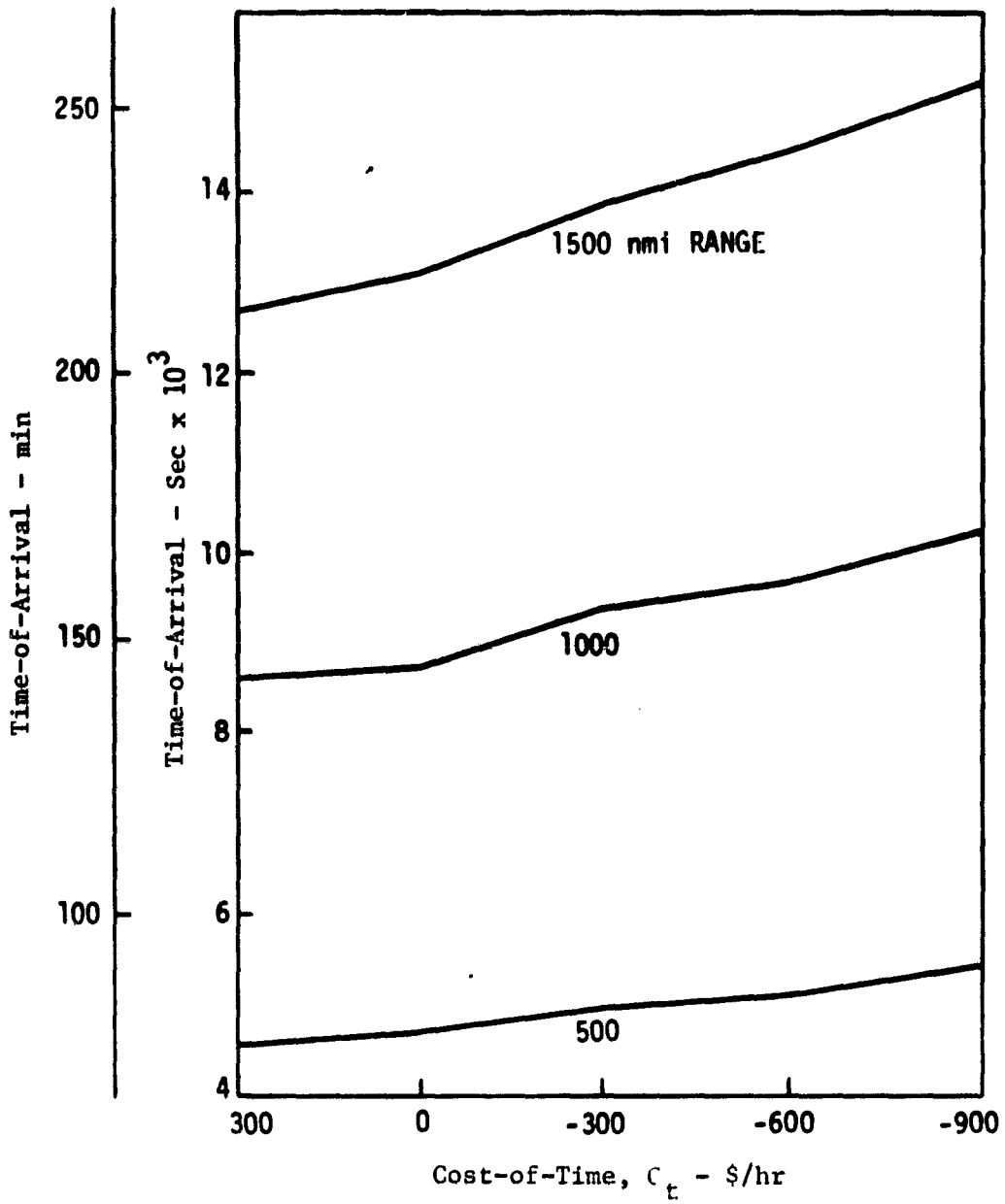

Figure 10. Time-of-Arrival Variations as a Function of Range and Cost-of-Time C_t. Initial Mass of 68182 kg (150000 lb) and Cruise Altitude Fixed at 10 km (33000 ft).

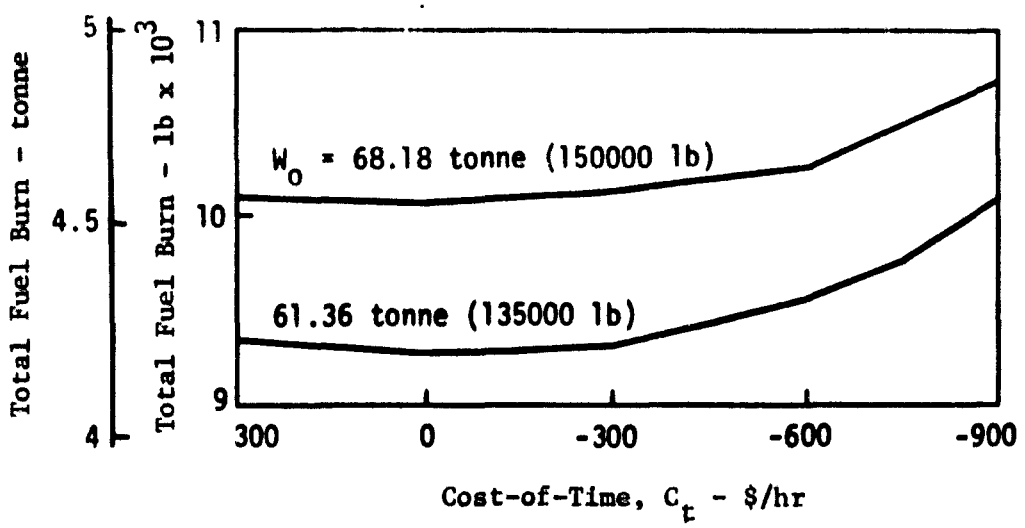

Figure 11. Fuel Burned Variations as Functions of Takeoff Weight and Cost-of-Time C_t. Cruise Altitude Fixed at 10 km (33000 ft). 500 n.mi. Range.

quadratic equation is derived to pass through the points (T_o, T_1, T_2) as a function of C_t. This quadratic equation is then solved for the value of C_t that will produce t_{fd}. This process is repeated using the last three values of time-of-arrival until convergence is reached.

If the time-of-arrival T_o is less than t_{fd}, then the minimum fuel profile is too fast. In this case, C_t must be negative. The next trial value the program uses is C_{tmin} from Eq. (22). This produces the maximum time of t_{fmax}. If t_{fd} is greater than t_{fmax}, a holding pattern (or path stretching) is required to make up the additional time. If t_{fd} is less than t_{fmax} (= T_1), then linear interpolation is used to obtain the next value of C_t. This produces time-of-arrival T_2. After that point, three values of time-of-arrival are available to compute a quadratic equation and solve the C_t. This procedure is again repeated until convergence is reached.

As predicted from Fig. 10, a convergence problem did arise in testing the fixed time-of-arrival option. This is illustrated in Fig. 12 which shows the variation in time-of-arrival for a 61.4 tonne (135000 lb) aircraft with C_t varying from $300/hr to $600/hr. As can be seen, there is

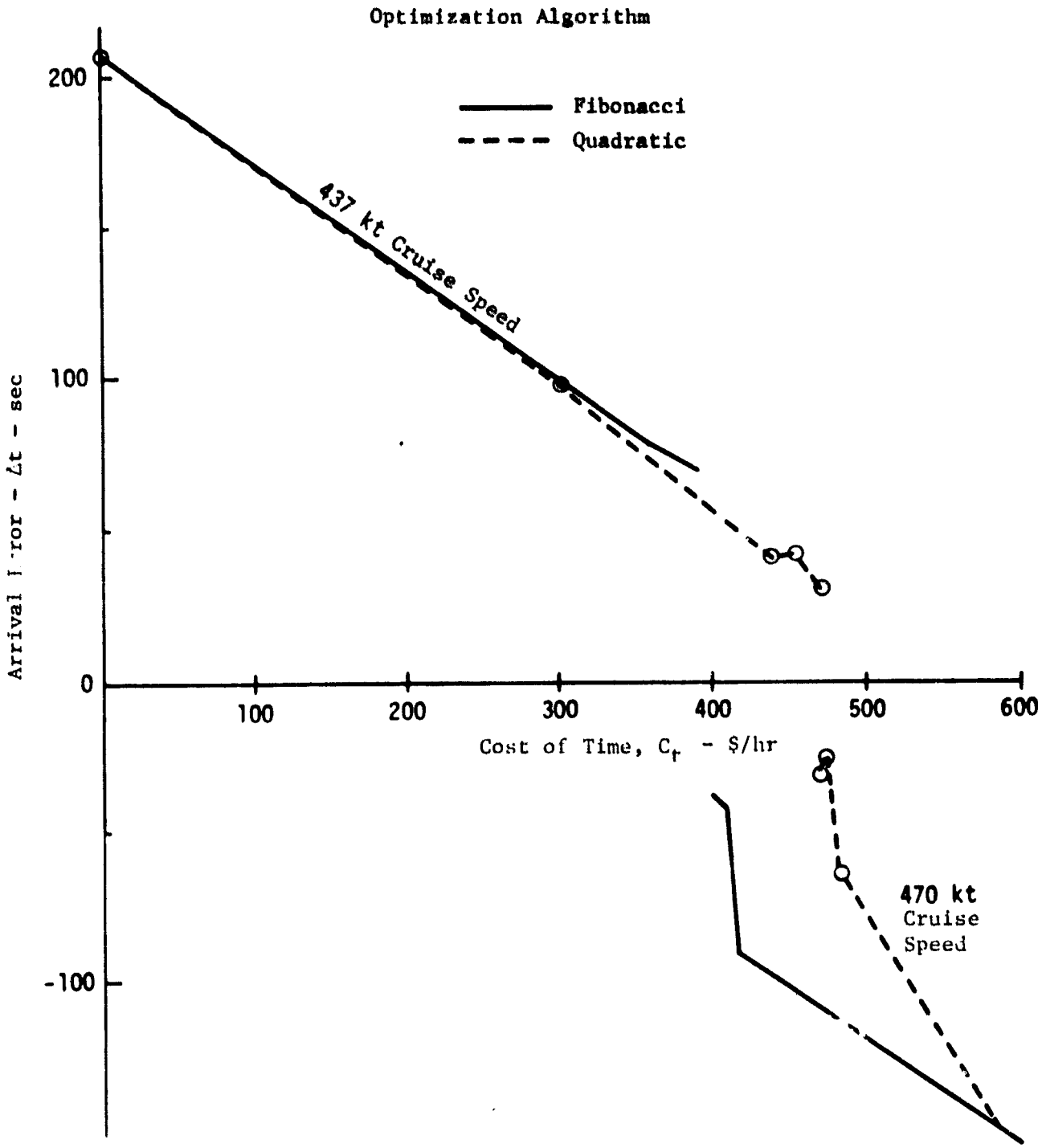

Figure 12. Illustration of Time-of-Arrival Convergence Problem

about a 100 sec gap in arrival time around C_t of \$400/hr. A quadratic optimization algorithm was tried in place of the original Fibonacci search technique to determine if the optimization routine was the source. This produced some improvement but did not remove the problem as is shown in Figure 12. Tightening the tolerances on the cruise trim conditions also did not remove the problem.

The problem was traced to the way the coefficient of drag C_D was determined by OPTIM in computing the cruise table. Currently, C_D is computed as a polynominal function of lift coefficient C_L, with Mach number as a parameter, as illustrated in Fig. 13. Linear interpolation is then used to obtain C_D for the given cruise Mach number.

Figures 14 and 15 show detailed plots of cruise cost λ of the tri-jet as a function of cruise speed, with cost of time set at \$300/hr and \$600/hr. Cost of fuel is \$.33/kg (\$.15/lb). Cruise altitude is a parameter. Note from these figures that:

1. There is a double minimum at the upper altitudes. The OPTIM program is based on there being only one minimum λ at each cruise altitude. The optimization routines used also are based on the assumption of a single minimum.

2. The minimums are along the Mach 0.76 and 0.82 lines. The Mach 0.80 line tends to pull the cost curves up creating the double minimums.

The drag coefficient C_D should be a continuous function of C_L and Mach. The minimum cruise cost should not always be at either M of 0.76 or 0.82 as indicated in the cost curves. The cost curves should be smooth with a single minimum at each altitude. Thus, the aerodynamic data, as currently stored in OPTIM, produces a convergence problem in attempting to obtain fixed time-of-arrival with tolerance on the order of 2 sec.

An effort is now underway to correct the convergence problem. Steps being taken are:

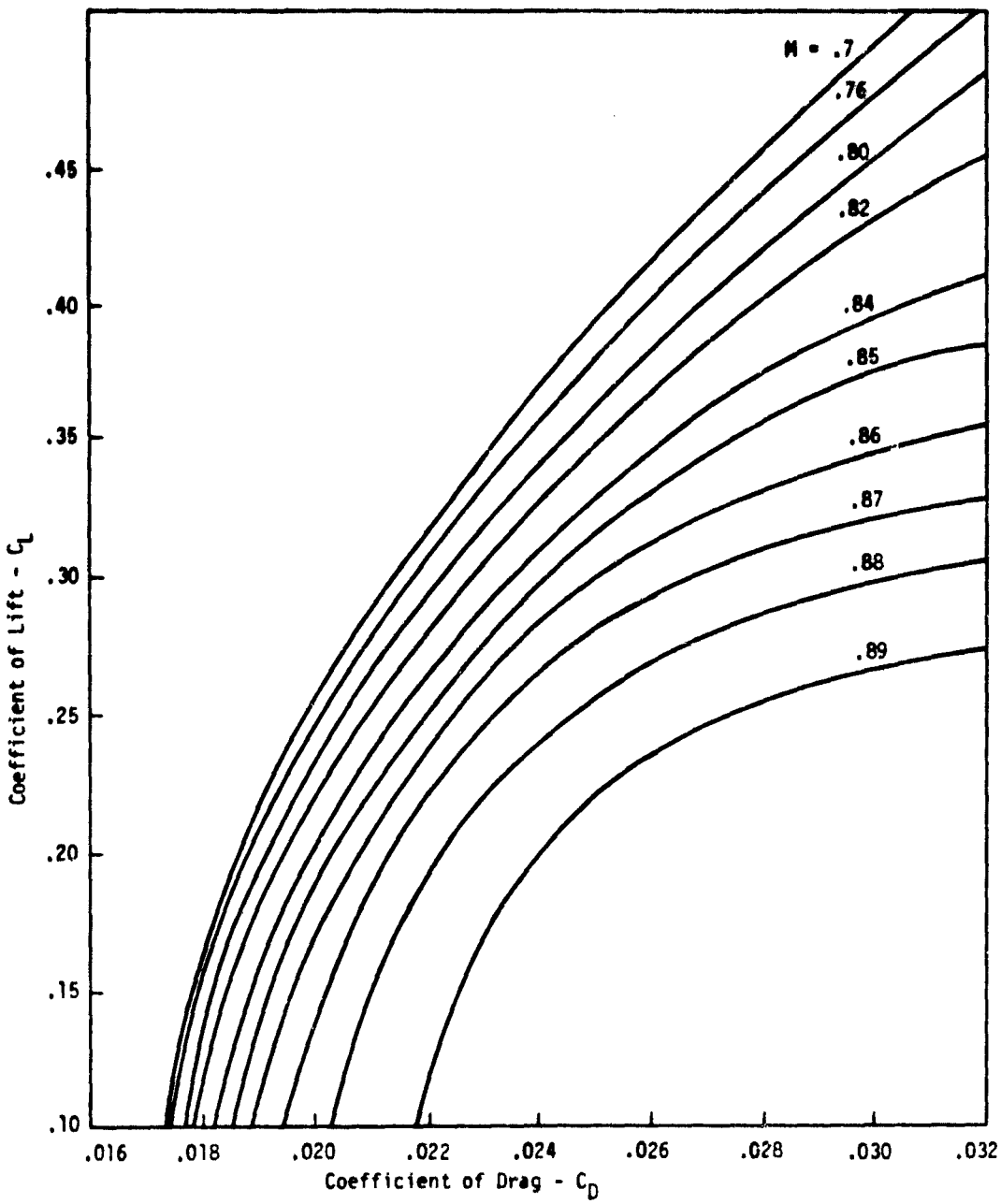

Figure 13. Typical C_D vs C_L - Lift/Drag Polars

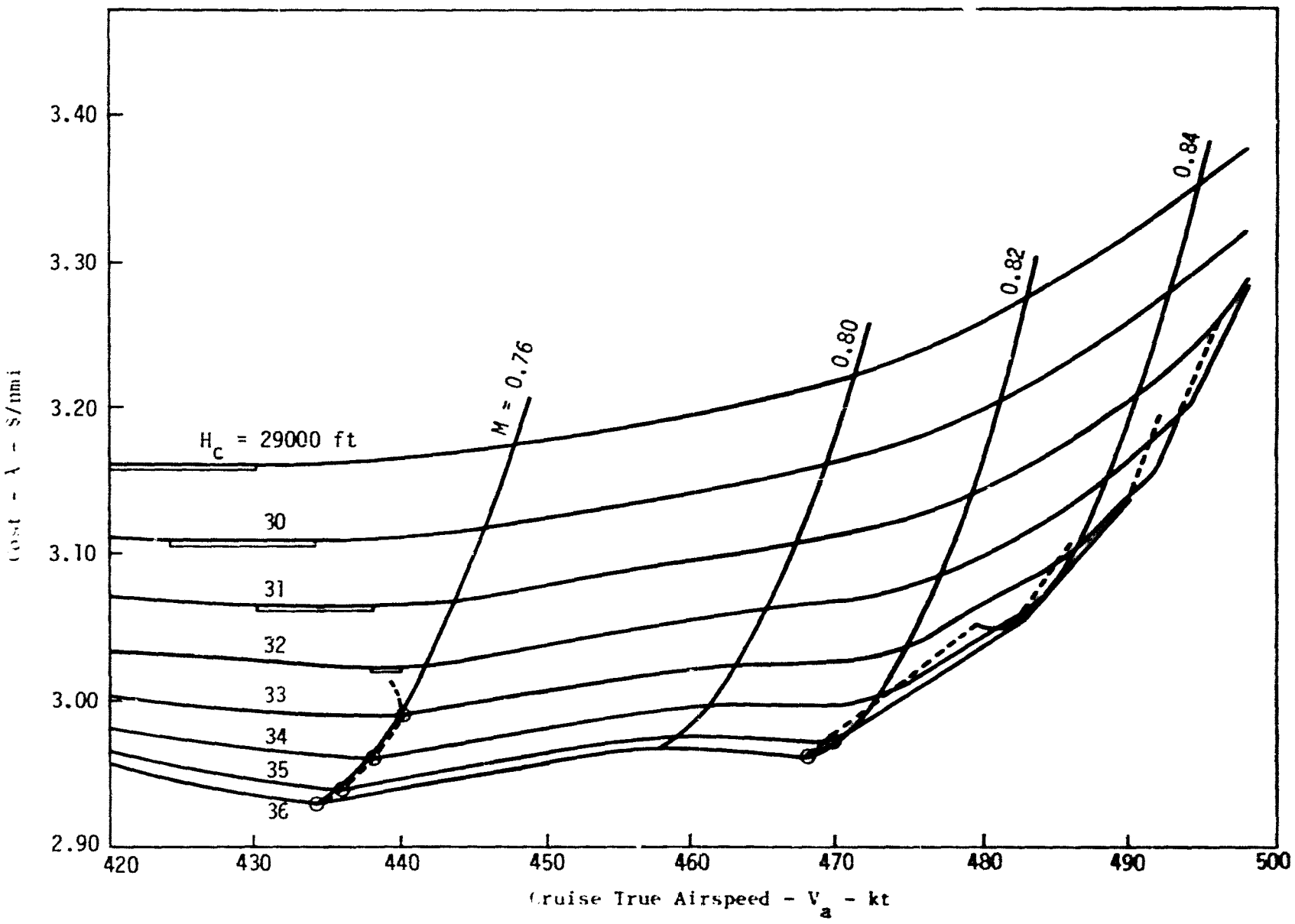

Figure 14. Cruise Cost as Function of Altitude and Cruise Speed for Cost-of-Time of $300./hr.

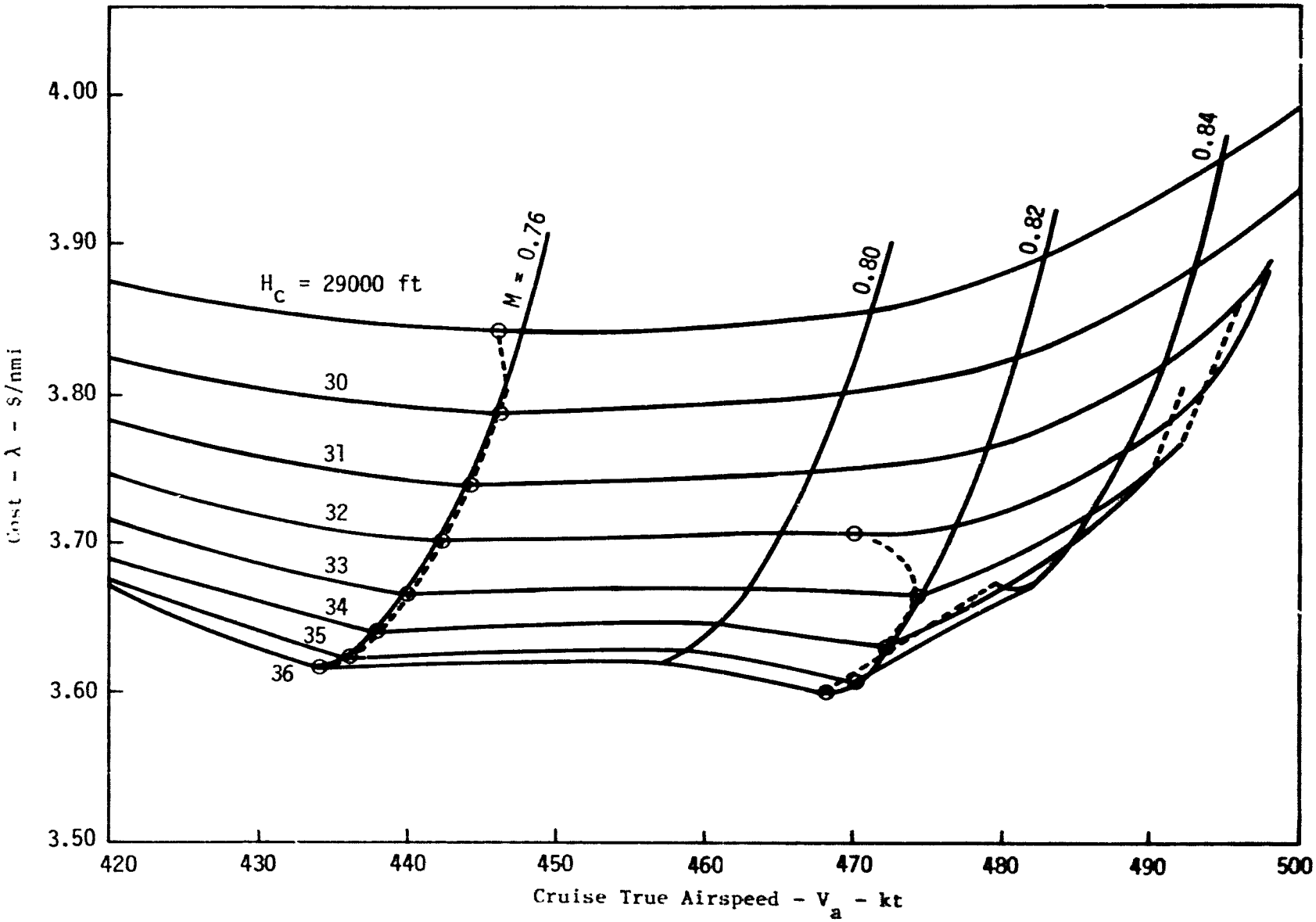

Figure 15. Cruise Cost as Function of Altitude and Cruise Speed for Cost-of-Time of $600./hr.

1. The C_D vs C_L and M data are being checked carefully to ensure that there are no kinks or bends in the curves.

2. Linear interpolation is being eliminated. Polynominal functions are being developed to ensure that all data vary continuously and smoothly.

The same constraints need to be applied to modeling the propulsion data. The lesson learned is that numerical optimization is based on the natural existance of continuous, smooth surfaces, and any departure from this type of model will produce a faulty result.

Despite the current existence of the convergence problem, there is a logical solution to its removal. Also, as seen in the next chapter, having fixed time-of-arrival capability can produce a significant flight fuel savings.

III

PROGRAM VERIFICATION AND SENSITIVITY RESULTS

The previous chapter and Appendix A describe an efficient way in which near-optimum flight profiles can be generated without using time-consuming numerical techniques. Instead of iteratively solving the two-point boundary value problem, assumptions are made so that the dynamics are simplified to two state variables. One state variable (either range or energy) becomes the independent variable, and the other is included as the single state in the Hamiltonian. Thus, the problem of solving for minimum cost profiles reduces to algebraic minimization of the Hamiltonian at each point along the profile.

Now, although this method is a convenient way of generating a trajectory, the resulting trajectory must be verified by using a more accurate model of the aircraft dynamics. Verification implies that:

1) The reference trajectory that is generated must be flyable when the full aircraft equations of motion and constraints are taken into account.

2) The trajectory cost (Eq. (2)) as predicted by OPTIM must be essentially identical to that experienced by simulating more complete aircraft equations of motion.

Thus, the first objective of this chapter is to describe a companion program to OPTIM which was developed for verification of the optimization results. This program is referred to as TRAGEN (for trajectory generation).

With OPTIM and TRAGEN as computer tools, the user has the capability to study the characteristics of optimum profiles in great detail and to examine alternate ways these profiles can be implemented on-board. Trajectory characteristics are obtained by exercising OPTIM's options and by making sensitivity studies with OPTIM and TRAGEN which are the subjects of the second part of this chapter.

Optimization Verification

To achieve optimization verification required the development of a companion computer program to OPTIM which can be used to simulate the longitudinal trajectory of an aircraft commanded to follow the reference path output from OPTIM. Some details of this program (TRAGEN) are presented in Appendix E, and a separate user's guide for this program has also been written [23].

In addition to verification of the optimization program's results, the TRAGEN program has the following utility:

1). It provides a means for testing guidance laws for steering the aircraft to follow the input reference trajectory.

2). It enables study of the effect of following an incorrect reference trajectory. For example, if the OPTIM results were based on one particular wind profile and initial aircraft weight, and a different weight and wind profile actually existed, the TRAGEN simulation would allow assessment of the effect of these errors on trajectory cost.

3). It can be used to determine the flight cost that would result from the aircraft being commanded to follow a reference trajectory suggested in the manufacturer's aircraft handbook. For example, for climb, handbook reference trajectories usually consist of following a constant indicated airspeed until a given Mach number is reached. Then, the reference trajectory follows this fixed Mach number until the reference cruise altitude is reached.

4). It can be used to test perturbation control schemes for removing the effect of wind gusts and other non-nominal performance sources (navigation errors, transient temperature profiles, non-standard engine performance).

5). It is expandable to test candidate on-board mechanizations of a system of equations for generating the near-optimum vertical profile.

A five state-variable model of the aircraft is currently used in TRAGEN to simulate longitudinal motion. State variables are altitude, altitude rate, longitudinal range, airspeed, and aircraft mass. Currently neglected are the rapid transient dynamics of throttle response, angle-of-attack, and pitch rate (δ_T, α, q). The throttle is assumed to be set so

that maximum thrust is achieved during climb and idle thrust is used during descent. The cruise phase is not simulated. The altitude control variable is taken to be the angle-of-attack which has maximum and minimum limits. This degree of sophistication is adequate for testing the OPTIM results.

The TRAGEN program can readily be expanded to include throttle dynamics and short period dynamics. This would be required for further study of autothrottle and autopilot design to steer the aircraft to follow input reference trajectories. The control variables would be throttle position and elevator deflection for this expanded capability. A requirement for implementing this expanded simulation would be to obtain the necessary stability and control derivatives to complete the dynamic model.

The specification of reference profiles used in TRAGEN is based on using altitude as the independent variable for climb and range-to-go to the destination as the independent variable for descent. For climb, the reference trajectory consists of specifying airspeed and flight path angle (with respect to the air mass) as piecewise linear functions of altitude. At the 3048 m (10000 ft) point, the aircraft is commanded to level off and accelerate until the airspeed is reached where the climb should again continue.

To generate the control law to follow the commanded climb profile, a linear perturbation model was made of the dynamic equations,

$$\begin{aligned} T\cos\alpha - D(\alpha,h,V_a) - W\sin\gamma &= m\dot{V}_a \ , \\ T\sin\alpha + L(\alpha,h,V_a) - W\cos\gamma &= mV_a\dot{\gamma} \ . \end{aligned} \tag{24}$$

The perturbation equations and transfer functions from Eqs. (24) are given in Eqs. (E.10) and (E.11) in Appendix E. Here, it is assumed that a perturbation $\delta\alpha$ to the nominal angle-of-attack can be used to obtain the desired perturbations in flight path angle ($\delta\gamma$) and airspeed (δV_a) maintain the aircraft on the desired reference climb profile.

Because both commanded values of airspeed and flight path angle are assumed to vary linearly with altitude, they are ramp functions, and a Type 1 control system is suggested. The original climb control law was thus set to be

$$\delta\alpha = \left(K_1 + \frac{K_2}{s}\right)(V_c - V_a) + \left(K_3 + \frac{K_4}{s}\right)(\gamma_c - \gamma) \tag{25}$$

where V_c and γ_c are the commanded reference values of V_a and γ. K_1, K_2, K_3, and K_4 are control gains. The commanded values were derived according to Eqs. (E.12) and (E.13).

Experience with this control law revealed two points:

1) The integral control gain K_2 on airspeed error was not needed and did not particularly improve performance. Thus, it was nominally set to zero.

2) Constant values of the gains K_1, K_3, and K_4 could be selected to provide good, stable performance throughout the climb phase. Thus, there was no need to have altitude dependent gains programmed.

No attempt was made to select the control gains so that the perturbation response was optimized. The main objective was to obtain a set of gains which caused the aircraft simulation to track the input reference trajectory with only a small amount of error (which was accomplished). Gain selection for control response optimization should remain as a task to be conducted when an actual autopilot/autothrottle is being implemented and the complete aircraft dynamics are being considered.

Evaluation of Optimum Profiles Several optimum trajectories were computed by using OPTIM and then subsequently used as inputs to drive the TRAGEN simulation. For example, Table 2 presents a comparison of OPTIM and TRAGEN results at the end of the climb portion of a tri-jet aircraft model having an initial mass of 61236 kg (135000 lb), and traveling a total range of 150, 225, and 275 n.mi. with no wind. As can be seen, the match is exceptional. The same degree of comparison was found using the two programs for different range and different initial mass flights.

Table 2. Comparison of Optimization and Trajectory Generation Program Climb Results for Different Range Flights. No Wind. 61236 kg (135000 lb) Takeoff Mass.

Range n. mi.	Fuel Burn - kg (lb)		Time - Sec		Altitude - m (ft)		Airspeed - m/s (ft/s)		Range - m (ft)	
	OPTIM	TRAGEN	OPTIM	TRAGEN	OPTIM	TRAGEN	OPTIM	TRAGEN	OPTIM	TRAGEN
150	1405 (3097)	1405 (3097)	682	680	7597 (24924)	7597 (24926)	230 (756)	229 (752)	125127 (410522)	125054 (410281)
225	1931 (4258)	1931 (4258)	1060	1060	9760 (32021)	9760 (32021)	244 (801)	244 (800)	211441 (693704)	212936 (698609)
275	2075 (4574)	2073 (4570)	1185	1178	10319 (33855)	10321 (33861)	244 (802)	244 (800)	242116 (794345)	241033 (790790)

The results with head and tail winds were not as close. Table 3 presents a comparison of OPTIM and TRAGEN results at the end of climb when the wind profile of Fig. 7 was used as both a head and tail wind for the 225 n.mi. range flight. In both cases, the more detailed simulation from TRAGEN shows that it takes a longer time period (14-22 sec) and greater range (4000 - 5000 m (14000 - 15000 ft)) than predicted by OPTIM (However, range traveled is not significant for climb.) The biggest discrepancy is the 2.6% extra fuel required for the tail wind case. In the future, the modeling simplifications of OPTIM and the steering accuracy of the TRAGEN control law should be investigated to resolve this point.

Table 3. Comparison of Optimization and Trajectory Generation Program Climb Results in the Presence of Winds. 225 n.mi. Range. 61236 kg (135000 lb) Takeoff Mass.

Type Wind	Fuel Burn - kg (lb)		Time - Sec		Altitude - m (ft)		Airspeed - m/s (ft/s)		Range - m (ft)	
	OPTIM	TRAGEN	OPTIM	TRAGEN	OPTIM	TRAGEN	OPTIM	TRAGEN	OPTIM	TRAGEN
Head	2084 (4594)	2082 (4591)	1180	1202	10294 (33772)	10362 (33996)	244 (802)	244 (802)	225177 (738770)	229818 (753997)
Tail	1701 (3751)	1747 (3851)	897	911	9145 (30003)	9074 (29770)	233 (766)	235 (772)	183238 (601174)	187433 (614936)

For the descent portion of the flight, the more likely variable - range-to-go to the destination point - was used as the independent variable for specifying the reference path. In this case, the descent altitude was specified as a function of range. This defined the inertial flight path angle that the aircraft should be on which is defined by Eq. (E.16). In the current version of TRAGEN, no attempt was made to control airspeed during the descent. The control law to compute the perturbation to the angle-of-attack was of the form

$$\delta\alpha = \left(K_3 + \frac{K_4}{s}\right)(\gamma_{Ic} - \gamma_I) , \tag{26}$$

where γ_{Ic} is the commanded inertial flight path angle.

Despite the lack of control of true airspeed during descent, the descent steering provides the same degree of matching performance between OPTIM and TRAGEN results as was experienced during the climb simulation (where true airspeed was controlled) above 3048 m (10,000 ft). Table 4 compares OPTIM and TRAGEN results at about 3048 m (10,000 ft) for the tri-jet descending with idle thrust from 10668 m (35,000 ft). The three cases are with no wind and the Denver head and tail winds shown in Fig. 7. The biggest error is in airspeed where variations of +5.8 to -1.5 m/s (+19 to -5 ft/sec) are seen.

Table 4. Comparison of Optimization and Trajectory Generation Program Results Descending from 10668 m (35000 ft) to 3048 m (10000 ft).

Type Wind	Fuel Burn - kg (lb)		Time-to-go- s		Altitude - m (ft)		Airspeed- m/s (ft/s)		Range-to-go - m (ft)	
	OPTIM	TRAGEN	OPTIM	TRAGEN	OPTIM	TRAGEN	OPTIM	TRAGEN	OPTIM	TRAGEN
No Wind	117 (259)	117 (258)	444	447	3154 (10348)	3148 (10328)	149 (490)	151 (497)	56704 (186036)	56598 (185688)
Head	110 (242)	110 (242)	444	449	3154 (10348)	3148 (10328)	149 (490)	148 (485)	55465 (181973)	55494 (182066)
Tail	123 (271)	124 (273)	440	441	3154 (10348)	3148 (10329)	149 (490)	155 (509)	57911 (189998)	57856 (189816)

These same cases are compared again at the altitude of 1.8 m (6 ft) in Table 5. The head wind case has a -3.4 m/s (-11 ft/sec) difference in true airspeed which causes 7 sec time and 4.5 kg (10 lb) fuel burn differences at this point. The tail wind case has a +5.8 m/s (+19 ft/sec) difference in airspeed which causes - 14 sec time and -1.8 kg (-4 lb) fuel burn differences. These differences could possibly be lessened with true airspeed control added.

Table 5. Comparison of Optimization and Trajectory Generation Program Results. Descending from 10668 m (35000 ft) to 1.8 m (6 ft).

Type Wind	Fuel Burn - kg (lb)		Time-to-go - s		Altitude - m (ft)		Airspeed - m/s (ft/s)		Range-to-go - m (ft)	
	OPTIM	TRAGEN	OPTIM	TRAGEN	OPTIM	TRAGEN	OPTIM	TRAGEN	OPTIM	TRAGEN
No Wind	237 (523)	237 (523)	0	8	1.8 (6)	-3.1 (-10)	124 (407)	126 (413)	0	-49 (-157)
Head	230 (506)	234 (516)	0	7	1.8 (6)	-5.2 (-17)	124 (407)	121 (396)	0	-96 (-314)
Tail	243 (535)	241 (531)	0	-14	1.8 (6)	-4.3 (-14)	124 (407)	130 (426)	0	-85 (-280)

Despite the differences between OPTIM and TRAGEN results, it is believed that the match between them is very good. That is, the results provided by OPTIM (fuel burn, time expired, trajectory followed) can be concluded to be accurate, and sensitivity runs based on using both programs will also produce accurate conclusions. A better match between the two programs can be obtained by minor adjustments to both programs.

Evaluation of Handbook Profiles It is also desired to use TRAGEN to evaluate and compare the cost of climb and descent profiles as specified in the pilot handbook with those generated by OPTIM. Thus, it was required to simulate flight along profiles specified in the pilot handbook. This required adding the capability of computing a typical handbook reference trajectory as part of the TRAGEN code.

Typical reference climb trajectories consist of the following sequence:

1. Climbing at 250 kt indicated airspeed (VIAS1) to 3048 m (10,000 ft.) (250 kt below 10,000 ft is an ATC maximum airspeed constraint).

2. Leveling off at 10000 ft and accelerating to a new climb indicated airspeed (VIAS2) (e.g., 320 KIAS).

3. Climbing at VIAS2 until a Mach number (M3) (e.g., M = 0.78) is reached.

4. Continue climbing at Mach number M3 until cruise altitude is reached.

During this climb, full throttle is typically used.

The handbook descent profile is the reverse of the above sequence with throttle set to idle. Thus, during descent M3, VIAS2, VIAS1 are used with the same constraint below 3048 m (10000 ft).

To compute the reference profile which follows that specified by a handbook, the following sequence of computations are used in TRAGEN. First, the altitude is incremented as

$$h = h_b + \Delta h \ , \tag{27}$$

Here, the subscript b refers to the value computed during the previous cycle. In TRAGEN, Δh is currently set to 152.4 m (500 ft). Next, the desired value of true airspeed V_T is computed from the specified indicated airspeed V_{IAS} or Mach number M by

$$p = f_1(h) \tag{28}$$

$$T_e = f_2(h) \tag{29}$$

$$\rho = p/3092.4T_e \tag{30}$$

$$a = 65.76\sqrt{T} \tag{31}$$

$$M = (5.((((V_{IAS}/29.)/p + 1.)^{2/7}) - 1.))^{1/2} \tag{32}$$

$$V_T = M\,a \tag{33}$$

Here, p and T_e are pressure and temperature which are computed in a subroutine as functions of altitude. Then, air density ρ and speed-of-sound a are computed as functions of p and T_e. If Mach number is given, Eq. (32) is skipped, and instead

$$V_{IAS} = 29.(p((1. + 0.2M^2))^{3.5} - 1.)^{1/2} , \tag{34}$$

is used to compute the indicated airspeed.

Next, the specific energy at h is

$$E = h + V_T^2/2g . \tag{35}$$

Then, for climb, the EPR is set at the maximum value, and thrust Th and fuel flow $\dot{w}$ are again obtained from subroutines as

$$Th = f_3(M,h) , \tag{36}$$

$$\dot{w} = f_4(M,h,Th) . \tag{37}$$

The approximation is made that lift L balances the aircraft weight w, or

$$L \cong W . \tag{38}$$

Then, the coefficient of lift C_L is

$$C_L \cong L/(1/2\ \rho\ V_T^2\ S) , \tag{39}$$

where S is the aircraft reference area. Then, another subroutine is used to compute the drag coefficient C_D as

$$C_D \cong f_5\ (C_L,M) . \tag{40}$$

From this, drag is

$$D \cong 1/2\ \rho\ V_T^2\ S\ C_D . \tag{41}$$

Then, energy rate is computed as

$$\dot{E} \cong (T - D)\ V_T/W . \tag{42}$$

The increment of time to reach this new state is

$$\Delta t \doteq (E - E_b)/\dot{E} \ . \tag{43}$$

The flight path angle to reach this state is

$$\gamma \doteq \sin^{-1} (2(\Delta h/\Delta t)/(V_{T_b} + V_T) \ . \tag{44}$$

The change in range between the two points is about

$$\Delta R \doteq (V_T + V_{T_b}) \cos \gamma \ \Delta t/2 \ . \tag{45}$$

The weight is incremented as

$$W = W_b - \dot{w} \ \Delta t \ . \tag{46}$$

The altitude is held constant to accelerate from the initial speed V_o to VIAS1 and to accelerate from VIAS1 to VIAS2.

For convenience, the descent reference profile is computed backwards in time from the final altitude to the cruise altitude. Then, the data points are reordered so that the descent reference profile is followed in real time.

Comparison of Optimum and Handbook Reference Profiles

One value of the TRAGEN program is that it can be used to compare the fuel and direct operating costs of various profiles followed in climbing to and descending from cruise. This capability gives the user a valid way of establishing the potential worth of any given flight management system.

Table 6, taken from Ref. 24, indicates the handbook climb and descent schedules for several types of commercial aircraft. For example, a 727-100 aircraft climbs (above 10000 ft) at 340 kt (IAS) until obtaining 0.78 Mach. The climb is continued at 0.78 Mach until cruise altitude is reached. Cruise is at 0.80 Mach. Descent is also at 0.80 Mach until obtaining 340 kt (IAS). Then, descent is continued at 340 kt until 3048 m (10000 ft) is reached. At that time the aircraft levels off and decelerates to 250 kt before continuing to descend.

Table 6. Typical Aircraft Characteristics as Specified in Manufacturer's Handbooks. [24]

Airplane Type	Final Cruise Altitude	Cruise Mach No.	Landing Weight*	Climb Schedule	Descent Schedule
737-200	8,839 m (29,000 FT)	.73	36,644 KG (80,800 LB)	320 IAS/.73 M	.73 M/320 IAS
727-100	10,668 m (35,000 FT)	.80	50,658 KG (111,700 LB)	340 IAS/.78 M	.80 M/340 IAS
727-200	10,668 m (35,000 FT)	.80	56,372 KG (124,300 LB)	340 IAS/.78 M	.80 M/340 IAS
DC-8-20	10,668 m (35,000 FT)	.80	75,011 KG (165,400 LB)	300 IAS/.78 M	.80 M/330 IAS
DC-8-50	10,668 m (35,000 FT)	.80	77,098 KG (170,000 LB)	300 IAS/.78 M	.80 M/330 IAS
DC-8-61	10,668 m (35,000 FT)	.80	88,707 KG (195,600 LB)	300 IAS/.78 M	.80 M/330 IAS
DC-8-62	10,668 m (35,000 FT)	.80	82,313 KG (181,500 LB)	300 IAS/.78 M	.80 M/330 IAS
DC-10-10	10,668 m (35,000 FT)	.83	128,844 KG (284,100 LB)	300 IAS/.82 M	.83 M/340 IAS
747-100	10,668 m (35,000 FT)	.84	194,784 KG (429,500 LB)	340 IAS/.82 M	.86 M/340 IAS

* Based on average 1973 Payload obtained from CAB Form 41, Sched. T-2(b).

TRAGEN was used to compare fuel and time costs of the handbook type profiles with optimum profiles generated by OPTIM. Figure 16 illustrates the speed/altitude profiles followed in a comparative example using the tri-jet aircraft. Shown are a handbook reference profile, an intermediate reference profile, and a minimum fuel profile generated by OPTIM. The intermediate reference profile was selected to have the characteristics of the handbook profile but to have speeds more nearly equal to the minimum fuel profile.

Table 7 presents the fuel used, time, and range covered in flying the three climb and descent segments illustrated in Fig. 16. An incremental cruise distance was added to the intermediate and minimum fuel climb profiles so that the same range would be covered for the climb comparison. Similarly, a cruise increment was added to the handbook descent profile so the same range would be covered for the descent comparison. (In Table 7, the second number after each + sign is the added cruise portion.)

As can be seen, the minimum fuel climb profile uses 169 kg (371 lb) less fuel (7.8%) than the handbook reference climb profile. It also takes 36 sec less time and covers 15.338 n.mi. less range to reach the cruise conditions. Note however, that the minimum fuel profile begins cruise at Mach 0.77 rather than 0.78. Also note that if the cruise segment is added to the minimum fuel climb so equal range is covered, the improvement in fuel is cut to 52 kg (115 lb), or 2.3%. The minimum fuel climb profile is essentially equivalent to the intermediate profile in that it only uses 6 kg (13 lb) less fuel.

The descent profile shows a different result. Here, the handbook descent profile taken alone uses 27 kg (60 lb) less fuel and 267 sec less time to descend than the "minimum fuel" profile. If the range traveled adjustment is made, however, the faster handbook descent requires 57 kg (125 lb) more overall fuel. This includes the estimated 84 kg (184 lb) required to maintain cruise at 0.8 Mach for 10 n.mi. Thus, this faster descent consumes about 20% more fuel, overall, than the minimum fuel profile (although about the same mass of fuel is gained in using the minimum fuel descent as in using the minimum fuel climb.)

Table 7. Comparison of Steering Techniques on Cost Performance for Tri-jet Aircraft. 500 n.mi. Range 10 km (33000 ft) Cruise Altitude.

Profile Climb Descent	Handbook 250/340/.78 .80/340/250	Intermediate 250/300/.77 .71/255/250	Minimum Fuel
Fuel Used - kg (lb)			
Climb + Cruise	2345 (5169)	2216 + 83 = 2299 (4885) (182) (5067)	2176 + 117 = 2293 (4798) (257) (5055)
Descent + Cruise	246 + 84 = 330 (542) (184) (726)	274 (604)	273 (601)
Time - Sec (min:sec)			
Climb + Cruise	1308 (21:48)	1282 + 90 = 1372 (21:22) (1:30) (22:52)	1272 + 126 = 1398 (21:12) (2:06) (23:18)
Descent + Cruise	912 + 80 = 992 (15:12) (1:20) (16:32)	1124 (18:44)	1179 (19:39)
Range - n.mi.			
Climb + Cruise	147.396	136.469 + 10.927	132.058 + 15.338
Descent + Cruise	87.506 + 10.321	97.827	97.827

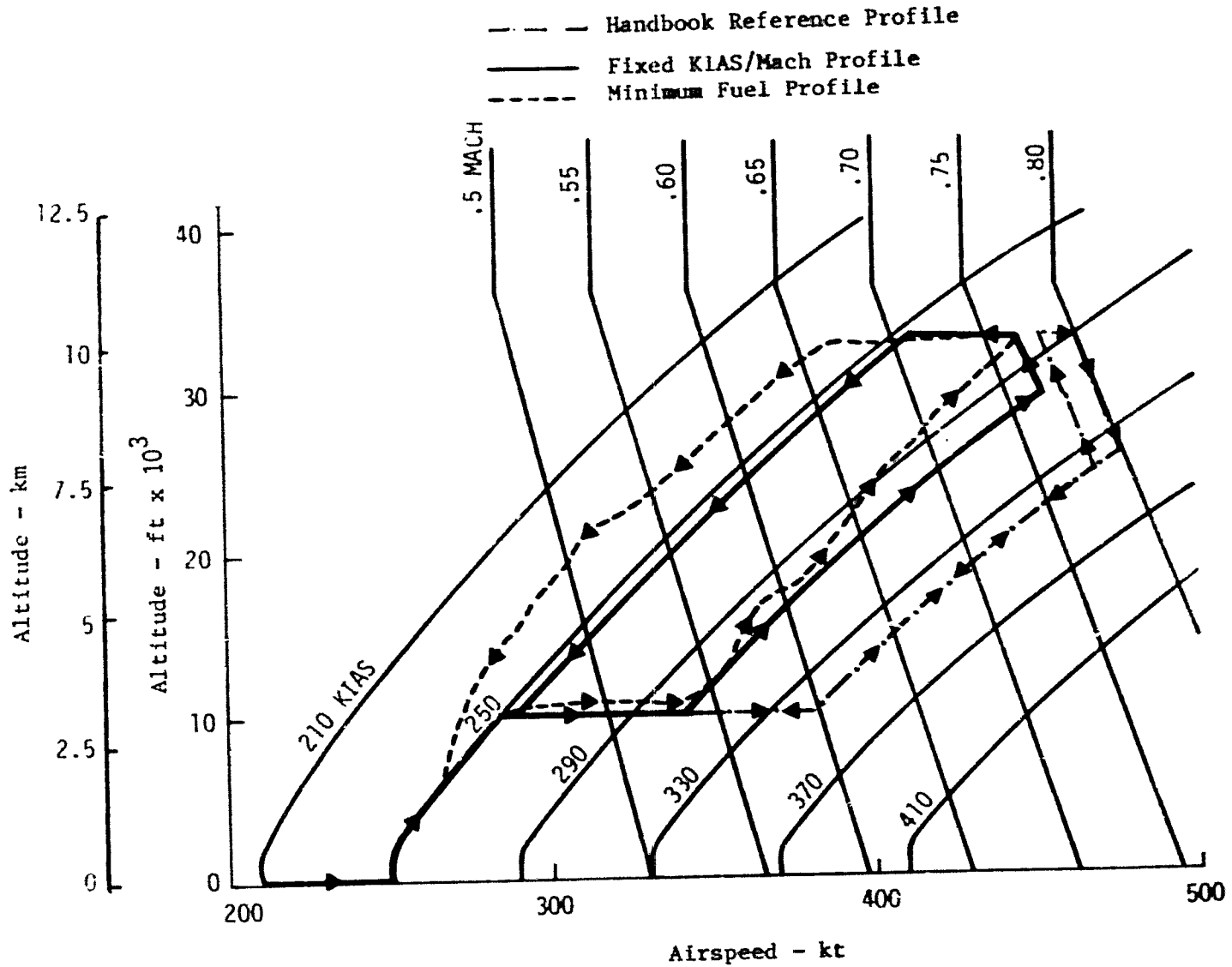

Figure 16. Comparison of Optimum and Handbook Reference Type Profiles

Other Profile Comparisons and Sensitivity Studies

Optimum Profile Characteristics In conducting the sensitivity analysis of the optimum profiles, there are two items that are of particular interest:

1). The establishment of how the characteristics of optimum profiles change with variations in initial mass, range-to-go, wind profiles, and other variables affecting the aircraft performance. Knowing these variations affects how an on-board algorithm should be constructed to account for measured changes in the flight conditions.

2). The analysis of the effect that errors in the assumed flight conditions (i.e., different initial mass, different wind profile) have on the cost of flying a particular profile. For example, if assuming the wrong initial mass of the aircraft has little effect on the overall cost, then the algorithm can be constructed so that initial mass is assumed to be a nominal value.

The purpose of this section is to begin to address these items for wind, initial mass, and range variations. Both OPTIM and TRAGEN are required for this purpose. Other variables that may have an effect are temperature, lift coefficient, drag coefficient, and thrust variations as well as measurement errors of altitude, flight path angle, airspeed (or Mach number), and range-to-go. These variations should be addressed at a future time.

It is assumed for climb that Mach number and flight path angle given as functions of altitude specify the optimum profile to a given cruise altitude. Thus, by presenting plots of these variables as functions of altitude, the effect of the variations to the nominal conditions is directly seen.

Figure 17 shows the variations in the climb profile as the total range is varied, in steps of 25 n.mi. from 75 n.mi. to 275 n.mi. for the tri-jet model. As can be seen, there is no variation below 3048 m (10000 ft). Above 3048 m (10000 ft), the flight path angle is initially higher and the climb Mach number is initially lower as the total range is increased. But it is seen that these curves are essentially parallel, and they merge into a common curve for range exceeding 175 n.mi. Thus, it would be relatively

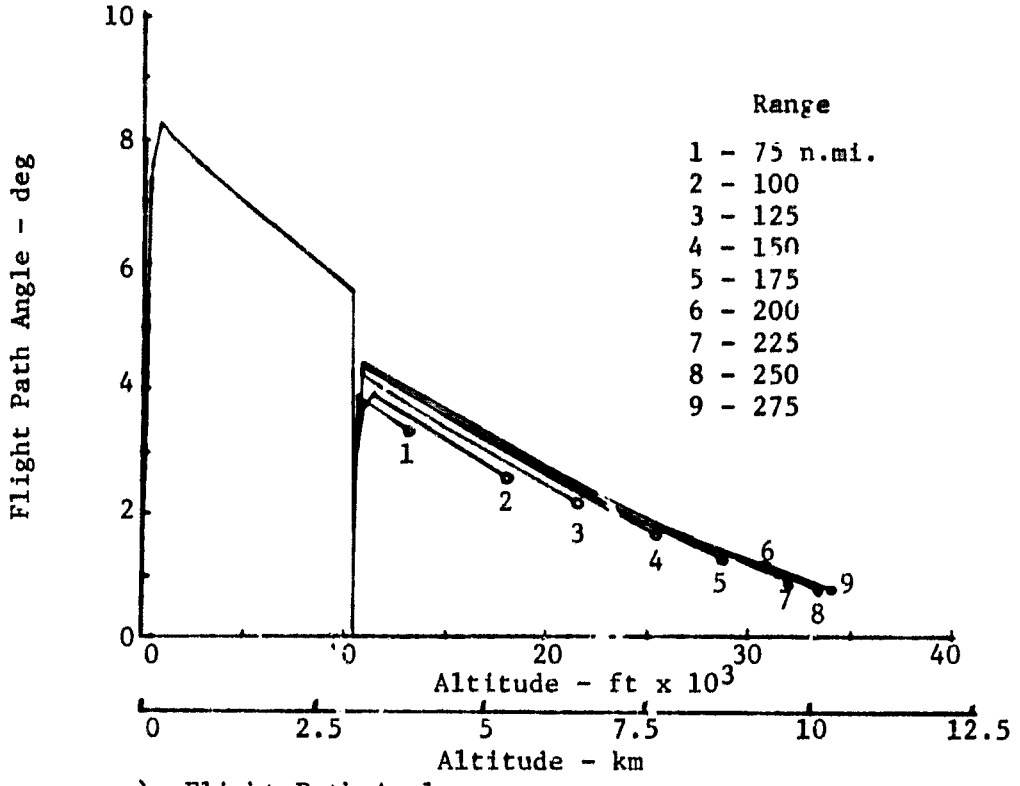

a) Flight Path Angle

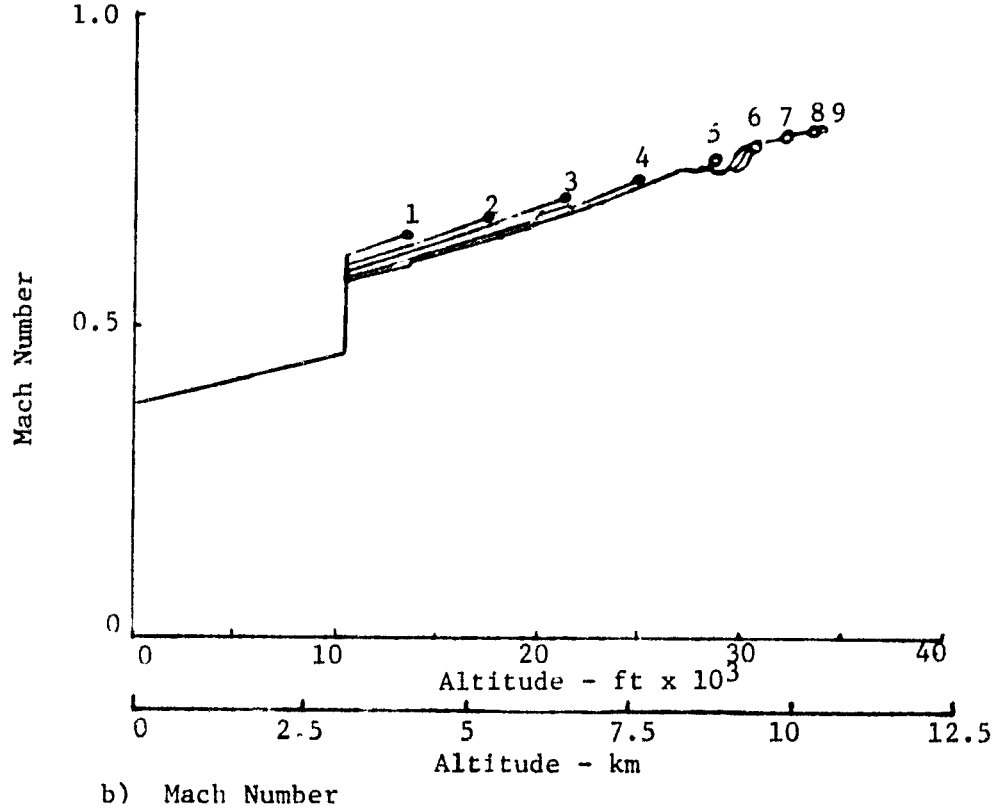

b) Mach Number

Figure 17. Effect of Range Variation on Optimum Climb Flight Path Angle and Mach Number

easy to model these curves as a polynominal function of altitude with parameter variation due to change in range.

Figure 18 shows the variation in the profile as initial mass is varied. Again, there appears to be a parallel offset with a greater effect on flight path angle. There is no effect on Mach number below 3048 m (10000 ft).) Also, again it can be seen that this variation would be easy to account for in specifying an on-board reference trajectory.

The biggest uncertainty that would be experienced during the climb and descent would be the variations in the longitudinal wind. To study this effect, the two wind profiles of Fig. 19 were used as program inputs. The Denver wind is the same as is shown in Fig. 7, but Fig. 19 also has the wind headings indicated at discrete points. The "triangle" wind is a constant 270^{o} heading wind varying linearly in magnitude with altitude at a rate of 1 knot per 305 m (1000 ft). These wind profiles were assumed to act as both tail and head winds by setting the aircraft heading to be 90^{o} or 270^{o}.

Figure 20 shows the effect of each of these wind profiles on the optimum climb trajectory compared to the nominal profile having no wind. As can be seen, the Mach number variation with altitude is essentially a parallel offset. The effect on flight path angle is mainly seen going from zero to 3048 m (10000 ft) where a fan out of $\pm 0.3^{o}$ is seen. Above 3048 m (10000 ft), the variation appears more as a steady offset. Thus, again it appears that accounting for various wind profiles can be done in the on-board system in a relatively simple way.

Figure 21 shows the effect of each of the wind profiles on the optimum descent from 10 km (33000 ft). There, the plots show altitude and Mach number as functions of range-to-go to the landing point. From the first plot, it is seen that wind causes a $\pm$ 10 n.mi. range variation in where the optimum descent should begin. This is predictable based on knowing how far the air mass moves due to the wind during the descent period. Also, there is up to a $\pm$ 0.05 variation in the optimum Mach number as a function of range-to-go. From the earlier results presented, it was shown that if

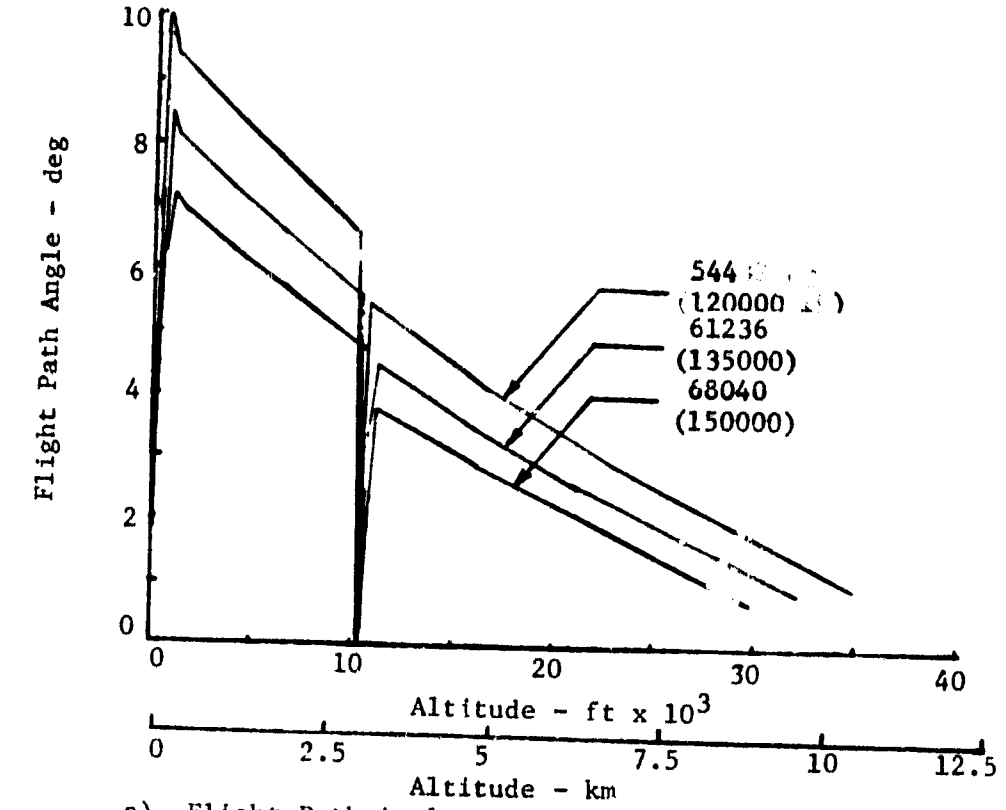

a) Flight Path Angle

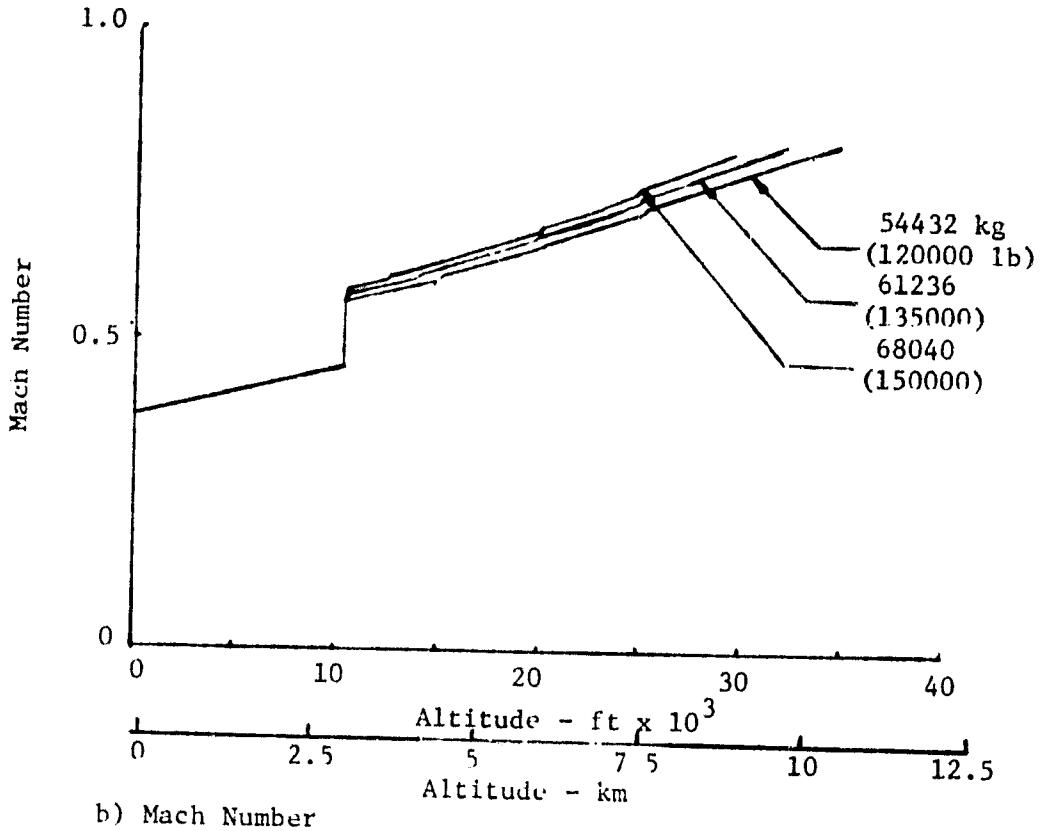

b) Mach Number

Figure 18. Effect of Initial Mass Variation on Optimum Climb Flight Path Angle and Mach Number

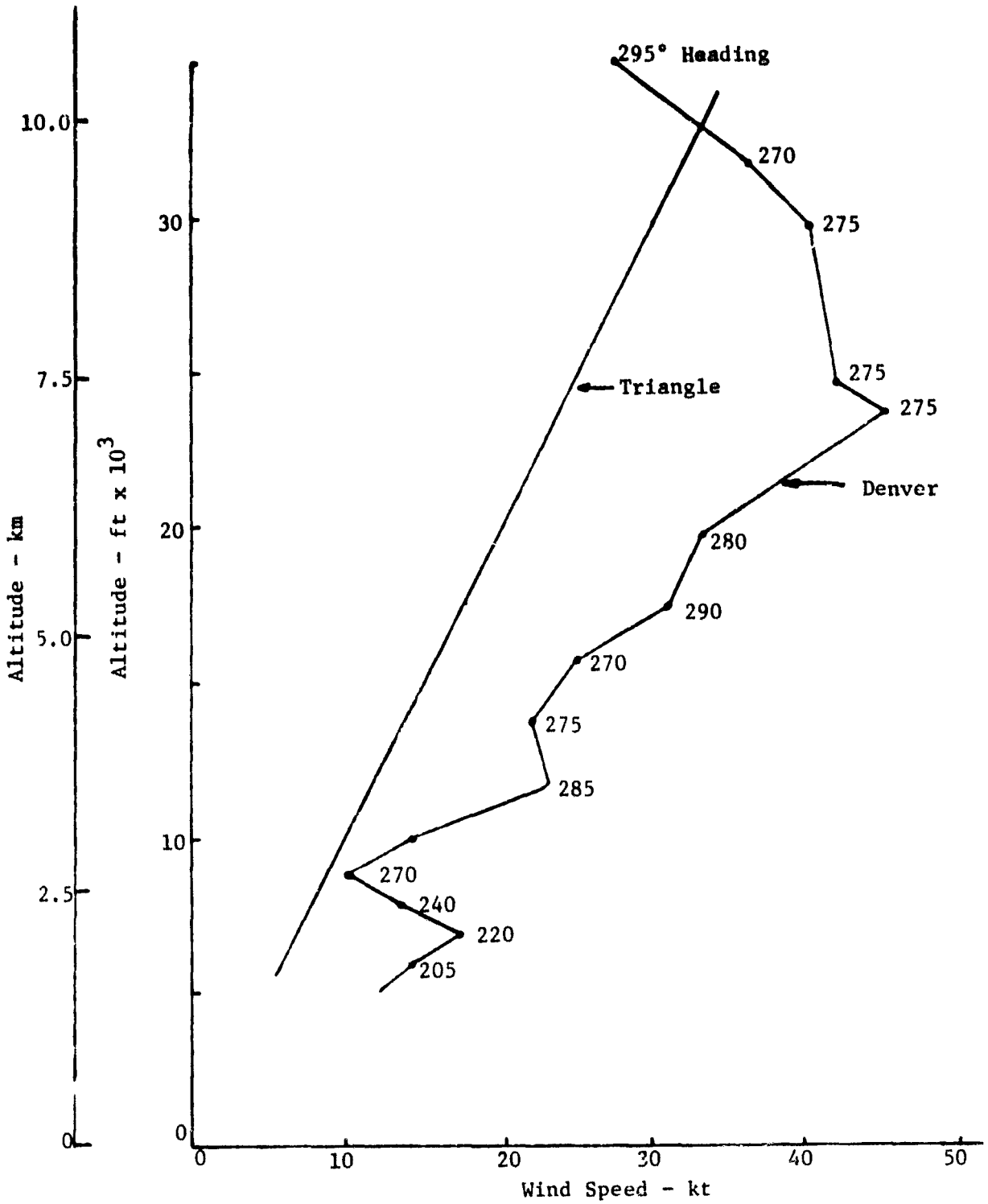

Figure 19. Wind Profiles Used to Study Sensitivity Effects on Optimum Profiles.

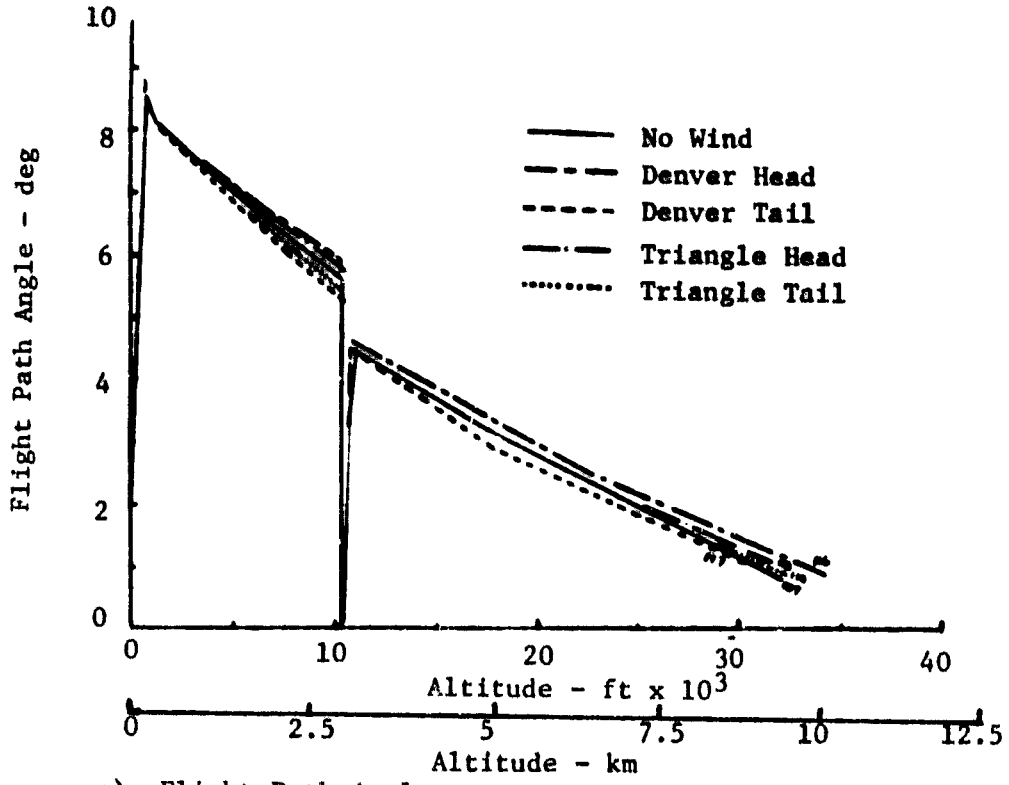

a) Flight Path Angle

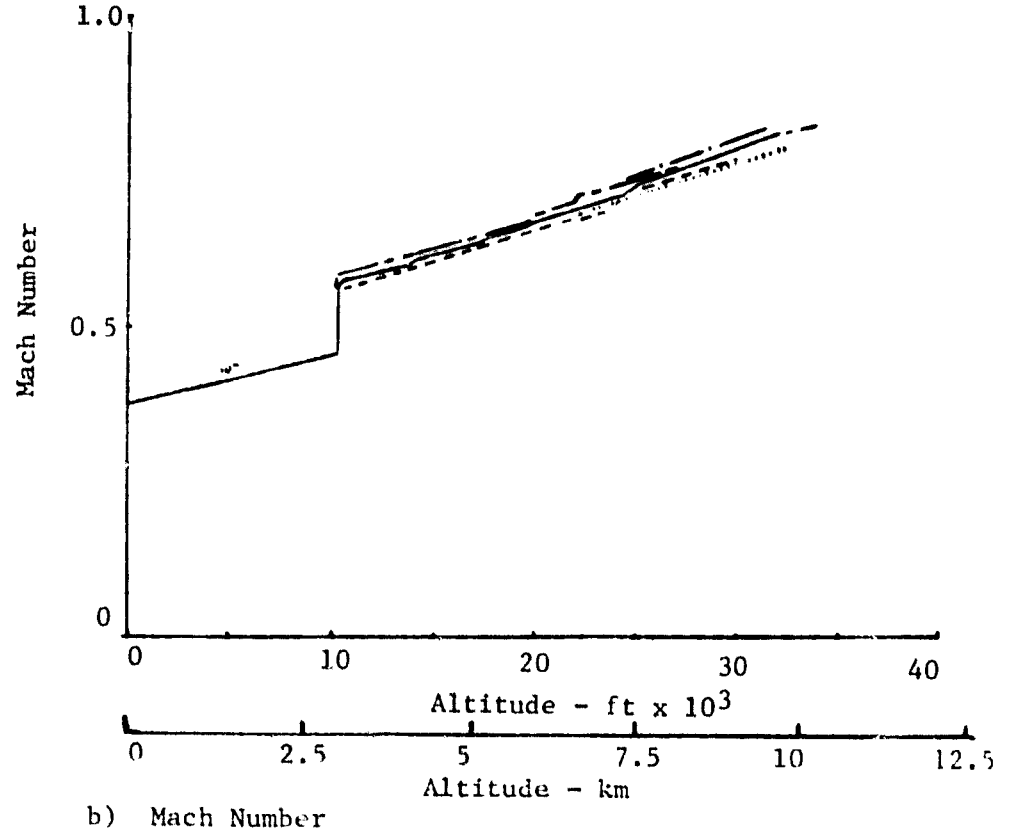

b) Mach Number

Figure 20. Effect of Wind Variations on Optimum Climb Flight Path Angle and Mach Number

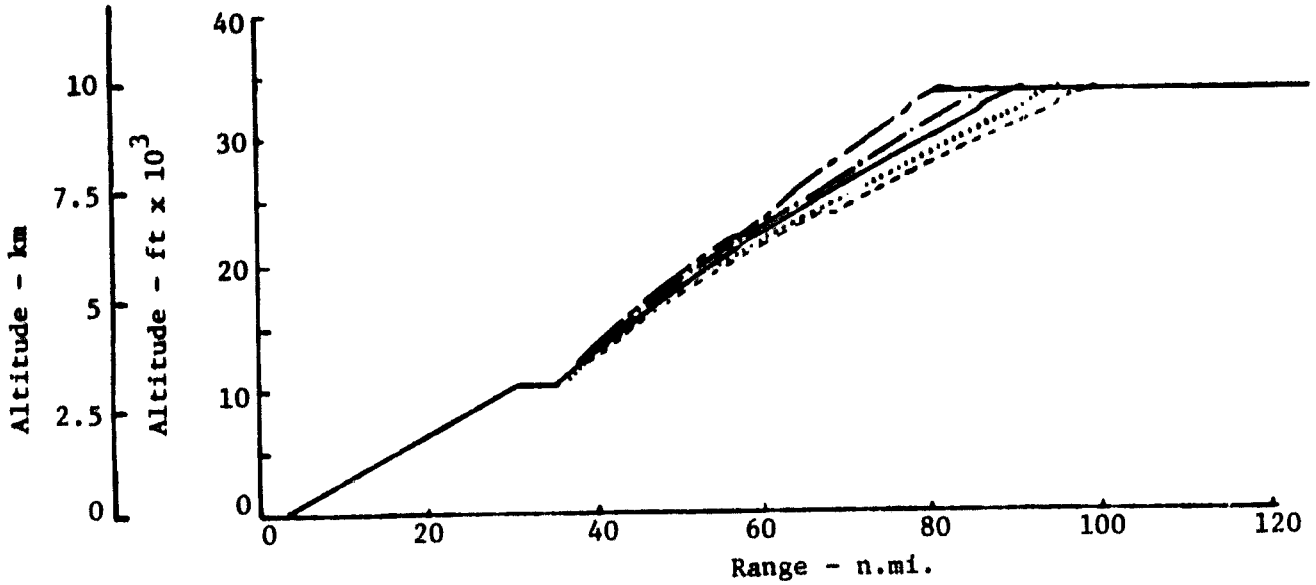

a) Altitude

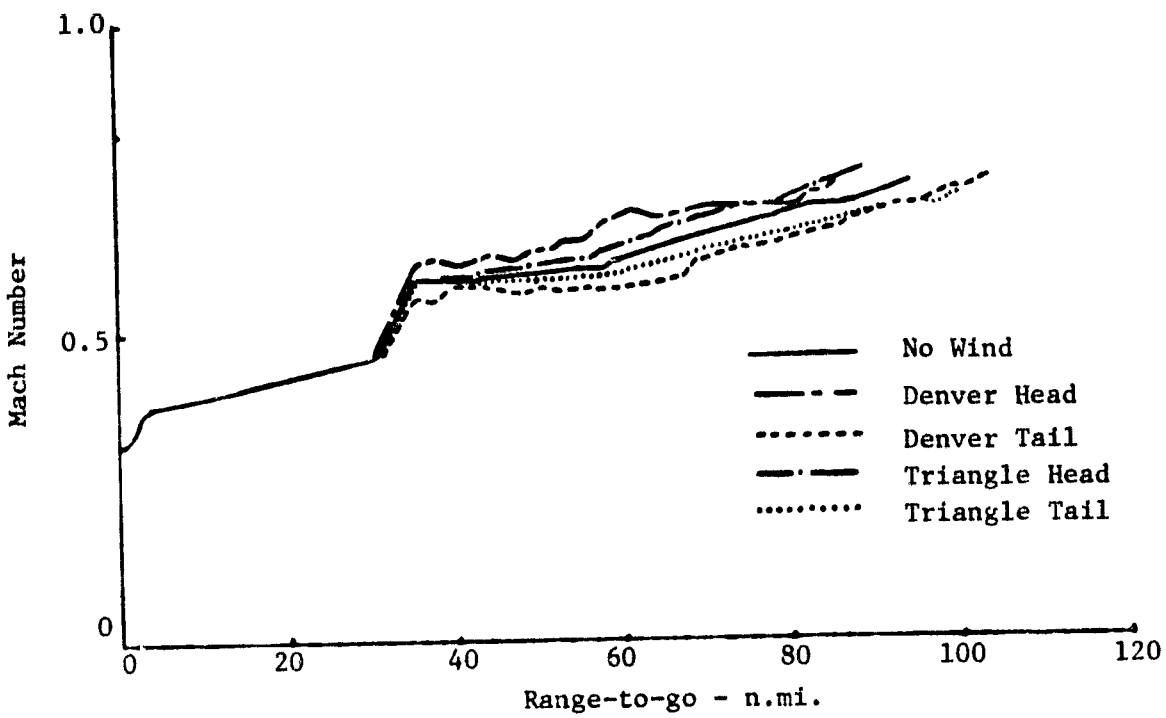

b) Mach Number

Figure 21. Effect of Wind Variations on Optimum Descent Altitude and Mach Number as Functions of Range-to-go.

the altitude-range profile was followed closely down to 3 km (10000 ft), the Mach number would probably follow the speed profile associated with the given altitude range profile. Thus, from an implementation point-of-view, the Mach variations seen above 3 km (10000 ft) in Fig. 21 are not of concern. Below 3 km (10000 ft), only one profile needs to be stored.

The results seen in Figs. 17-21 are limited in scope, in that all possible variations are not addressed. For example, the effects of variations in cruise mass and cruise altitude for the descent trajectories should be explored. However, the one thing that can be concluded is that variations of total range, initial mass, and wind profiles have predictable effects that can be easily used to modify the characterization of the nominal optimum trajectory. Thus, the process of computing the optimum climb-descent profiles does not have to take place on-board the aircraft. Instead, a nominal profile plus modifications to account for off-nominal parameter changes can be pre-computed and stored in the aircraft flight management system. This provides a very simple on-board method of computing the reference profile.

The second aspect of the sensitivity analysis was to study the effect of flying a non-optimal profile. This effort involved using TRAGEN to simulate following a given incorrect optimum profile when a different profile should have been used. Two error conditions were investigated:

a) Following an optimum profile specified for the incorrect initial mass

b) Following an optimum profile specified for the incorrect wind profile.

Only the climb phase was investigated.

For initial mass errors, four runs were made as shown in table 8. As can be expected, the increase in assumed initial mass causes a decrease in the optimum cruise altitude. Thus, if the aircraft is lighter than the assumed amount, it will climb faster to the lower altitude. This results in both time and fuel reduction from what was predicted to reach cruise. Cases 1a and 1d in Table 8 were of this nature, and they show a 13-14% reduction in fuel and a 14-16% reduction in climb time for an initial error of -6804 kg (-15000 lb) in initial mass.

Table 8. Initial Mass Error Cases Considered - Climb Profile

Run	Initial Mass - kg (lb)	Assumed Optimum Profile Mass - kg (lb)	Change in Climb Fuel kg (lb)-(%)	Change in Climb Time Sec - (%)
1a	61236 (135000)	68040 (150000)	-274 (-604) (-13.1%)	-159 (-14.4%)
b	61236 (135000)	54432 (120000)	+329 (+726) (+18.7%)	223 (+22.9%)
c	68040 (150000)	61236 (135000)	371 (+817) (+19.2%)	247 (+23.3%)
d	54432 (120000)	61236 (135000)	269 (-592) (-13.9%)	-167 (-15.8%)

On the other hand, if the initial mass is assumed too small, the heavier aircraft will attempt to climb to a higher than nominal altitude. Cases 1b and 1c of Table 8 show this condition for an initial mass error of +6804 kg (+15000 lb). The result was a 19% increase in required climb fuel and a 23% increase in required climb time. It was also seen that the aircraft did not achieve the required cruise airspeeds when the incorrect optimum input altitude was reached. Climb fuel estimation accuracy is important for choosing the optimum cruise conditions.

Based on the results of Table 8, it is seen that the initial mass is an important parameter to be entered into the computations. It is better to assume too large an initial mass than vice versa.

For the climb wind profile errors, four more cases were studied where optimum climb profiles based on the triangle wind profile of Fig. 19 were used. The results are shown in Table 9. As can be seen, if the tail wind is greater than assumed (Cases 2a and 2d), more time and possibly more fuel are required to achieve cruise conditions. Likewise, if the head wind is greater than assumed (Cases 2b and 2c), less time and possibly less fuel are required, although the results are mixed. It is seen that neglecting the wind profile can vary fuel cost up to $\pm$ 1.5%.

Table 9. Wind Profile Error Cases Considered - Climb Profile

Run	Actual Wind Profile	Assumed Profile for Computing Optimum	Change in Climb Fuel kg (lb) - (%)	Change in Climb Time Sec - (%)
2a	No Wind	Head	-1 (-2) (-.05%)	+7 (+0.7%)
b	No Wind	Tail	+11 (+24) (+0.6%)	-3 (-0.3%)
c	Head	No Wind	-27 (-60) (-1.4%)	-15 (-1.4%)
d	Tail	No Wind	+29 (+64) (+1.5%)	+18 (+1.7%)

These type of sensitivity studies are important because they produce information necessary for the implementation process. Computing the optimum profile with the wrong aircraft or environment models can cause a large percentage of the expected gain from the flight management system to not be realized.

Many more sensitivity cases than those described above need to be obtained for determining the sensor and measurement processing requirements associated with implementation of an optimum vertical flight management system. However, with the availability of the OPTIM and TRAGEN programs, the user is in a position to obtain these results.

Benefit of Free Cruise Altitude OPTIM was used to generate optimum profiles where the cruise altitude was both free and fixed. Figure 22 shows a comparison of twin-jet aircraft profiles where altitude is fixed at 10 km (33000 ft) and free. The initial mass of the aircraft is 40.78 tonne (90,000 lb). Range traveled is 750 n.mi. As can be seen, the climb and descent profiles for both cases are equivalent. The free-cruise altitude case begins cruise sooner (~ 32000 ft) and climbs during cruise to about 11.4 km (37500 ft).

Table 10 presents a cost comparison of the two profiles shown in Fig. 22. As can be seen, the free-cruise altitude profile takes 70 sec longer to complete, but it requires 154 kg (339 lb) less fuel than the fixed-cruise altitude case. (This is a reduction of 3.9%). These results were also based on generating optimum profiles using cost of fuel C_f of \$0.33/kg (\$0.15/lb) and cost of time C_t of \$600./hr. With these cost figures, the direct operating cost reduction of using the climb cruise is \$29.20 (or 1.37%) for this flight.

The fixed cruise results could have been improved perhaps, by selecting a fixed cruise altitude of some value other than 10 km (33000 ft). However, the pilot is not usually given that freedom. Another improvement could have been realized by allowing a step climb in the cruise segment of the fixed-cruise altitude case - e.g., from 10 km (33000 ft) to 11.28 km (37000 ft). An interesting and valuable addition to OPTIM would be to include the step climb option.

Benefit of Constraining Time-of-Arrival To understand the reasons why fixed time-of-arrival flight path control would be beneficial, we restate three assumptions made in Chapter I concerning the future scenario of commercial aviation:

1. Because of the increasing cost and scarcity of jet fuel, aircraft will soon be nominally flying along minimum fuel vertical flight paths.

2. Because of increasing demand for air travel, increasing congestion and delays of variable length will be occuring at the major terminal areas.

3. Because of increasing capabilities being developed and implemented in communication and computer technology, the ATC system will be able to anticipate terminal area delay times. The controller will be able to inform the pilot early in the flight what the expected delay will be, and he will be able to assign the pilot an open time slot (time-of-arrival) at the terminal feeder fix or outer marker.

If these assumptions hold, the pilot will have a choice of two strategies to follow to take a fixed delay into account:

Table 10. Cost Comparison for Fixed and Free Altitude Profiles

Range = 750 n.mi. Twin-Jet Aircraft W_o = 40.78 tonne (90000 lb)

C_f = \$0.33/kg (\$0.15/lb) C_t = \$600.00/hr. h_c = 10 km (33000 ft)

Quantity	Climb	Cruise	Descent	Total
Fuel - kg (lb)				
Fixed	1099 (2426)	2740 (6049)	167 (368)	4006 (8843)
Free	1091 (2409)	2580 (5695)	181 (399)	3852 (8504)
Distance - n.mi.				
Fixed	85.6	577.5	86.9	750.0
Free	84.6	566.1	99.4	750.0
Time - hr:m:s				
Fixed	13:39	1:20:27	15:32	1:49:39
Free	13:31	1:20:01	17:16	1:50:49
Cost - \$				
Fixed	427.73	1530.53	199.61	2157.86
Free	424.37	1483.67	220.63	2128.66

1. Continue to fly his nominal minimum fuel path and then enter a "minimum fuel flow" holding pattern to absorb the delay at the end of the cruise segment, or

2. Regulate his flight path by slowing down so that he arrives at the terminal area within an acceptable tolerance of the assigned time-of-arrival.

The algorithm developed in this study generates the optimum vertical flight path between a city pair which minimizes fuel and meets the delayed time-of-arrival constraint (Option 2 above). The fuel reduction of using this strategy is now compared to that of Option 1 as a function of the delay time.

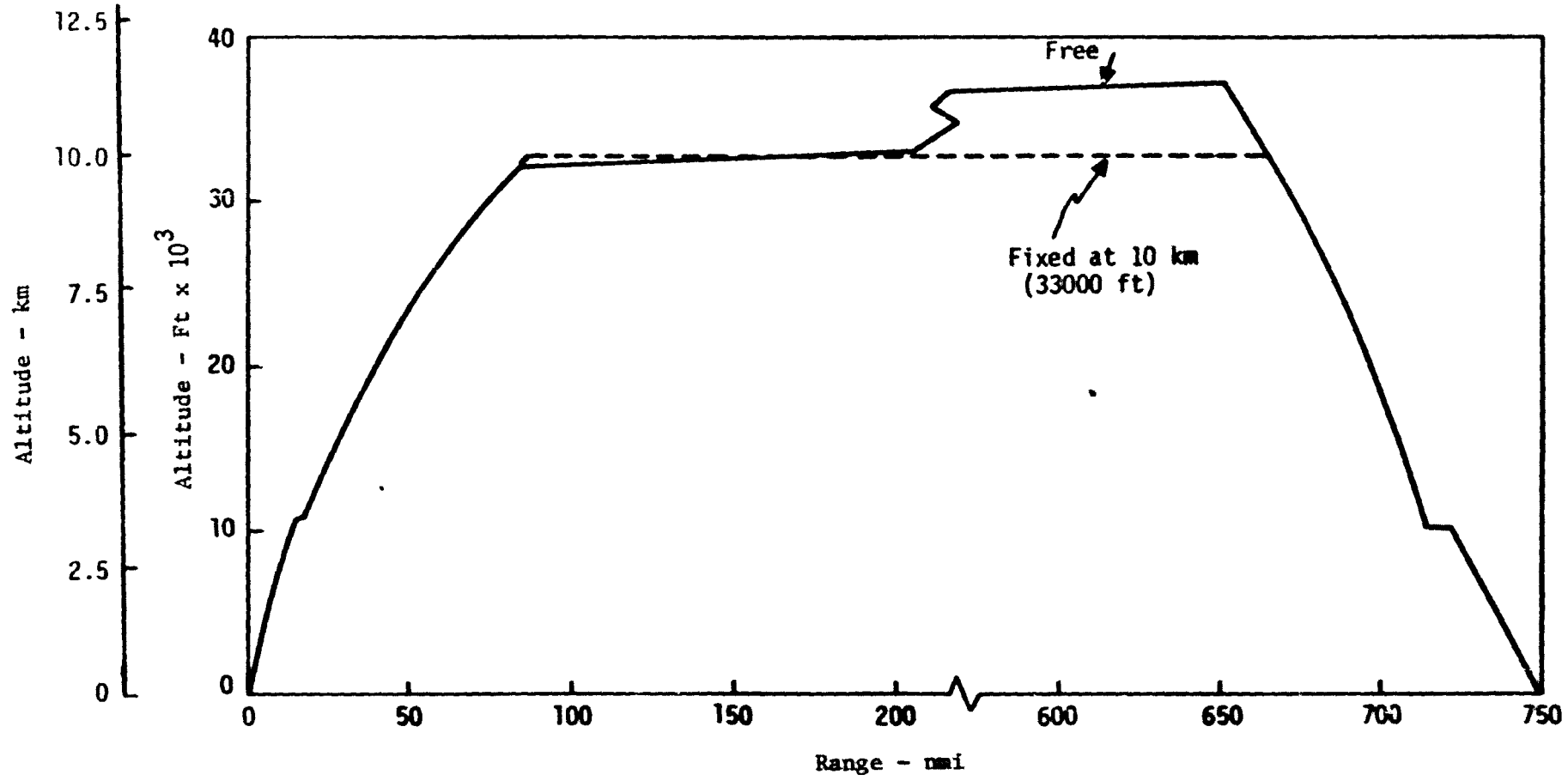

Figure 22. Comparison of Free and Fixed Cruise Altitude Profiles for the Twin-jet Aircraft.

The method used to generate a profile that follows the strategy of Option 1 can be described with the sketch shown in Fig. 23. It is assumed that the profile follows the segments between the sequence of points shown in Fig. 23. The segments followed are:

1-2: Climb along a minimum fuel segment.

2-3: Maintain a minimum fuel cruise segment to the point where descent would normally begin.

3-4: Continue at cruise altitude and airspeed until the range where the minimum fuel flow airspeed is obtained during the nominal descent.

4-5: Decelerate to the minimum fuel flow airspeed while maintaining cruise altitude. This begins the holding pattern.

5-6: Remain in the holding pattern at cruise altitude and minimum fuel flow airspeed to absorb the fixed delay time period.

6-7: Continue with minimum fuel descent.

The fuel burned during each of these segments can be obtained from the OPTIM program normal printout. This profile is optimistic in that it assumes that the aircraft leaves the holding pattern (at cruise altitude and minimum fuel flow) with no discontinuity with the optimum descent profile.

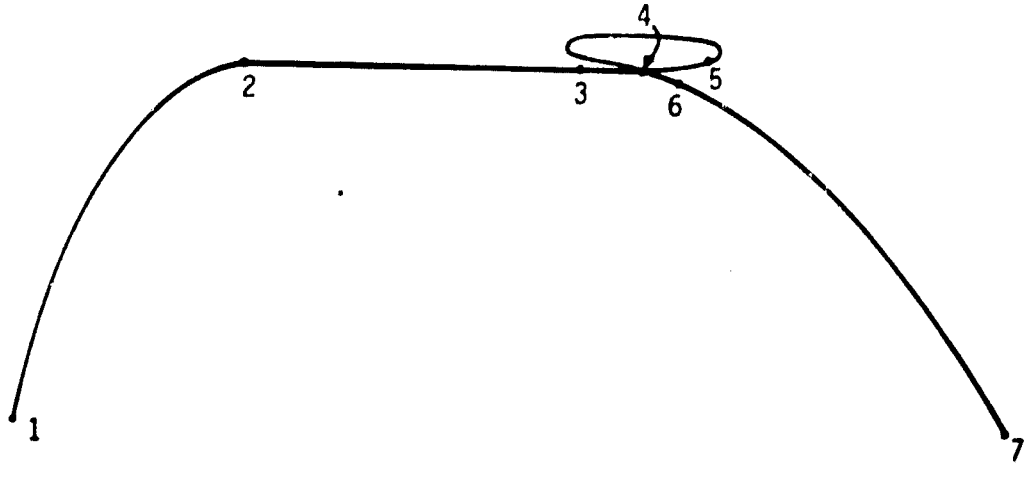

Figure 23. Sketch of Profile with Holding Pattern (Option 1).

Figures 24 and 25 show the amount and percent of fuel saved using Option 2 instead of Option 1. The independent variable is the arrival time delays for the medium range tri-jet aircraft with mass of 68275 kg (150,000 lb) at takeoff. The range traveled is the other variable parameter in these (29 min 10 sec), about 660 kg (1450 lb) of fuel can be potentially saved. Approximately 225 kg (500 lb) of fuel can be saved for anticipated 5 minute delay, independent of range.

Figure 25 shows the percentage of fuel saved for the cases shown in Fig. 24. Up to 6% of the fuel used by Option 1 can be saved with this controlled time-of-arrival capability. The values shown in Fig. 25 are computed by dividing the reduced fuel amount by that used for controlled time-of-arrival (Option 2).

The results just presented are conservative in the sense that the holding pattern assumed to obtain the Option 1 results is ideal. Usually, holding patterns are made at lower than cruise altitudes. The results are optimistic in the sense that for Option 2, it is assumed that the pilot is informed of the upcoming time delay right after takeoff. Thus, further study is necessary to model a more accurate representation of the holding pattern and to consider the cases where the pilot is informed of the delay somewhere during the cruise segment of flight. However, the potential savings are clearly indicated.

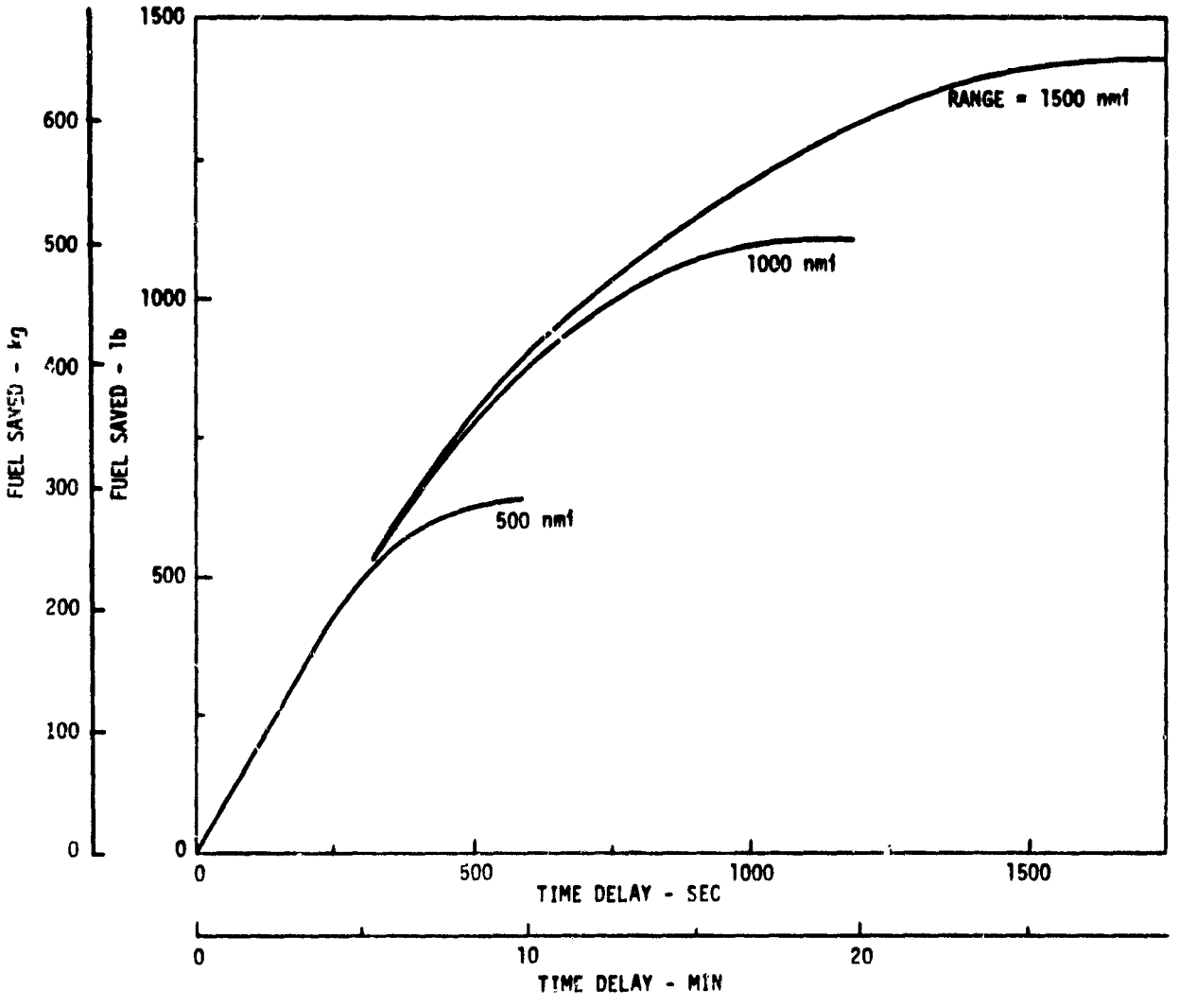

Figure 24. Fuel Saved Using Option 2 as a Function of Time Delay and Range.

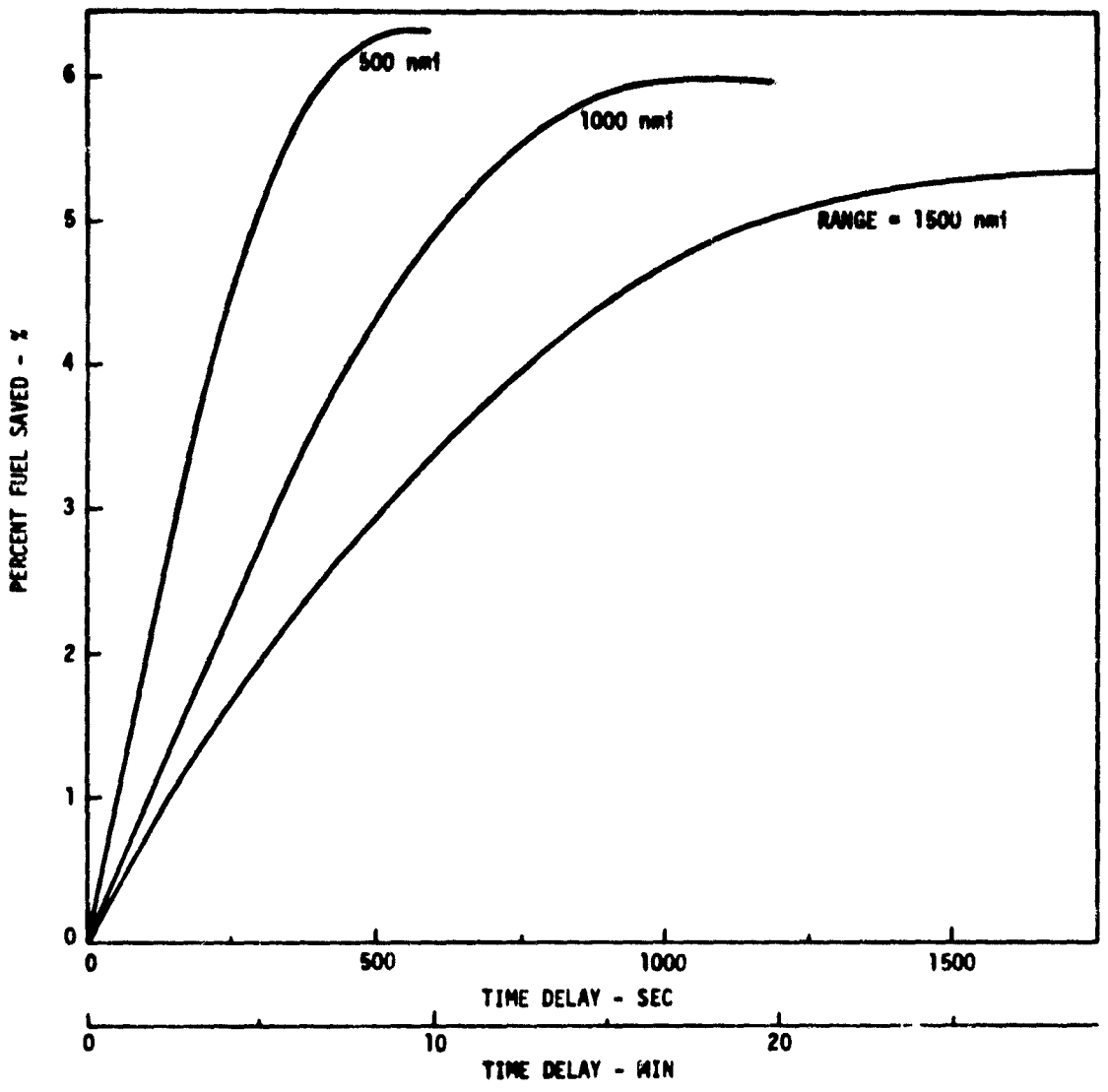

Figure 25. Percentage Fuel Saved Using Option 2 as a Function of Time Delay and Range.

IV

SUMMARY, CONCLUSIONS, AND RECOMMENDATIONS

Summary and Conclusions

All evidence indicates that we are rapidly consuming our supply of hydrocarbon fuels. This makes it mandatory that systems be developed that allow conservation of the remaining supplies until alternate fuels can be developed. This is especially true of aircraft flight which currently has no alternatives. This report addresses the development of on-board algorithms for vertical steering of the aircraft to minimize fuel consumption and cost.

Chapter II derives an algorithm for computing the optimum vertical profile using range as the independent variable. Both fuel and time are penalized, and the longitudinal wind effects are taken into account. The Hamiltonian is constant for this mechanization, and it is equal to the minimum cruise cost per unit distance traveled. To obtain optimum climb and descent profiles involves minimizing a single function at discrete points along the trajectory by proper choice of thrust and airspeed. This algorithm proved to be a dual to the one derived by Erzberger where energy was used as the independent variable. A computer program (called OPTIM, described in Appendix A) was used to obtain the optimum vertical profiles for typical medium range transport aircraft flights based on these algorithms.

Chapter II also presents a method of generating a minimum fuel flight path when the time-of-arrival (or length of flight is fixed. A convergence problem sometimes occurs when using this option because aerodynamic and propulsion data are stored in tabular forms rather than as continuous functions in the programs.

In Chapter III, the accuracy of the vertical profiles obtained from OPTIM are examined by using a more complete longitudinal model of the aircraft. This model was incorporated into a computer program called

TRAGEN (described in Appendix E) which steers the aircraft to follow an input or computed reference trajectory. Results show that the OPTIM reference trajectories are both flyable and accurate in terms of fuel burned and time expended.

Chapter III also presents the changes in characteristics of optimum reference trajectories due to changes in range, initial mass, and wind profile for a typical transport aircraft. It is concluded that these changes are simple modifications to the nominal reference profiles; they could be used to compute perturbations to a nominal profile on-board without recomputing the entire reference profile.

Chapter III also examines the effects of errors in the estimated values of initial mass and the wind profile on the performance obtained during climb. A 9% increase in initial mass (6804 kg (15000 lb)) can cause a 23% increase in time and a 19% increase in fuel required to achieve the desired cruise conditions. Wind errors have a smaller effect. These sensitivity studies are useful for specifying how accurately various parameters which affect the flight performance need to be measured.

Chapter III also illustrates further utility of the OPTIM and TRAGEN program capabilities. Results are given which:

a). Compare the fuel and time costs of a typical optimum profile flight where the cruise altitude is constrained to 10 km or is free. The range was 750 n.mi., and a twin-jet transport model was used. The path with the fixed cruise altitude constraint required 154 kg (339 lb) more fuel which is 3.9% of the total fuel burned.

b). Investigate the benefits of having fixed time-of-arrival guidance capability on-board the aircraft. The fuel that could be saved by using this capability to absorb delays rather than using holding patterns was computed for delays of up to 30 min and ranges of 500, 1000, and 1500 n.mi. About 225 kg (500 lb) of fuel could be saved for a 5 min delay of a tri-jet aircraft (regardless of range) using the fixed time-of-arrival option. Fuel saved could be as high as 6% of the total fuel used.

c). Compare handbook reference and optimum profiles. It was shown that an optimum climb for a tri-jet aircraft would use 169 kg (371 lb) less fuel (7.8%) than the handbook reference climb profile. However, after making adjustments for equal range traveled, this savings was reduced to 52 kg (115 lb) less fuel (2.3%). An optimum descent requires 57 kg (124 lb) less fuel than a faster handbook descent profile.

Many more interesting studies can be conducted with these complementary computer programs.

Recommendations

Based on the experience obtained by review of previous work, development of the OPTIM and TRAGEN program capabilities, and conversations held with many government and industry personnel associated with research and design in the air transportation and air traffic control fields, the following recommendations are made concerning immediate future work.

The following extensions to the OPTIM and TRAGEN programs would provide the capability to obtain more realistic reference flight paths, correct known minor program errors, and add capabilities which would be useful for obtaining improved solutions for other phases of flight:

a) Modeling of lift and drag

The aerodynamic data used to model the aircraft lift and drag in OPTIM and TRAGEN are quite complete. However, in the course of the study it was found that great care had to be taken in obtaining lift and drag coefficients from table look-up routines. This was particularly true for drag; the drag coefficient is currently given as a function of the lift coefficient and Mach number. From a cross plot of C_D against Mach number for a given C_L, a highly non-linear result occurs in the region of typical cruise points (e.g., M = .78 and C_L = .35). Thus, tables which interpolate linearly between the lines of constant Mach number will create ridges or kinks in the data which can have an adverse effect on the determination of the optimum cruise Mach number in the OPTIM program. The kinks produce discontinuities in attempting to converge on time-of-arrival. One solution would be to use curve fitting techniques to insure that the drag coefficient is always a continuous function of both C_L and Mach number. This also requires that the aerodynamic data be carefully checked to adjust any data points causing kinks to occur.

b). Modeling of propulsion data

The propulsion data used to model the turbofan engine for the twin-jet aircraft is strictly "uninstalled" data. For establishing trends and for making relative comparison, these data are sufficient. However, if one wishes to model a given aircraft more exactly and to predict absolute results, installation losses must be included in the model. The losses include inlet pressure recovery losses, exhaust nozzle losses and bleed and power extraction. The following table gives data for one particular engine model to illustrate the point.

Table 11. Example of Unmodeled Propulsion Losses

Mach Number = 0.78
Altitude = 9.144 km (30000 ft)
Standard Day
Reference Thrust = 18593 N (4180 lb) (uninstalled data)
Reference SFC = 0.773

Item	Thrust Change - $\frac{\Delta F_N}{F_N}$	SFC Change - $\frac{\Delta SFC}{SFC}$
Nozzle Gross Thrust Coefficient	-.0008	+.0004
Inlet Pressure Recovery	-.0041	+.0015
Bleed and Power Extraction	-.0462	+.0295
Total	-.0511	+.0314
∴ Installed Thrust = 17641 N (3966 lb)		
Installed SFC = 0.797		

These changes are nontrivial and should be considered when modeling an actual system. At idle conditions, the effects are even more pronounced for the bleed and power estraction because of the low level of thrust. It is recommended that these installation effects be modeled and that the results be compared with those of the present study to establish quantitatively the installation effects.

c). Correction of the time-of-arrival convergence problem.

Currently, because most of the aerodynamic and engine characteristics are obtained (for both aircraft models) from tables using linear interpolation, there are kinks in the data. This causes convergence problems when the time-of-arrival is constrained. Steps to correct this problem would be to

a). Convert aero and engine data to continuous functions so that interpolation can be eliminated, as discussed above,

b). Ensure that there are no double minimums in the cruise cost at a particular altitude,

c). Replace or improve the optimization routine, and

d). Check out OPTIM with the modifications.

This correction is vital to smooth running of the algorithm onboard an aircraft.

d). Optimum cruise - step change in altitude.

Currently, OPTIM is based on optimum cruise climbs. This added option would be an extension to using fixed cruise altitudes. OPTIM would determine where to change altitudes in a step fashion as fuel is burned off during cruise.

e). Extend TRAGEN to simulate the entire flight path.

Currently, TRAGEN can be used to simulate either the climb or the descent profile. This addition would add logic so that cruise (constant altitude, step climb or cruise climb) could be simulated along with a three-segment climb-cruise-descent profile.

f). Takeoff performance modeling.

Currently, OPTIM begins flight path optimization calculations at an arbitrarily selected speed and altitude which is designated as the beginning of climb. If this program is to be used as a flight planning tool, some allowance must be made for the time, fuel burned and altitude attained during the takeoff phase. This phase includes the ground roll, rotation and climb during flap retraction. The takeoff performance should be studied to develop sufficient parametric data to be able to predict the velocity and altitude at the beginning of climb and the fuel burned during the takeoff. Both the ambient temperature profile and airport altitude must be taken into account.

g). Descent performance modeling.

Currently, OPTIM computes the descent portion of the trajectory with the engines usually at a flight idle power setting. In doing so, two potential constraints are ignored - the rate of increase in cabin pressure and the maximum allowable fuselage angle. Both factors are important for a commercial transport aircraft. The descent trajectory for both aircraft should be studied to determine if these constraints are significant in relation to the overall flight path optimization methodology used in OPTIM. If these constraints do prove to be significant, it is necessary to include these effects in both OPTIM and TRAGEN. In addition, the fuel, time, range, and altitude covered during the final descent phase with flaps and landing gear deployed need to be determined. These effects would also be included in the OPTIM and TRAGEN programs.

h). Cruise control to account for wind and temperature

Currently, OPTIM uses a single wind profile which specifies magnitude and direction as a function of altitude. This profile is used to compute the optimum climb, cruise, and descent portions of flight. There is an eventual need to develop variable profile models of the wind and temperature as functions of both

altitude and horizontal position. Then, by using these models, the optimization techniques need to be modified to account for the modeled wind and temperature variations. This is especially important for the cruise phase of flight which may cover a large range over which the wind changes may be considerable.

APPENDIX A

TRAJECTORY OPTIMIZATION USING THE ENERGY STATE METHOD

The purpose of this Appendix is to summarize briefly the theoretical background used for optimization of trajectories. These principles form the basis of the numerical process used for computing the optimum vertical profile of a jet aircraft. More details are given in Refs. 17, 21, and 25. Reference 25 derives the principles upon which trajectory optimization is based. In Refs. 17 and 21, Erzberger and Lee apply these principles using the energy state approximation to obtain a practical, efficient means of generating the optimum vertical profile.

OPTIM is an extension of the original computer code developed by Erzberger and Lee that encompasses these principles and is based on their methods. The latter part of this appendix describes how OPTIM is organized.

In the following sections, the theory of trajectory optimization is first presented. Then, the application of this theory to minimizing the direct operating cost (DOC) of an aircraft traveling over a fixed range is outlined. This is followed by a discussion of the details of going from theoretical expressions to a practical computer code. The theoretical points are presented without proof, for conciseness. The reader wanting more detail should review the references.

Theoretical Principles

In Ref. 25., a description is given of the requirements for solving an optimization problem involving a continuous dynamic system with no terminal constraints but with fixed terminal time. This description is repeated here because it presents the basic principles which extend to the aircraft profile optimization problem.

A system (the aircraft) is governed by the nonlinear differential equations

$$\dot{x} = f(x,u,t) \quad ; \qquad x(t_o) \text{ given}; \qquad t_o \leq t \leq t_f \; ; \tag{A.1}$$

where x is the n-dimensional state vector and u is the m-dimensional control vector. The cost function which is to be minimized is of the form

$$J = \phi(x(t_f),t_f) + \int_{t_o}^{t_f} L(x,u,t)\, dt. \tag{A.2}$$

Here, ϕ is the terminal cost function, and L is the cost per unit time along the trajectory. The problem is to find the sequence of controls u(t) that minimize J.

First, the system equations are adjoined to J with the multiplier vector $\lambda(t)$:

$$J = \phi(x(t_f),t_f) + \int_{t_o}^{t_f} \{L(x,u,t)+\lambda^T(t)\{f(x,u,t)-\dot{x}\}\}\, dt. \tag{A.3}$$

Then the Hamiltonian function is defined as

$$H(x,u,t) = L(x,u,t) + \lambda^T(t) f(x,u,t). \tag{A.4}$$

Equation (A.3) is integrated by parts to yield

$$J = \phi(x(t_f),t_f) - \lambda^T(t_f)\, x(t_f) + \lambda^T(t_o)\, x(t_o) + \int_{t_o}^{t_f} \{H(x,u,t) + \dot{\lambda}^T(t)\, x(t)\}\, dt. \tag{A.5}$$

Next, the change in J due to variations in u(t) and x(t) is considered for fixed t_o and t_f:

$$\delta J = \left\{ \left(\frac{\partial \phi}{\partial x} - \lambda^T \right) \delta x \right\}_{t=t_f} + (\lambda^T \delta x)_{t=t_o} \qquad (A.6)$$

$$+ \int_{t_o}^{t_f} \left\{ \left(\frac{\partial H}{\partial x} + \dot{\lambda}^T \right) \delta x + \frac{\partial H}{\partial u} \delta u \right\} dt.$$

The elements of $\lambda(t)$ are chosen to cause the coefficients of δx in Eq. (A.6) to vanish under the integral and at t_f:

$$\dot{\lambda}^T = -\frac{\partial H}{\partial x} = -\frac{\partial L}{\partial x} - \lambda^T \frac{\partial f}{\partial x} ; \qquad \lambda^T(t_f) = \frac{\partial \phi}{\partial x} . \qquad (A.7)$$

Equations (A.7) are called the co-state equations. Then, Eq. (A.6) becomes

$$\delta J = \lambda^T \delta x(t_o) + \int_{t_o}^{t_f} \frac{\partial H}{\partial u} \delta u \, dt. \qquad (A.8)$$

For J to be minimum, δJ must be zero for arbitrary $u(t)$; this implies that for no bounds on u,

$$\frac{\partial H}{\partial u} = 0 \qquad , \quad t_o \leq t \leq t_f \qquad (A.9)$$

on the optimum path. If the control variables are constrained as

$$C(u,t) \leq 0, \qquad (A.10)$$

then for $u(t)$ to be minimizing, we must have $\delta J \geq 0$ for all admissible $u(t)$. This implies, from Eq. (A.8) that

$$\frac{\partial H}{\partial u} \delta u \triangleq \delta H \geq 0, \qquad (A.11)$$

for all t and all admissible $\delta u(t)$. In other words, H must be minimized over the set of all possible u; this is known as the minimum principle [25].

In summary, to solve for $u(t)$ that minimizes J, the differential equations (A.1) and (A.7) must be solved simultaneously, where $u(t)$ is determined from Eqs. (A.9) or (A.11). The boundary conditions on the state x at t_o and λ at t_f are specified, resulting in a two-point boundary-value problem.

If L and f are not explicit functions of t, then

$$\dot{H} = \frac{\partial H}{\partial t} + \frac{\partial H}{\partial x}\dot{x} + \frac{\partial H}{\partial u}\dot{u} + \dot{\lambda}^T f, \tag{A.12}$$

$$= \frac{\partial H}{\partial t} + \frac{\partial H}{\partial u}\dot{u} + \left(\frac{\partial H}{\partial x} + \dot{\lambda}^T\right) f.$$

Each element of Eq. (A.12) is zero on the optimum trajectory, from which we can conclude that H is constant on the optimum trajectory. This latter point is used in the analysis presented in Chapter II.

Application to Aircraft Profile Optimization Using the Energy State Approximation

Here we are concerned with applying the above theory to the problem of choosing the thrust and airspeed values to control the aircraft vertical profile in going from one point to another. The cost function J is the direct operating cost (DOC) which is the sum of fuel and time costs. This is, in integral form,

$$J = \int_0^{t_f} (C_f \dot{w} + C_t)dt \triangleq \int_0^{t_f} C_d \, dt, \tag{A.13}$$

where C_f is the cost of fuel (\$/kg or \$/lb), $\dot{w}$ is fuel flow (kg/lb/nr), C_t is the cost of time (\$/hr), C_d is the direct operating cost, and t_f is the time to fly the specified distance traveled d_f. It is also assumed that the typical vertical profile is as shown in Fig. A.1 - that is, it contains climb, cruise, and descent portions which have the constraint that

$$d_{up} + d_{dn} \leq d_f \tag{A.14}$$

where

$d_{up} = x(t_{ci})$ = the distance traveled from the start point to where the cruise segment begins (at time $t = t_{ci}$).

$d_{dn} = d_f - x(t_{cf})$ = the distance traveled from the end of cruise (at time $t = t_{cf}$) to where the descent segment ends.

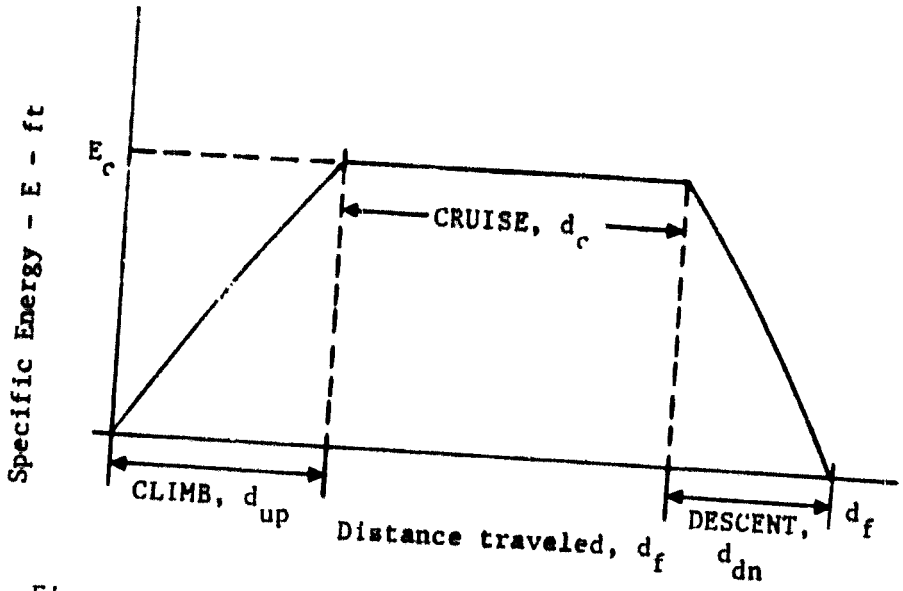

Figure A.1. Assumed Structure of Optimum Trajectories

Thus, the cost function (Eq. (A.13)) can be rewritten as

$$J = \int_0^{t_{ci}} C_d dt + (d_f - d_{up} - d_{dn})\psi + \int_{t_{cf}}^{t_f} C_d dt, \qquad (A.15)$$

$$= \int_0^{t_{ci}} C_d dt + (d_f - x(t_{ci}) - [d_f - x(t_{cf})])\psi + \int_{t_{cf}}^{t_f} C_d dt.$$

where ψ is the cost per unit distance while in cruise.

Simplified point-mass equations of longitudinal motion of the aircraft are

$$\begin{aligned} \dot{V}_c &= (T-D)/m - g \sin \gamma , \\ \dot{h} &= V_a \sin \gamma , \\ \dot{x} &= V_a \cos \gamma + V_w , \end{aligned} \qquad (A.16)$$

where the flight path angle (γ) dynamics and mass loss due to fuel burn are neglected. Here,

V_a = true airspeed,
h = altitude,
V_w = longitudinal component (tangent to earth's surface) of wind speed,
m = aircraft mass,
T = thrust,
D = drag.

Also, it is assumed that lift $L = mg \cos\gamma$. The effect of mass loss is accounted for by continuously updating mass without adding another state variable.

Specific energy E is defined as

$$E = h + V_a^2/2g \ , \tag{A.17}$$

which is the sum of potential and kinetic energy per unit mass. Its time derivative is found to be

$$\dot{E} = V_a (T-D)/mg \ . \tag{A.18}$$

The energy state approximation is based on the assumption that potential and kinetic energy can be interchanged instantaneously. In this approximation, the energy state variable replaces altitude and airspeed state variables [16]. Thus, Eq. (A.17) can be used in place of $\dot{V}_a$ and $\dot{h}$ in Eq. (A.16).

It is assumed that the aircraft specific energy increases monotonically during climb and decreases monotonically during descent. This assumption is used in the development to change the independent variable in Eq. (A.15) from time to energy. This uses the transformation

$$dt = \frac{dE}{\dot{E}} \ . \tag{A.19}$$

It is mathematically convenient to evaluate the last integral in Eq. (A.15) backwards in time so that the energy state is monotonically increasing during its evaluation. This means that the running distance (range) variable during the descent can be measured backwards from the end point. Thus, we can think of range measured in two ways as shown in Fig. A.2.

C-2

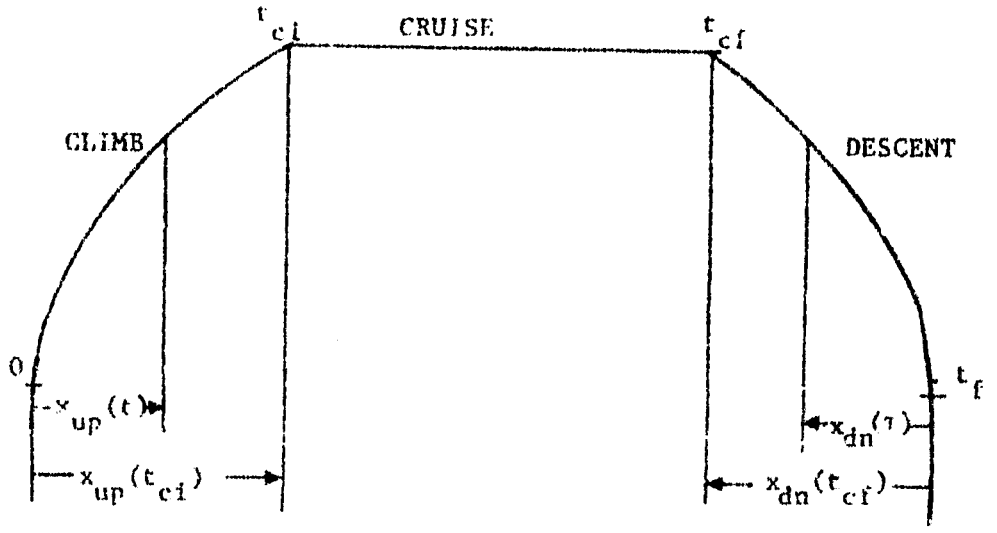

Figure A.2. Measurement of Range from the Origin or to the Destination.

In this sketch,

$x_{up}(t)$ = range measured on the way up in forward time t,

$x_{up}(t_{ci})$ = value of x_{up} when initial cruise is reached,

$x_{dn}(\tau)$ = range measured on the way up in backward time τ,

$x_{dn}(\tau_{cf})$ = value of x_{dn} when final cruise is reached ($\tau_{cf}=|t_{cf}-t_f|$).

Also, we define the variable x to be range traveled during climb and descent. The distance traveled during cruise is then constrained to be $(d_f - x)$. We can then see that an incremental change dx in the range variable x is equivalent to incremental changes in both x_{up} and x_{dn}. That is

$$dx = d(x_{up} + x_{dn}) . \tag{A.20}$$

From this discussion, the second of Eqs. (A.15) can be written as

$$J = \int_{0_i}^{t_{ci}} C_d dt + (d_f - x_{up}(t_{ci}) - x_{dn}(\tau_{cf}))\,\psi + \int_{0_f}^{\tau_{cf}} |C_d| d\tau . \tag{A.21}$$

We use Eq. (A.19) and the transformation

$$d\tau = \frac{dE}{|\dot{E}|} \tag{A.22}$$

to rewrite Eq. (A.15) as

$$J = \int_{E_i}^{E_{cf}} \left(\frac{C_d}{\dot{E}} \, dE \right)_{\dot{E}>0} + (d_f - (x_{up}(E_{ci}) + x_{dn}(E_{cf}))) + \int_{E_f}^{E_{cf}} \left(\frac{dE}{|\dot{E}|} \, dE \right)_{\dot{E}<0} \tag{A.23}$$

Here, E_i, E_{ci}, E_{cf}, and E_f are the values of specific energy evaluated at time t equal to 0 and t_{ci} and time t evaluated at t_{cf} and t_f respectively.

Note from Eq. (A.23) that the range variable x only appears as the sum of climb and descent distances ($x_{up} + x_{dn}$). Thus, the state equation for this system of equations can be written as

$$\frac{dx}{dE} = \frac{d(x_{up} + x_{dn})}{dE} = \left(\frac{(V_{up} + V_{wup})}{\dot{E}} \right)_{\dot{E}>0} + \left(\frac{(V_{dn} + V_{wdn})}{|\dot{E}|} \right)_{\dot{E}<0} \tag{A.24}$$

Here, V_{wup} and V_{wdn} are the longitudinal components of the wind speed for climb and descent. Then, analogous to Eq. (A.4), the Hamiltonian is

$$H = \left[\left(\frac{C_d}{\dot{E}} \right)_{\dot{E}>0} + \left(\frac{C_d}{|\dot{E}|} \right)_{\dot{E}<0} + \lambda \left\{ \left(\frac{(V_{up}+V_{wup})}{\dot{E}} \right)_{\dot{E}>0} + \left(\frac{(V_{dn}+V_{wdn})}{|\dot{E}|} \right)_{\dot{E}<0} \right\} \right] \tag{A.25}$$

This can be divided as

$$H = \left[\frac{C_d + \lambda (V_{up}+V_{wup})}{\dot{E}} \right]_{\dot{E}>0} + \left[\frac{C_d + \lambda (V_{dn}+V_{wdn})}{|\dot{E}|} \right]_{\dot{E}<0} \tag{A.26}$$

Now, analogous to Eq. (A.7), the costate equation for λ can be written as

$$\frac{\partial\lambda}{\partial E} = -\frac{\partial H}{\partial x} = -\frac{\partial H}{d(x_{up}+x_{dn})} = 0 \qquad (A.27)$$

and from Eqs. (A.7) and (A.23), this costate has the final value

$$\lambda(E_{ci}) = \lambda(E_{cf}) = \frac{\partial\phi}{\partial(x_{up}+x_{dn})} = \frac{\partial([d_f-x_{up}-x_{dn}]\psi)}{\partial(x_{up}+x_{dn})} = -\psi \qquad (A.28)$$

where ψ is the cruise cost per unit distance.

Note, this problem could be placed in a slightly more conventional form by dividing it into two problems - one for climb and one-half of the cruise distance and the other for decent and the other half of the cruise distance. Then Eqs. (A.27) and (A.28) would be replaced by

$$\frac{\partial\lambda}{\partial E} = -\frac{\partial H}{\partial x_{up}} = 0 \qquad (A.29)$$

$$\lambda(E_{ci}) = \frac{\partial([d_f/2 - x_{up}]\,\psi(E_{ci}))}{\partial x_{up}} = -\psi(E_{ci}),$$

for climb. For descend,

$$\frac{\partial\lambda}{\partial E} = -\frac{\partial H}{\partial x_{dn}} = 0 \qquad (A.30)$$

$$\lambda(E_{cf}) = \frac{\partial([d_f/2 - x_{dn}]\,\psi(E_{cf}))}{\partial x_{dn}} = -\psi(E_{cf})$$

This allows splitting the Hamiltonian defined in Eq. (A.26) and allows for $\psi(E_{ci}) \neq \psi(E_{cf})$. In fact, in the actual implementation $E_{ci} \neq E_{cf}$ because optimum cruise energy changes as fuel is burned off. The principal results are unchanged, however.

Thus, from Eq. (A.11), (A.29) and (A.30) the trajectory optimization problem becomes

$$H_{up} = \min_{\substack{V_{up} \\ \pi_{up}}} \left[\frac{C_d}{\dot{E}} - \psi(E_{cf}) \left(\frac{V_{up} + V_{wup}}{\dot{E}} \right) \right]_{\dot{E}>0} , \tag{A.31}$$

$$H_{dn} = \min_{\substack{V_{dn} \\ \pi_{dn}}} \left[\frac{C_d}{|\dot{E}|} - \psi(E_{cf}) \left(\frac{V_{dn} + V_{wdn}}{|\dot{E}|} \right) \right]_{\dot{E}<0} .$$

Thus, the optimization problem reduces to solving pointwise minimum values of the algebraic functions defined by Eq. (A.31) during the climb and descent portions of the trajectory.

Equations (A.29) and (A.30) are the transversality condition for the free final state problem ($d_{up} + d_{dn} < d_f$) with terminal cost. Thus, the constant value of λ for climb and descent is found to be the negative of the cost per unit distance for cruise.

The cruise cost ψ ($= -\lambda$) is found by assuming that the aircraft is in static equilibrium during cruise (T = D), and that

$$\psi(E_c) = \min_{V_c} \frac{C_d}{(V_c + V_w)} , \tag{A.32}$$

In other words, for any cruise altitude, there is an optimum thrust and airspeed such that the cost per unit distance $\psi(E_c)$ is minimized. The optimum cruise cost as a function of cruise energy is typically of the shape shown in Fig. A.3. Thus, there is also an optimum cruise energy E_{copt} where cruise cost $\psi(E_{copt})$ is minimized. If the range is long enough so that there is sufficient range to reach optimum cruise energy E_{copt}, it should be done, and the cruise conditions should be set so that $\psi(E_c) = \psi(E_{copt})$.

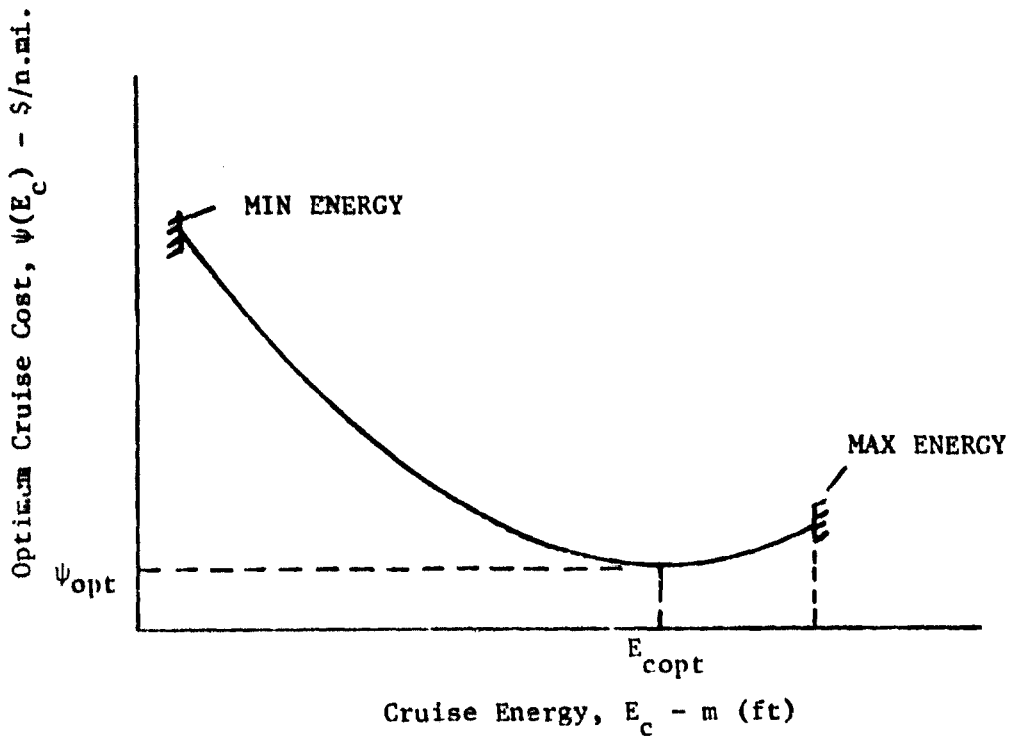

Figure A.3. Optimum Cruise Cost as a Function of Cruise Energy

For the case where there is no cruise segment ($d_f = d_{up} + d_{dn}$), the cost function contains only integral terms. Then, the transversality condition yields $\lambda = -\psi(t_c)$. That is, λ would be the negative of $\psi(t_c)$, where $\psi(t_c)$ is the optimum cost for cruising at the highest point reached on the climb trajectory.

The optimum cruise energy E_{copt} is only specifically reached when there is range enough to climb to and descend from the optimum altitude/airspeed values, where $\psi(E_c)$ is minimum. For ranges less than this value, the maximum value of E_c that is reached is a free variable less than the optimum value. Its choice is made to optimize the cost function of Eq. (A.23).

From Eqs. (A.23) and (A.25), one can write

$$\frac{\partial J}{\partial E} = H + \left[\frac{\partial [(d_f - d_{up} - d_{dn})\ \psi(E_c)]}{\partial E} \right] = 0, \qquad \text{(A.33)}$$

at $E = E_c$. This is

$$H_c + d_c \frac{\partial \psi}{\partial E_c} = 0 \quad , \tag{A.34}$$

where d_c is the cruise distance, and H_c is the total value of H ($H_{up} + H_{dn}$) at the cruise point. Thus, Eq. (A.34) can be used, along with other characteristics of ψ and H, to determine the relationship between ψ, E_c, and d_c. The Hamiltonian evaluated at $E = E_c$ is the cost penalty to achieve a unit increase in cruise energy. For $H_c > 0$, Eq. (A.34) can be written as

$$d_c = -H_c/(\partial\psi/\partial E)_{E = E_c} \tag{A.35}$$

Figure A.4 shows the family of trajectories which have this characteristic. These occur at values of E_c below E_{copt} where $\partial\psi/\partial E < 0$ (see Fig. A.3). That is, non-zero cruise segments occur at short ranges with cruise energies less than the optimum energy value for long range.

For the case where $H_c = 0$, d_c is zero for $\partial\psi/\partial E < 0$. The distance d_c can be non-zero only at optimum cruise energy where $\partial\psi/\partial E = 0$. This family of trajectories is shown in Fig. A.5.

Thus, we have a situation where positive values of H_c dictate one type of trajectory and zero values dictate another. In Ref. 17, it is shown that if the aircraft engine specific fuel consumption S_{FC} is independent of the thrust T (so that $\dot{w} = S_{FC}T$), then the structure of the trajectories will be like Fig. A.5 with no cruise segment occuring except at E_{copt}. (This implies that the Hamiltonian H_c is zero at the maximum energy point). For this case, the optimum thrust setting for climb is T_{max}, and the optimum setting for descent is T_{idle}.

If the engine specific fuel consumption is dependent on thrust, and the thrust values are not constrained during climb or descent, it is shown in Ref. 17, that the Hamiltonian H_c is again zero at the cruise energy, and again the trajectory structure is like those of Fig. A.5.

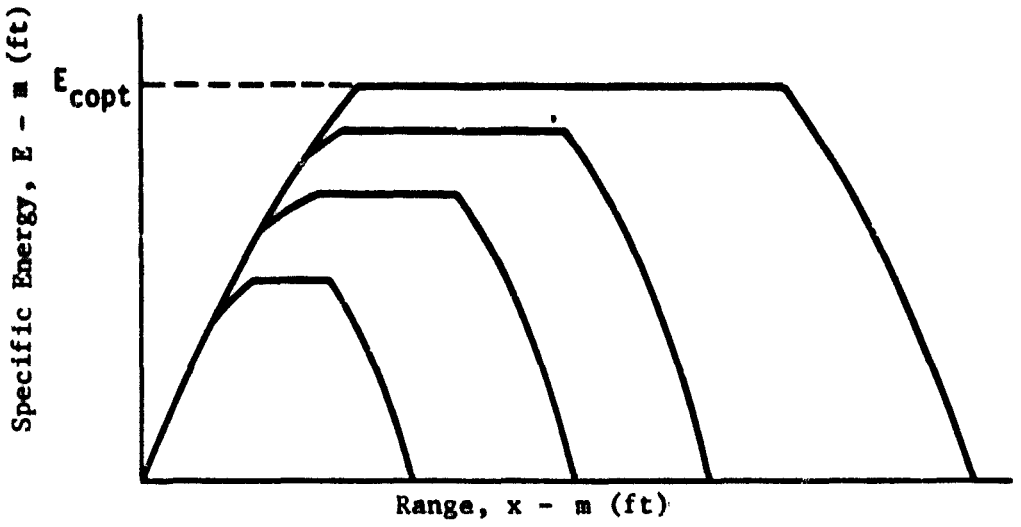

Figure A.4. Optimum Profile Energy vs Range for $H_c > 0$ at Cruise.

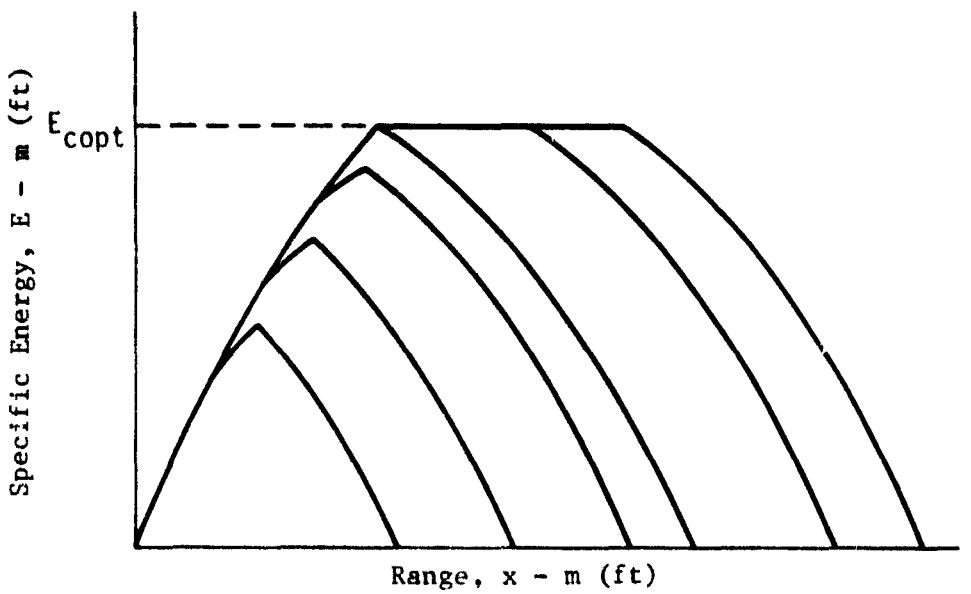

Figure A.5. Optimum Profile Energy vs Range for $H_c = 0$ at Cruise.

If the S_{FC} is dependent on thrust, and constrained to the maximum value for climb and to the minimum idle value for descent, then the Hamiltonian is positive at cruise. This causes positive cruise segments according to Eq. (A.35) at cruise energies below the optimum. For this case, the optimum trajectories will have shapes similar to Fig. A.4. These trajectories are slightly less efficient than those of Fig. A.5. because one less control is available for optimization.

Some Mechanization Details of the Computer Program

The remaining sections of this Appendix describe how the previous theoretical material has been utilized to construct an offline computer program for generating optimum vertical profiles for models of medium range tri-jet and twin-jet transport aircraft. This material is presented in an alternate way in Ref. 21, and the program is referred to here as OPTIM.

By examining the specific fuel consumption data of the turbojet engine, it is determined that S_{FC} is dependent on thrust. Thus, for the transport models, two types of short range profiles must be considered - those represented by Fig. A.4 (Type 1 profile) when thrust is constrained and airspeed is the single control - and those represented by Fig. A.5 (Type 2 profile) when both thrust and airspeed are used as controls.

The solution to optimum climb and descent profiles is found by minimizing the Hamiltonian expressed in Eqs. (A.31). The independent variable (energy) is stepped along in fixed increments (e.g., 150 m (500 ft)), and the Hamiltonian is minimized at each energy setting. Minimization occurs by finding the best values of airspeed (V_{up}, V_{dn}) (and optionally thrust (π_{up}, π_{dn})) so that the climb function and the descent function are individually minimized.

To solve Eqs. (A.31) requires knowing two more quantities:

λ or $\psi(E_c)$ - the cruise cost per unit distance. This comes from evaluating Eq. (A.32) at the desired cruise altitude.

E_c - the cruise energy. This is a function of the cruise altitude and the associated cruise airspeed obtained in Eq. (A.32).

Note that for the Type 2 profile at short ranges, there is no cruise segment. In this case, the maximum energy achieved at maximum altitude is referred to as the cruise energy E_c. At that altitude, there still is defined a minimum cruise cost according to Eq. (A.32).

For the Type 1 trajectory of short range, there exists a non-zero cruise segment which is determined by use of Eq. (A.35). To solve Eq. (A.35) requires that the Hamiltonian defined by Eqs. (A.31) be solved at the point of transition from climb-to-cruise. It also requires knowing the slope $\partial\psi/\partial E$ of the cruise cost for a change in cruise energy at that point.

Cruise Optimization

The first step that must be taken to compute optimum trajectories is to derive the optimum cruise cost ψ and its derivative $\partial\psi/\partial E$. This is done by computing what is referred to as the "cruise table". The parameters that affect this table are the assumed cruise mass, the wind profile, and the lift L, drag D, thrust T, and fuel flow $\dot{w}$ characteristics of the aircraft. The optimization process searches over the acceptable ranges of altitude and airspeed for a given mass. The results are collected in tabular form for a series of different assumed cruise masses.

Again, the minimum cost of flight during cruise per unit distance for a fixed cruise mass W_c is found by

$$\lambda = \psi(W_c) = \min_{V_a} \left[\frac{C_f \dot{w} + C_t}{V_a + V_w} \right] . \qquad (A.36)$$

This assumes that the aircraft is in static equilibrium during cruise, i.e.,

$$T \cos \alpha = D, \qquad (A.37)$$
$$L + T \sin \alpha = mg,$$

where the angle-of-attack α is found by solving these equations simultaneously. The altitude is stepped in 305m (1000 ft) increments from sea level to ceiling altitude (where maximum thrust just balances drag). At altitudes below ceiling altitude, the airspeed - dependent drag curve crosses the maximum thrust curve at two points (V_1 and V_2) as illustrated in Fig. A.6. Thus, for each altitude level, the values of V_1 and V_2 are determined, and then $\psi(W_c, E_c)$ is minimized with respect to airspeed V_a between these two limits. Restrictions are that V_1 be greater than 0.1 Mach and that V_2 be less than 0.89 Mach for the tri-jet (0.84 for the twin jet) for structural reasons.

After the cruise cost is minimized at each discrete altitude level, these numbers are stored in a table with altitude as the independent variable. Typical results are plotted in Fig. A.7. Presented here are also the optimum cruise Mach number M_{opt} and the optimum thrust setting EPR_{opt}. After results are obtained in steps of 305 m (1000 ft), the minimum cost point is found as a function of altitude. In the OPTIM program, the cruise table optimization results are obtained by using a Fibonacci search with ten Fibonacci numbers. (See Ref. 22).

The cruise table results are obtained for cruise mass varying as dictated by the program input. Usually, the cruise mass is incremented in steps of 2268 kg (5000 lb). Up to ten values of cruise mass can be used. For each cruise mass, the optimal cruise altitude, cost, speed, power setting, fuel flow and specific energy are computed. An example of optimum cruise cost and a function of cruise mass is shown in Fig. A.8.

Climb Optimization

After the cruise tables are generated, the program proceeds with obtaining the optimum climb trajectory. This requires guessing what the cruise mass will be, based on the takeoff mass. The guess is used to obtain a trial value for ψ_c (or λ) in the Hamiltonian from the cruise tables. The procedure to obtain this guess is based on an empirical formula which iterates until convergence is made.

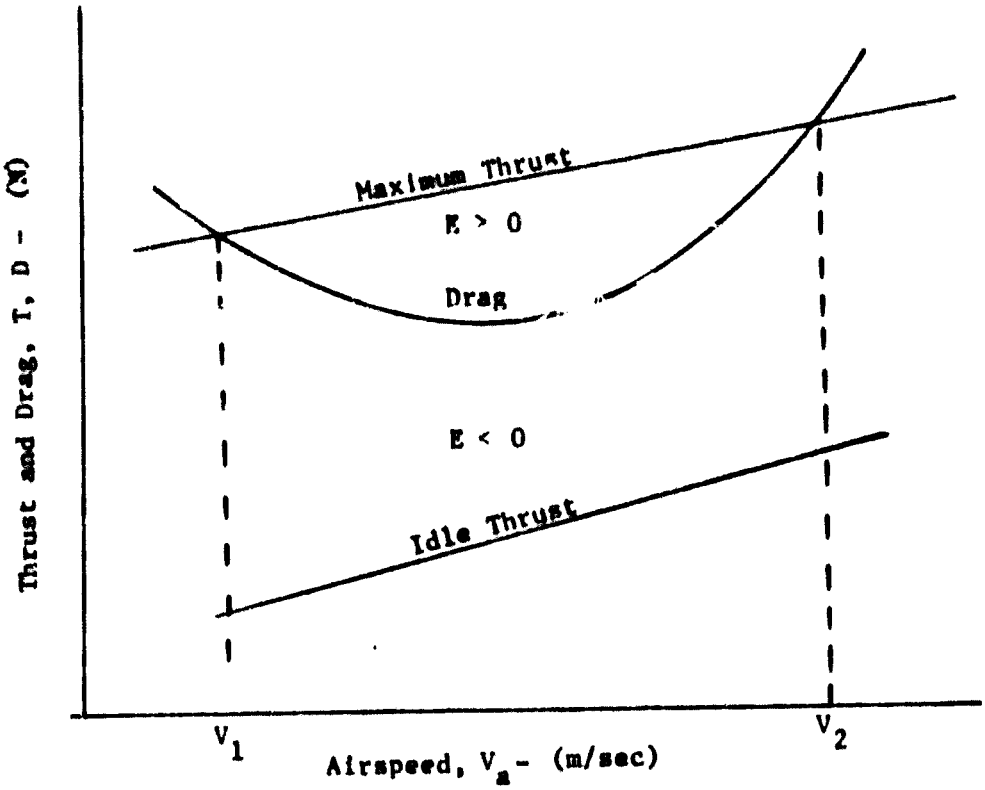

Figure A.6. Plot of Thrust and Drag vs True Airspeed at a Particular Altitude

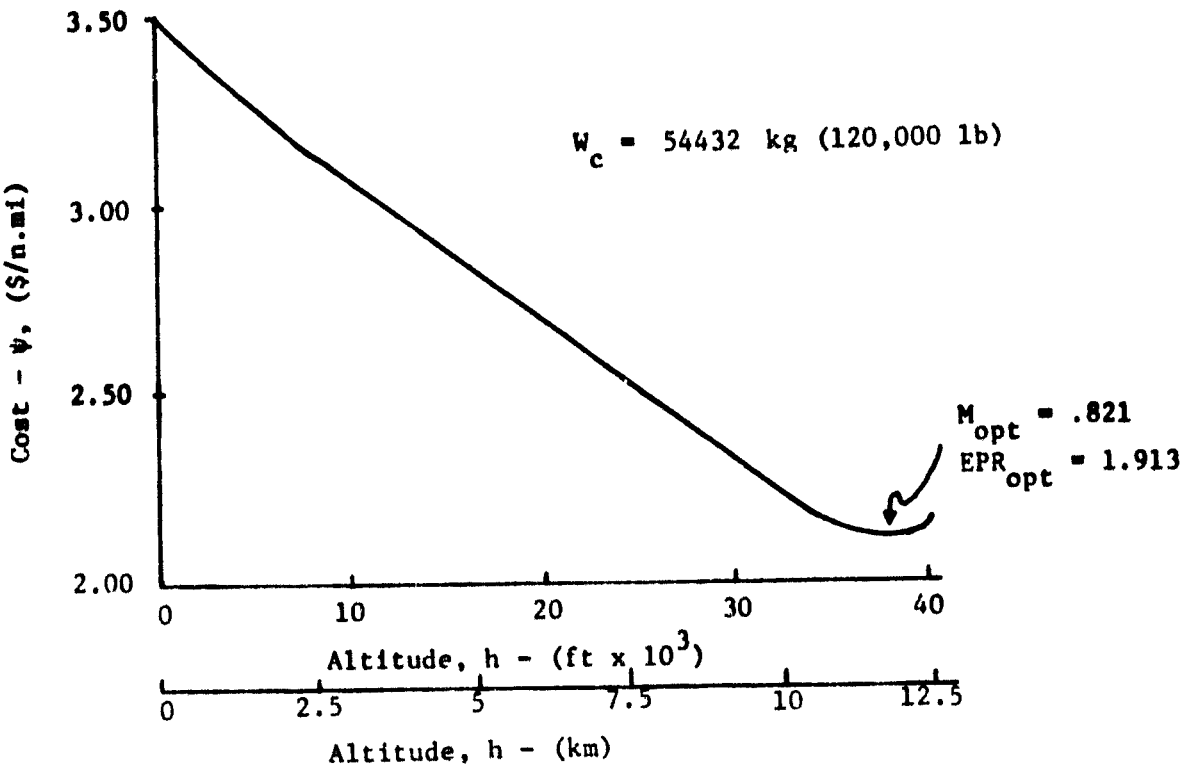

Figure A.7. Optimum Cruise Cost as a Function of Altitude for Cruise Mass of 54432 kg (120,000 lb).

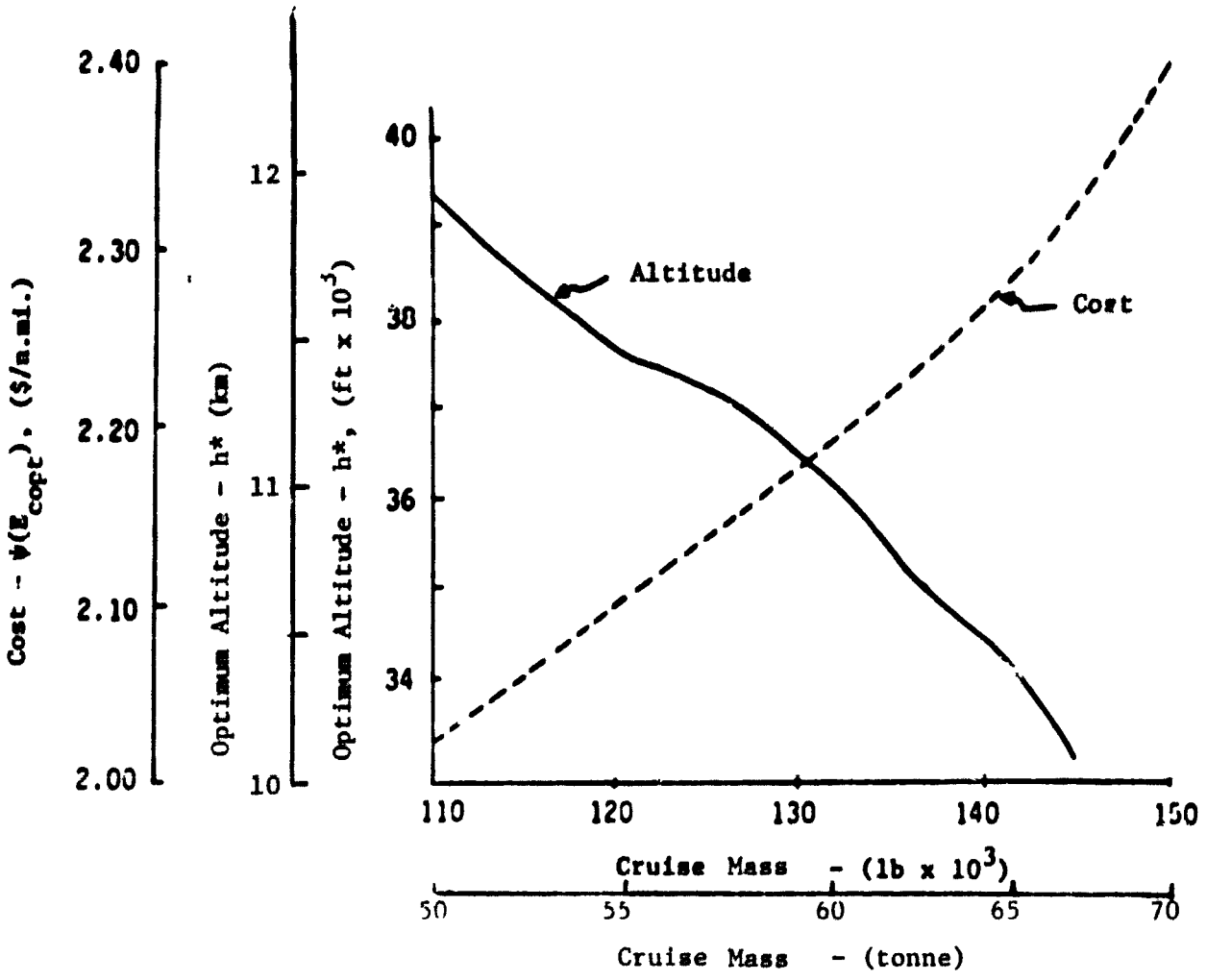

Figure A.8. Optimum Cruise Cost and Cruise Altitude as Functions of Cruise Mass for a Tri-jet Aircraft Flying into a particular Head Wind.

The climb optimization process starts by assuming $\psi(E_c) = 1.5\,\psi(E_{copt})$, where $\psi(E_{copt})$ is first obtained by setting the initial cruise mass W_{ci} equal to the takeoff mass (an input). The appropriate cruise tables are used to interpolate to find the corresponding value of E_c associated with $1.5\,\psi$. Then, an empirical formula of the form

$$F_{up} = 0.11\ (E_{ci} - E_i)\ (1 + 4.7\ C_t/C_f)\ W_{ci}/W_{ref}\ , \qquad (A.38)$$

is used to obtain an approximation to the fuel burned to reach E_c. Here, E_i is the takeoff aircraft energy, W_{ref} is a reference mass (61690 kg (136000 lb) for the tri-jet) and W_{ci} is the previous value of cruise mass.

Then, the cruise mass is updated at $W_{ci} = W_{ci} - F_{up}$. This process is repeated until the difference in consecutive estimates of F_{up} falls below 45 kg (100 lb).

When the cruise mass estimate is obtained, the corresponding values of E_c and $\psi(E_c)$ are obtained from the cruise tables. Then, the program is ready to generate points on the optimum climb trajectory. This is done by incrementing specific energy and minimizing the Hamiltonian function

$$H_{up}(E) = \frac{C_f \dot{w} + C_t - \psi(E_c)\ (V_a + V_w)}{\dot{E}} \qquad (A.39)$$

at each point. (This is the first of Eqs. (A.31)). That is, the program starts with initial energy $E_o = h_o + V_o^2/2g$. It steps the energy a fixed amount ΔE (say 150 m (500 ft). At this point, it searches over true airspeed V_a (and possibly thrust setting π) so that Eq. (A.39) is minimized. For the turbojet engines, thrust is governed by EPR settings which vary between 1.1 (idle thrust) and some maximum value less than 2.4. The true airspeed has an upper limit governed by

a). 0.89 Mach structural limits (tri-jet); 0.84 (twin jet)
b). 250 kt (IAS) below 3048 m (10000 ft) for ATC restrictions,
c). $\sqrt{2g(E-h)}$ which insures that the aircraft climbs, and
d). V_2, the upper value shown in Fig. A.6 where max thrust equals drag.

The lower limit is governed by

a). V_1, the lower value shown in Fig. A.6 where max thrust equals drag,
b). 0.1 Mach
c). 1.5 m/sec (5 ft/sec) less than the previous value of V_a to limit large jumps in flight path angle.

The Fibonacci search technique is again used to determine V_a and π which minimize Eq. (A.39) for the fixed value of energy E. The value chosen for airspeed is accurate to within .0056 Mach, and EPR is accurate

to within .009. Associated with these values of V_a and π are values of energy rate $\dot{E}$ (Eq. (A.16)) and altitude h:

$$h = E - V_a^2/2g \ . \tag{A.40}$$

From these, approximate values of time, range, flight path angle, and fuel burned are obtained from

$$\begin{aligned} \Delta t &= \Delta E/\dot{E}, \\ \sin\gamma &= (\Delta h/\Delta t)/V_a \ , \\ x &= \Sigma\Delta x \ ; \quad \Delta x = (V_a \cos\gamma + V_w(h))\ \Delta t \\ F &= \Sigma\Delta F \ ; \quad \Delta F = \dot{w}\ \Delta t. \end{aligned} \tag{A.41}$$

The above process is repeated by stepping along energy in increments of ΔE until E_c is reached. The last value of Eq. (A.39) is stored for possible use in evaluating the cruise distance.

The above climb optimization procedure is repeated with $\psi = 1.5\psi_c$, $1.0\psi_c$, and perhaps other values until the total range of flight converges to the appropriate value. This is discussed in further detail later.

Descent Optimization

The descent optimization is very similar to the climb optimization with regard to the equations which are evaluated. The optimization process requires estimated values of E_c and W_c at the beginning of descent, and an estimate of mass W_f at the end of descent. The method used to obtain these estimates is discussed in the next section.

If there is a cruise portion of flight, fuel will be burned during cruise. Thus, the value of E_{cf}, ψ, and W_{cf} at the beginning of descent will usually be different than at the beginning of cruise. If there is no cruise portion, then these values will be identical.

The descent profile is obtained by starting at the final energy state and then going backwards in time. The energy rate is constrained to be negative with respect to forward time.

Similar descent profile constraints exist on true airspeed as for those of the climb profile. The thrust level is on or near the idle value during descent.

Cruise Fuel Burn

To estimate the final mass during cruise (W_{cf}) and landing (W_f), the following steps are taken:

1). Determine ψ_c, the initial cruise cost based on the initial cruise mass W_{ci} obtained from the climb optimization.

2) Use the initial cruise mass and ψ_c to compute the fuel flow $\dot{w}(\psi_c)$

3). Estimate the cruise range d_c by the empirical equations,

$$P = \psi_c/\psi_{copt} = 1.5 \ , \tag{A.42}$$

$$d_c = b_1P^4 + b_2P^3 + b_3P^2 + b_4P + b_5 \ .$$

4). Compute the cruise fuel as

$$F_c = \dot{w}(\psi_c)\ d_c/(V_c + V_w(h_c)) . \tag{A.43}$$

5). Estimate the average cruise mass as

$$\bar{W}_c = W_c - 0.5F_c \tag{A.44}$$

6). Use the cruise table to obtain the corresponding cruise cost $\bar{\psi}_c$, altitude $\bar{h}_c$, fuel flow $\dot{\bar{w}}(\bar{\psi}_c)$, true airspeed $\bar{V}_c$, and wind speed $\bar{V}_w(\bar{h})$.

7). Recompute Eq. (A.43), and then find the final cruise mass,

$$W_{cf} = W_{ci} - F_c . \tag{A.45}$$

8). Use the value W_{cf} in the cruise tables to obtain $\psi(W_{cf})$. As with the climb, set $\psi = 1.5\ \psi(W_{cf})$.

9). Use this value of ψ to obtain h_{cf} and E_{cf} from the cruise tables. These are the end conditions for the descent trajectory obtained backwards in time.

10). Estimate the landing mass from the empirical formula

$$P = 1.5, \tag{A.46}$$
$$W_f = W_{cf} - (c_1 P^2 + c_2 P + c_3).$$

The values of ψ, E_{cf} and W_f obtained by the above procedure are used for obtaining the optimum descent trajectory. The descent portion of the Hamiltonian is of the form

$$H_{dn}(E) = \frac{C_f \dot{w} + C_t - \psi(E_{cf})\ (V_a + V_w)}{|\dot{E}|}; \tag{A.47}$$

this function is also minimized at each of the given values of energy.

After the first descent profile is completed, a new estimate of cruise distance is obtained by using Eq. (A.35), or

$$d_c = -(H_{up} + H_{dn})/(\partial\psi/\partial E) \quad . \tag{A.48}$$

Then, step (4) above is repeated to obtain an improved cruise fuel burn. Then, the improved landing mass estimate is

$$W_f = W_i - (F_{up} + F_c + F_{dn}) \ . \tag{A.49}$$

The landing trajectory is reoptimized with this new value of landing mass. Then, improved values of total range traveled, time required, and fuel burned during climb, cruise, and descent are made.

For short range flight, the above steps assumed that a Type 1 trajectory is generated because thrust is constrained to maximum value during climb and idle value during descent. If thrust is free, then a Type 2 trajectory will result, with no cruise portion. For this case, the steps required to estimate cruise distance d_c and final cruise cost, mass, and energy can be eliminated.

Cruise Cost Estimation

The first climb and descent profiles are generated with $\psi_c = 1.5\psi(E_{copt})$. The next set is generated with $\psi_c = 1.0\psi(E_{copt})$. Each of these values of cruise cost have an associated range on the curve shown in Fig. A.9. If the total range desired is greater than R_{max} (the value obtained using $1.0\psi(E_{copt})$), then it is assumed that the optimum cruise altitude and energy are reached. Then a third set of climb and descent profiles is generated using $\psi(E_{copt})$. In this case, the cruise distance is computed so that the desired overall range is exactly achieved.

If the desired range is between R_{min} and R_{max} in Fig. A.9, then an iterative process is used to obtain $\psi(E_c)$ and the associated desired range. Iterations are stopped when the total range traveled is within some small distance ε of the desired range. (In OPTIM, ε is set at 5 n.mi.)

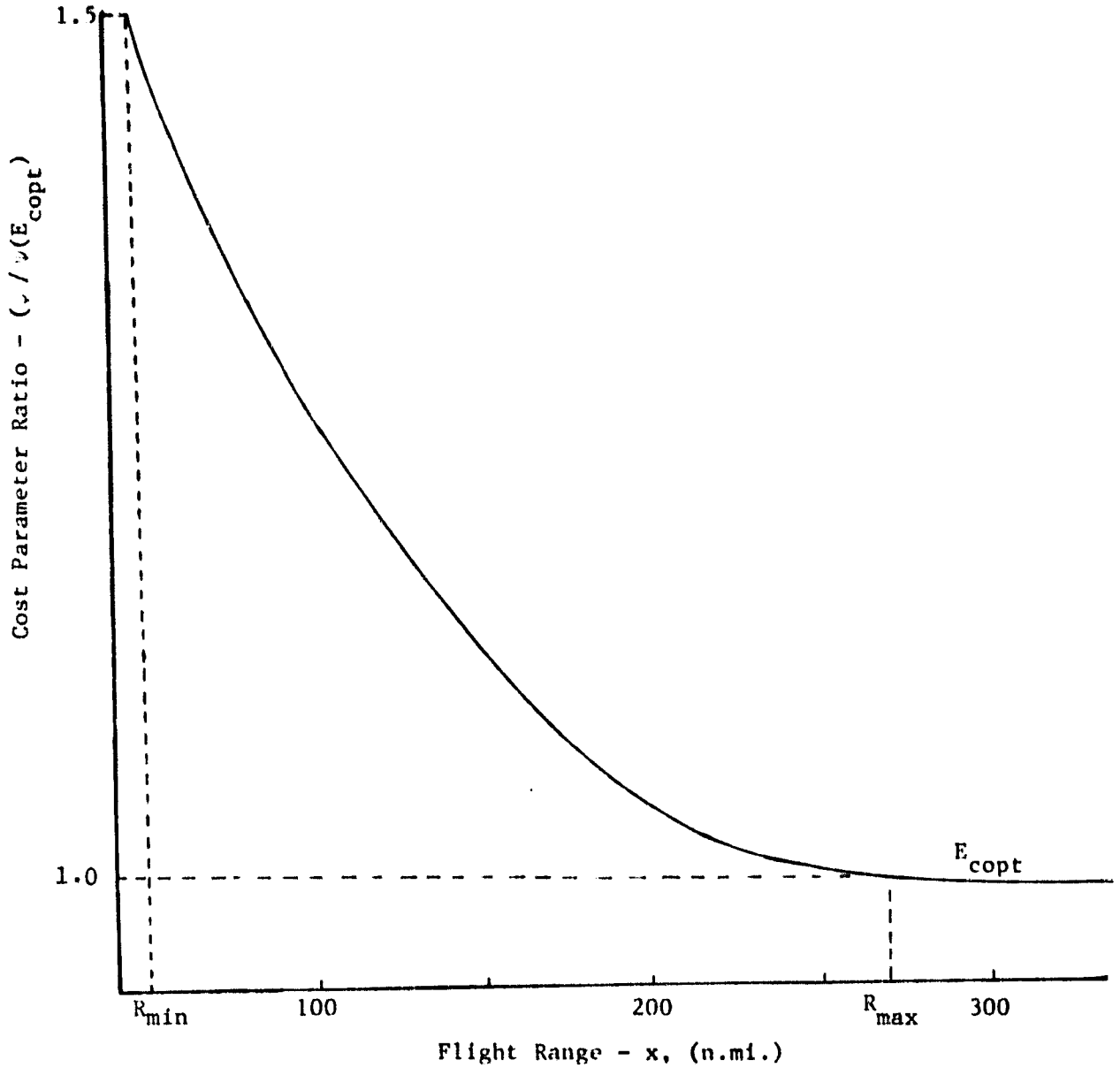

Figure A.9. Relationship between the Cruise Cost Parameter ψ and the Associated Range of Flight

APPENDIX B

ENGINE MODEL DEVELOPMENT

The modeling of the turbofan engine for the twin-jet aircraft in program OPTIM required changes to subroutines FCLIMB, ENGEPR, and ENGIDL [22]. Idle thrust and idle fuel flow are computed in ENGIDL and FCLIMB, and thrust and fuel flow at all other power settings are computed with a call to subroutine ENGEPR. The actual computations are done in subroutine ENGEP3. All engine data is stored in tables in the BLOCK DATA subprogram.

Idle Performance

Figure B.1 shows idle performance (net thrust and fuel flow) for the engine taken from the engine installation handbook. Note that surge bleeds can be either open or closed depending upon altitude and flight Mach number. To model this phenomena, two sets of tables were developed - one for bleeds closed and one for bleeds open (see Figs. B.2 and B.3). Then, an additional table was developed to determine the altitude for surge bleed closure as a function of flight Mach number (see Fig. B.4). Figures B.5 and B.6 show idle performance for cold and hot days. It is assumed that the fuel flow varies in inverse proportion to the square root of the T_{T2} ratio. This is expressed as

$$\frac{\dot{w}_{\text{fuel non STD}}}{\dot{w}_{\text{fuel STD}}} = \sqrt{\frac{T_{T2\ \text{non STD}}}{T_{T2\ \text{STD}}}} \quad . \tag{B.1}$$

T_{T2}, in degrees absolute, is the stagnation temperature at the compressor inlet. There is essentially no change in idle thrust due to temperature variation.

No Service Bleed
Standard Atmospheric Conditions

No Power Extraction
100% Ram Recovery

ICAO Standard Atmosphere

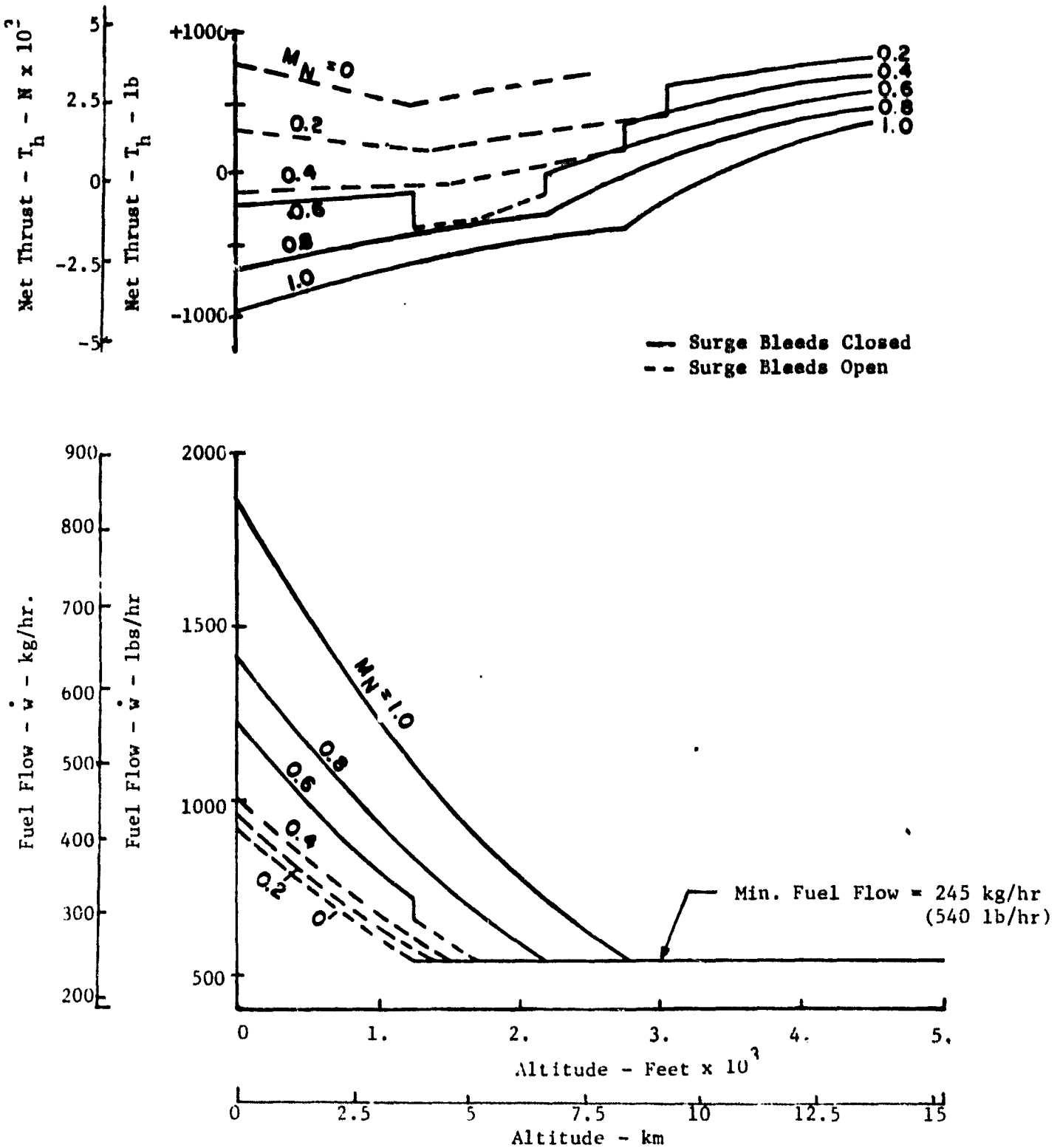

Figure B.1 Estimated Engine Performance at Flight Idle as a Function of Altitude

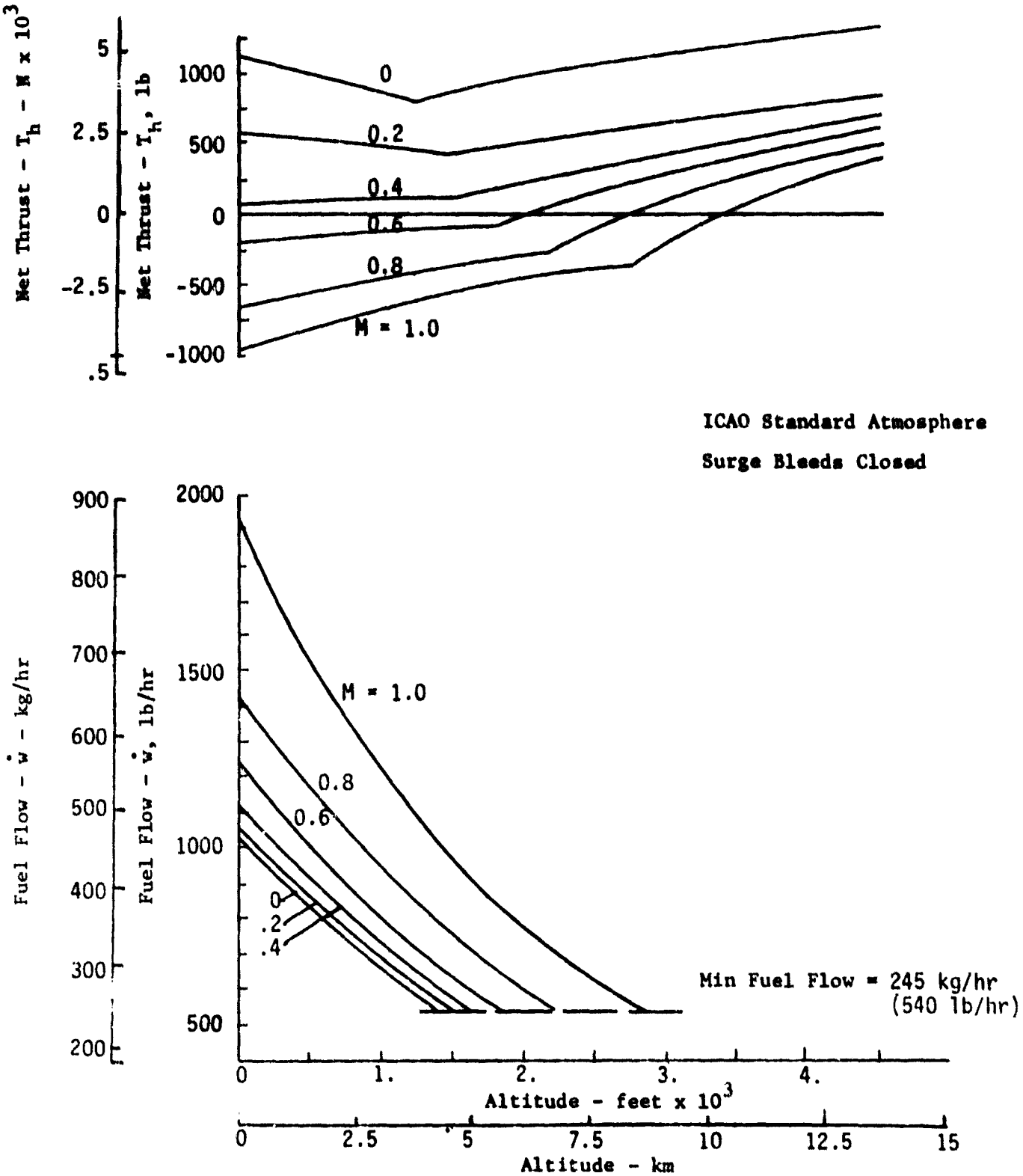

Figure B.2 Engine Idle Performance - Surge Bleeds Closed

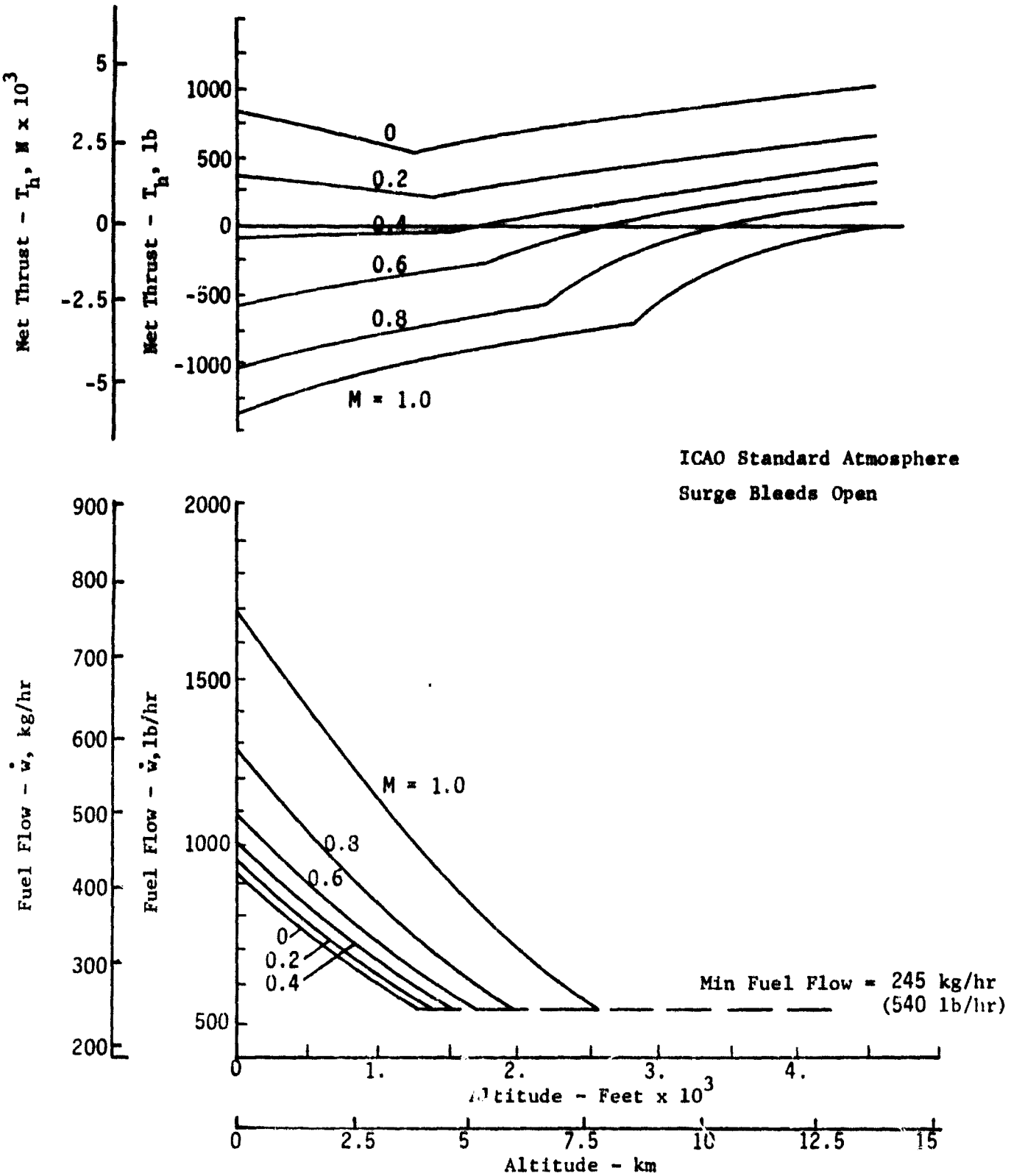

Figure B.3 Engine Idle Performance - Surge Bleeds Open

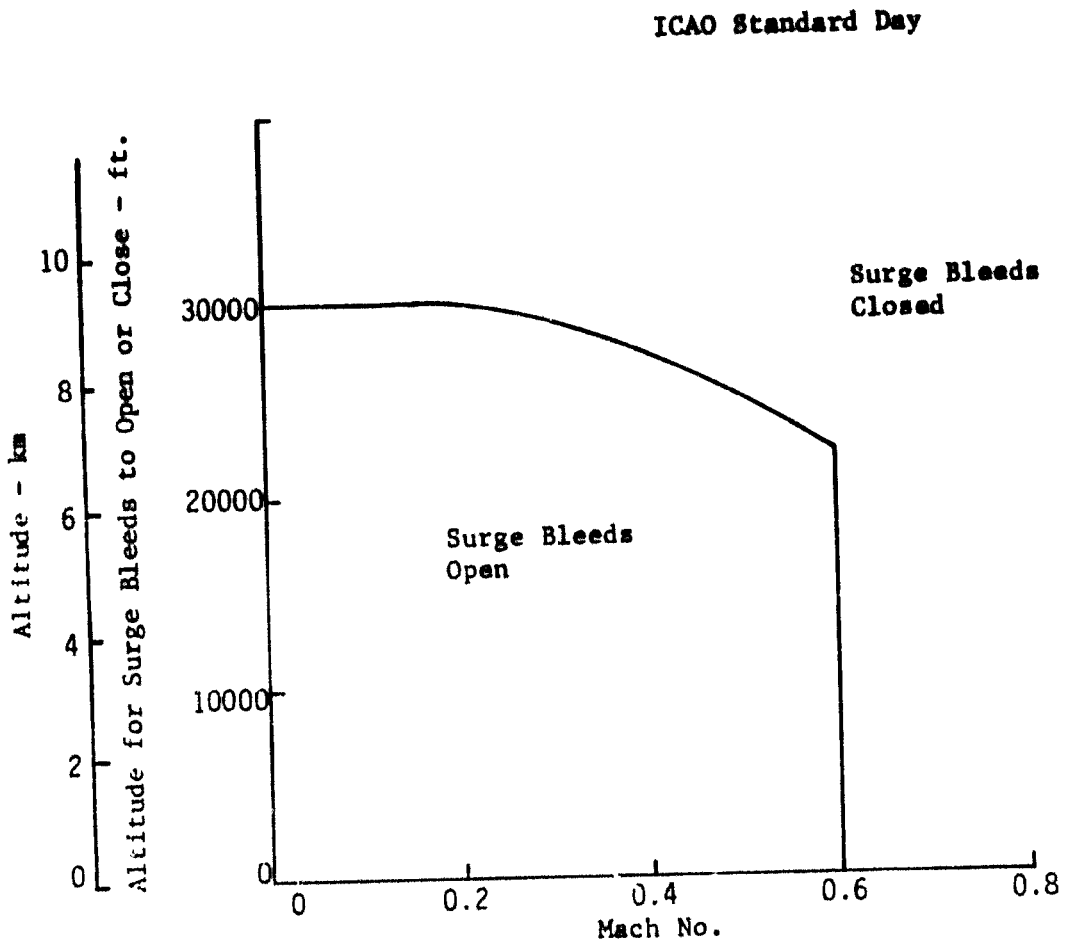

Figure B.4 Altitude for Surge Open/Closed

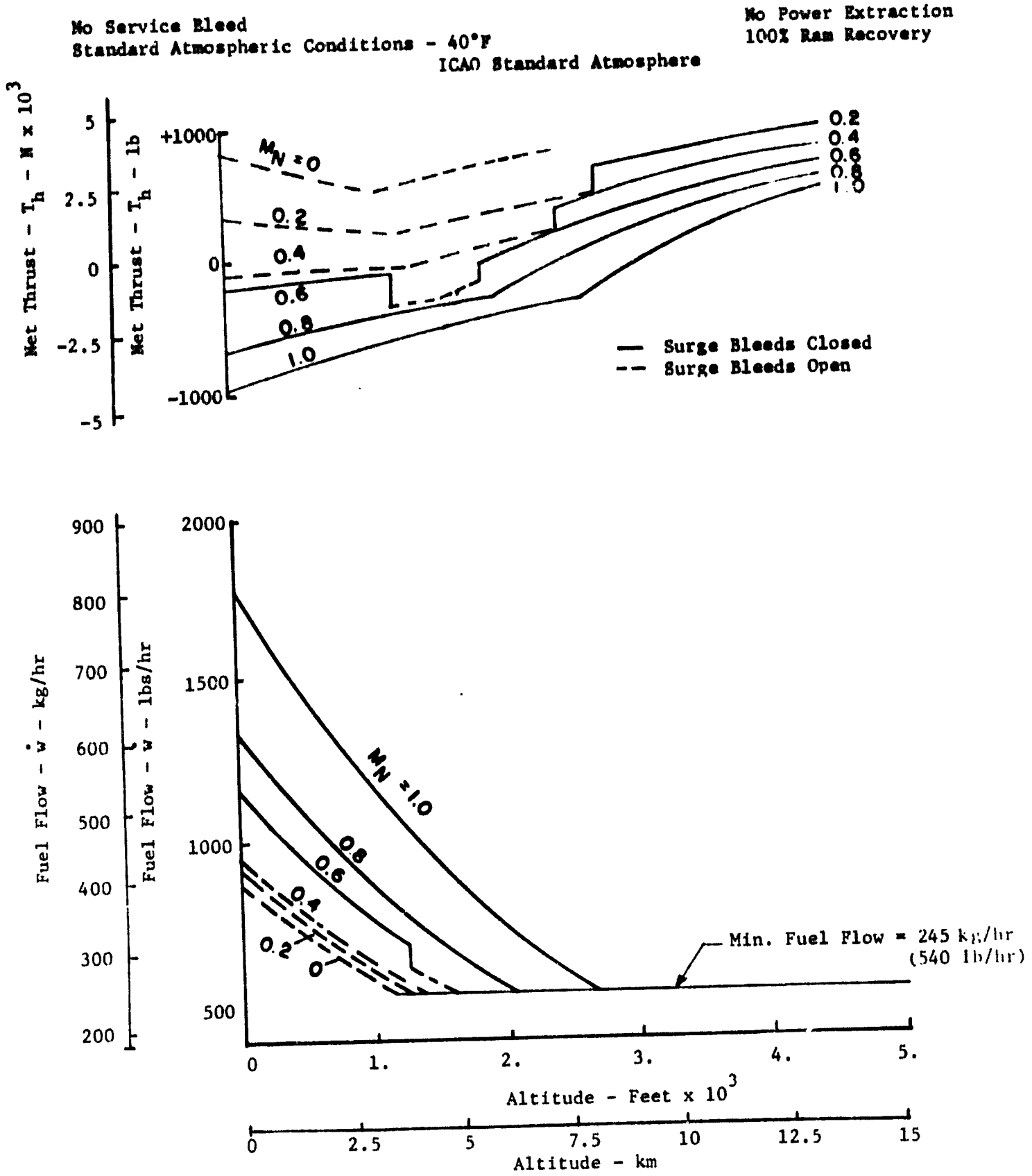

Figure B.5. Estimated Engine Performance at Flight Idle on a Cold (-22°K) Day

No Service Bleed
Standard Atmospheric Conditions - 40°F

No Power Extraction
100% Ram Recovery

ICAO Standard Atmosphere

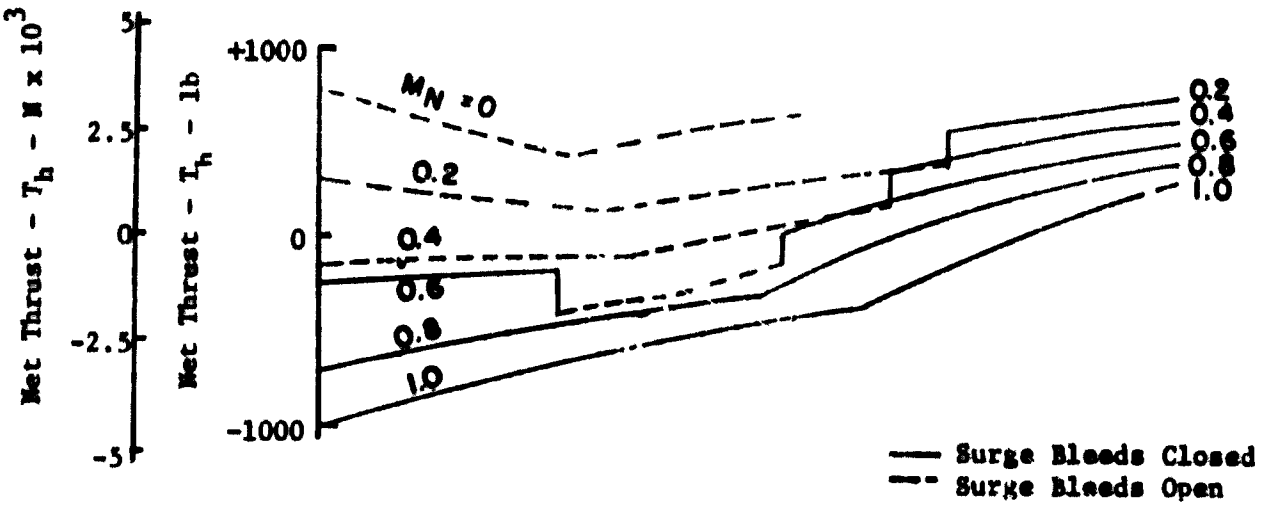

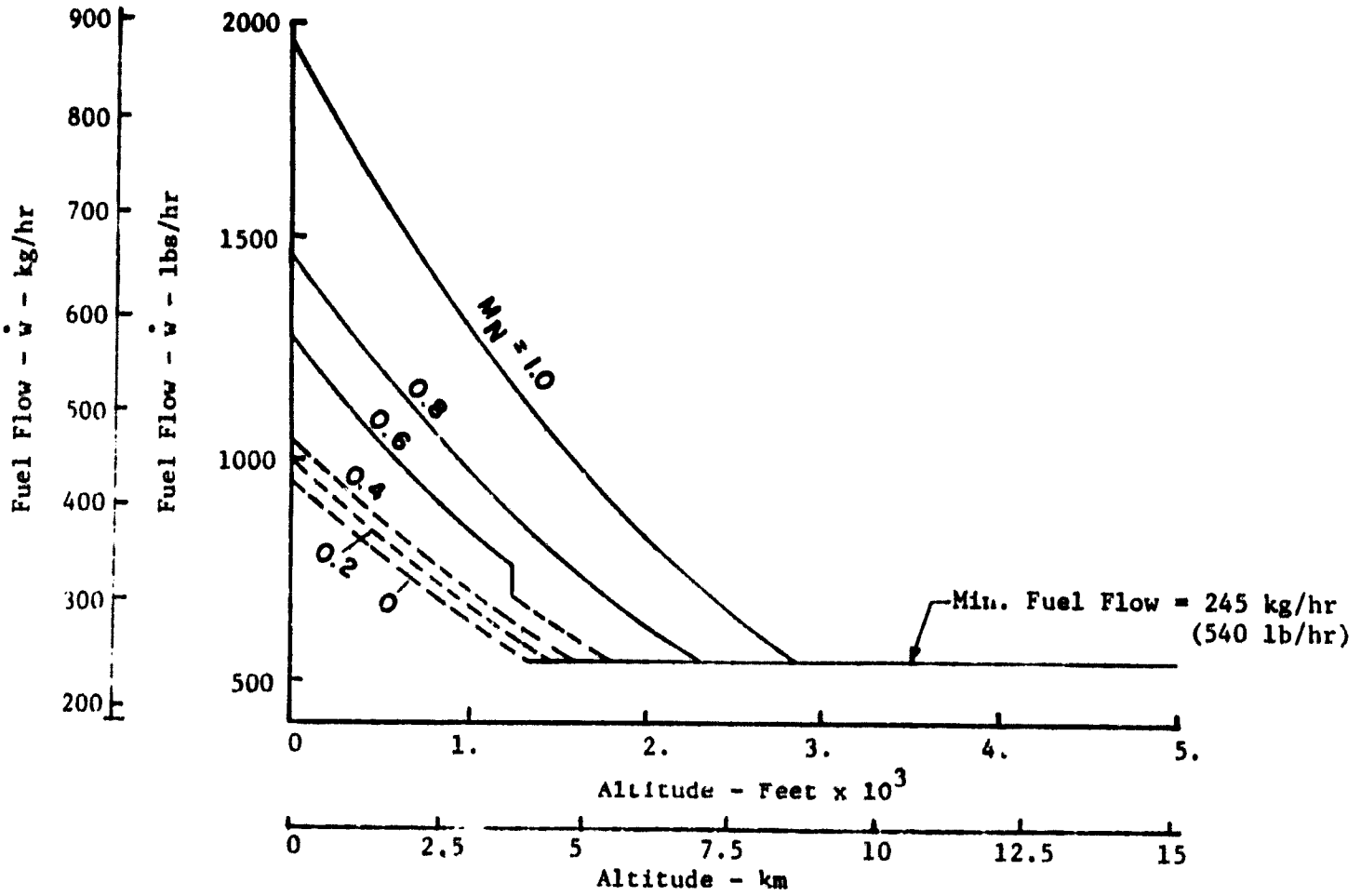

Figure B.6. Estimated Engine Performance at Flight Idle on a Hot (+22°K) Day

Maximum Engine Pressure Ratio

Maximum engine pressure ratio (EPR) is determined at each flight condition to insure that the engine is not set beyond its operational limits. As shown in Fig. B.7, the maximum EPR for climb is a function of the compressor inlet temperature (T_{T2}) only (which is computed from Mach number and altitude). Likewise, maximum EPR at cruise is a function of T_{T2} only. Two different curves are used: one for altitude $\leq$ 9.144 km (30000 ft) and one for altitude $\geq$ 10.668 km (35000 ft). Between 9.144 and 10.668 km (30000 and 35000 ft), and the maximum EPR is assumed to vary linearly.

Engine Thrust

Figure B.8 gives corrected thrust (thrust/ambient pressure ratio) as a function of flight Mach number and the engine pressure ratio for the twin-jet aircraft. Figure B.9 is a repeat of Fig. B.8 with additional data which represents the same engine performance in the tri-jet aircraft. It can be seen that with one exception the tri-jet data lies below the twin-jet data.* It was found that the tri-jet engine data represented installed thrust with the values being an average of the three engines on the aircraft. Because the middle engine on the tri-jet aircraft suffers greater installed losses because of the "S" shaped inlet duct, it is not surprising that the thrust shown in less. The program selects the appropriate engine data for each aircraft.

Engine Fuel Flow

Engine corrected fuel flow is shown in Fig. B.10 as a function of the engine pressure ratio and altitude. Note that the corrected fuel flow is also a function of flight Mach number for EPR less than 1.6. The correction

---

* The one exception is at M = 0.7 and EPR = 1.85. This data point was presumed to be in error, and a smooth curve is assumed.

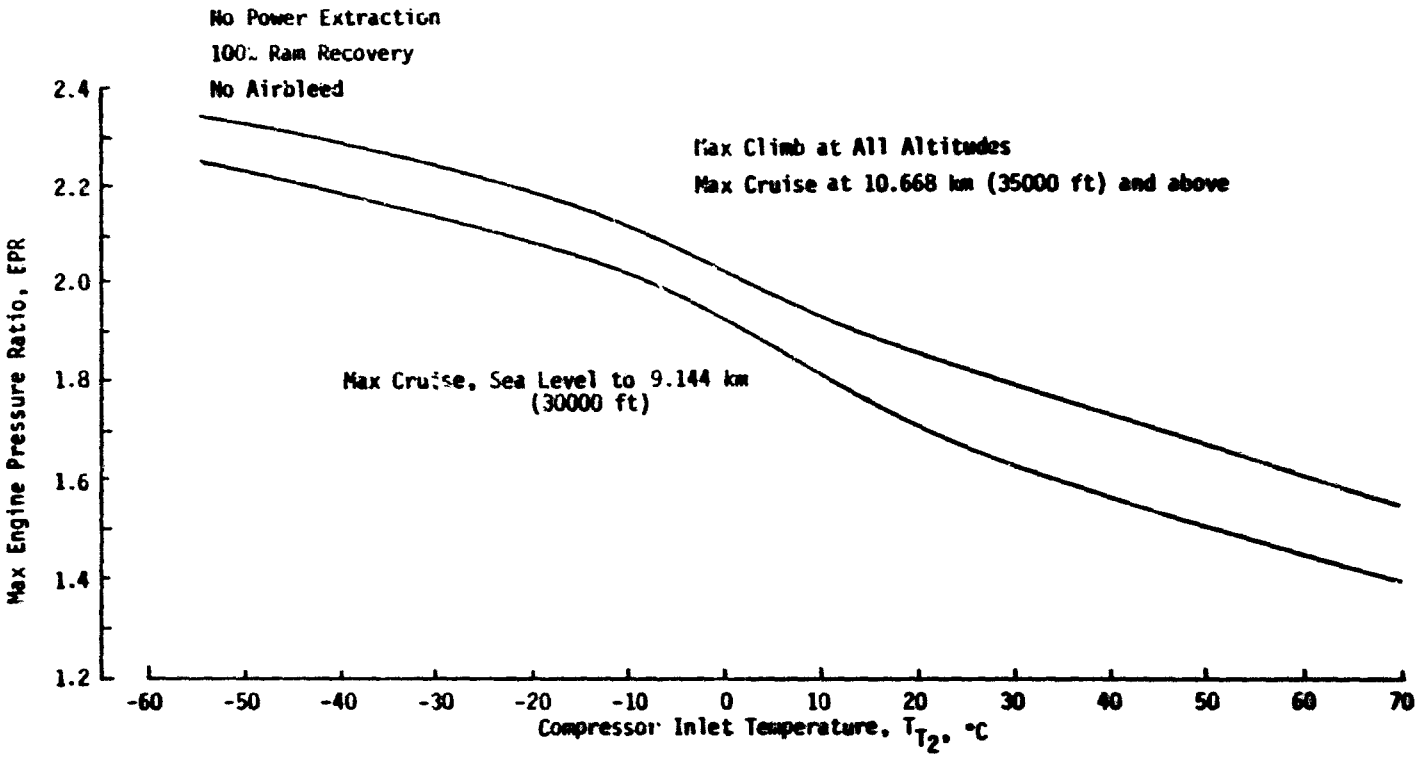

Figure B.7. Maximum Engine Pressure Ratio as a Function of Temperature.

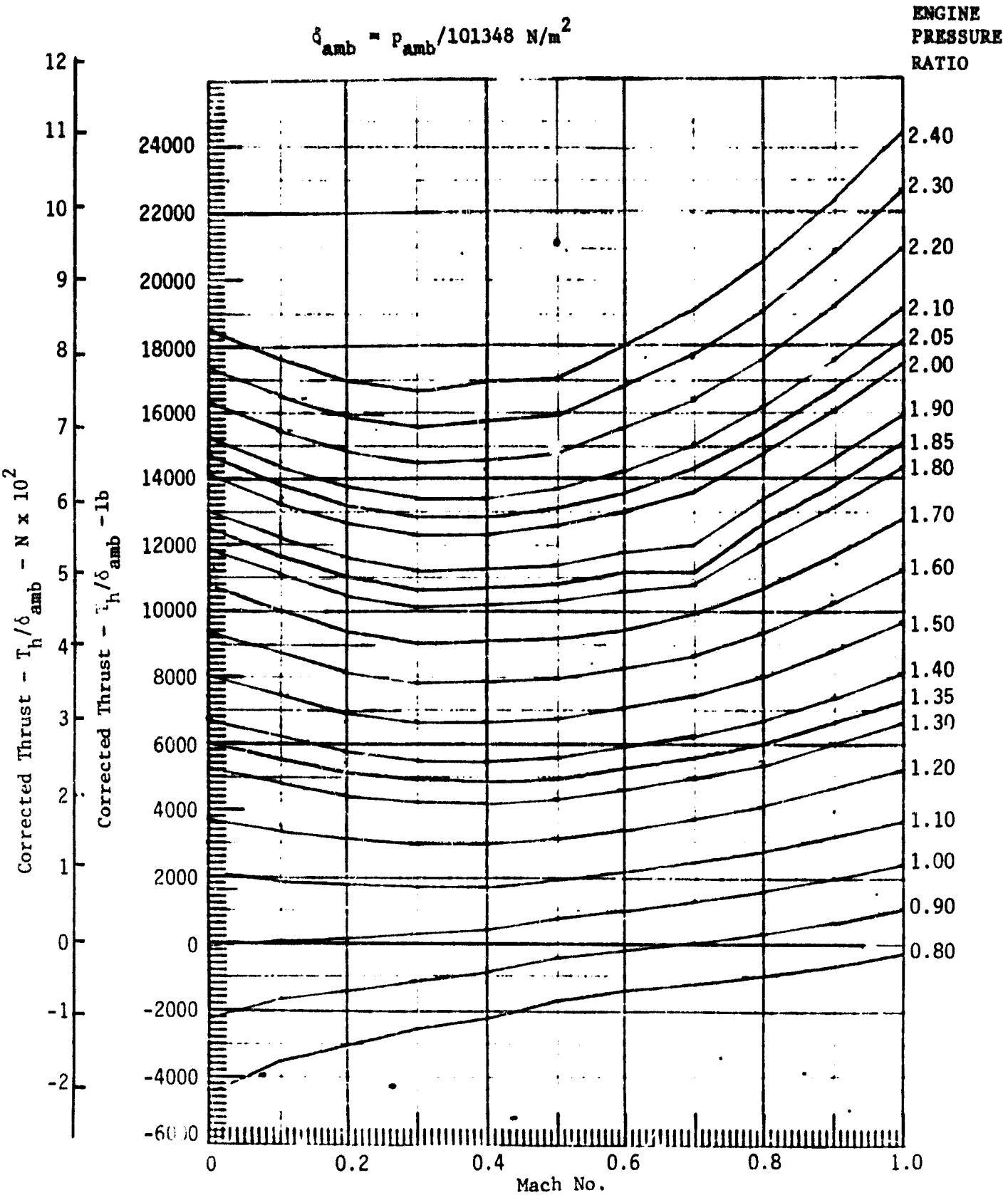

Figure B.8 Engine Thrust at Different Power Settings

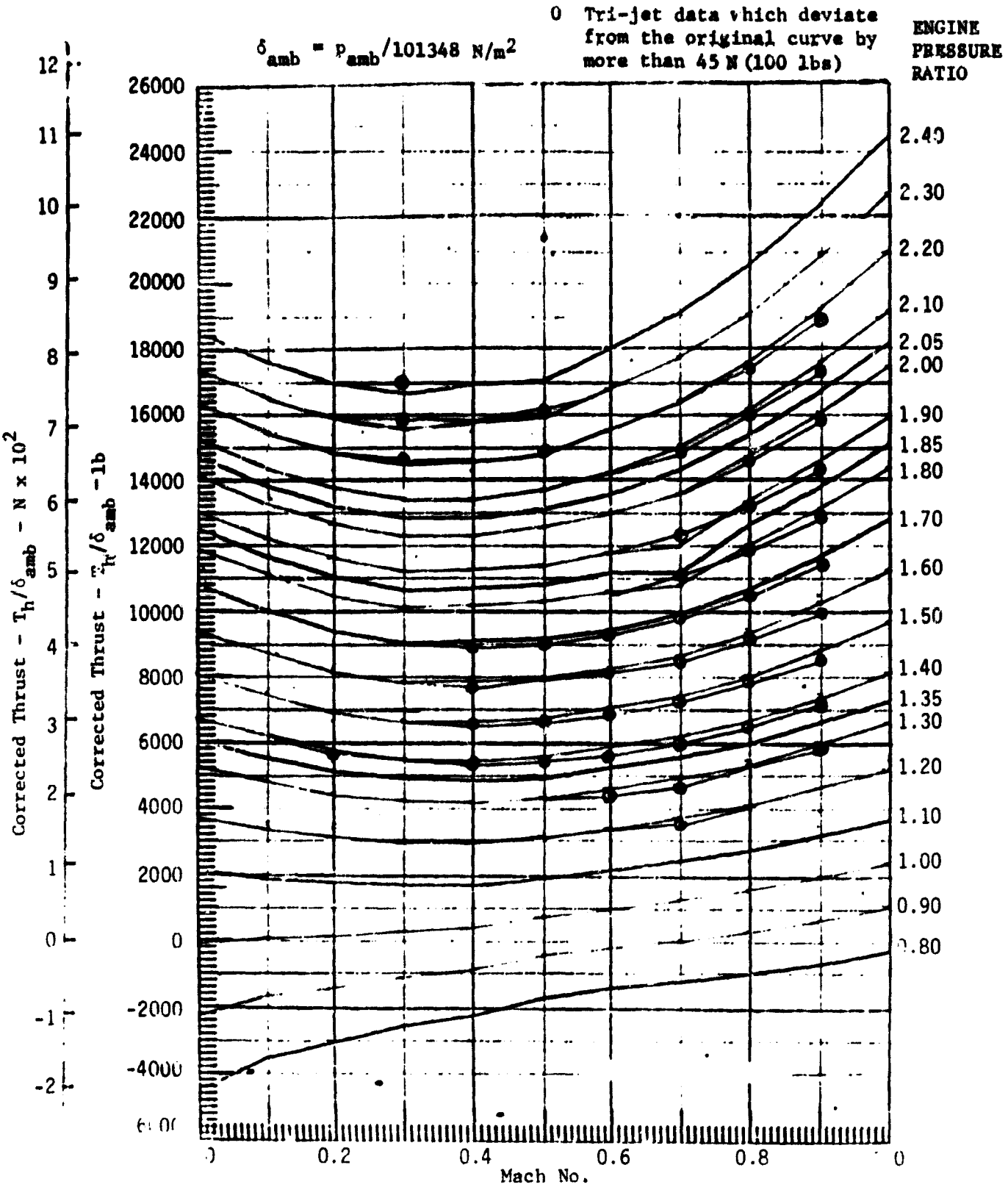

Figure B.9 Comparison of Engine Thrust Data

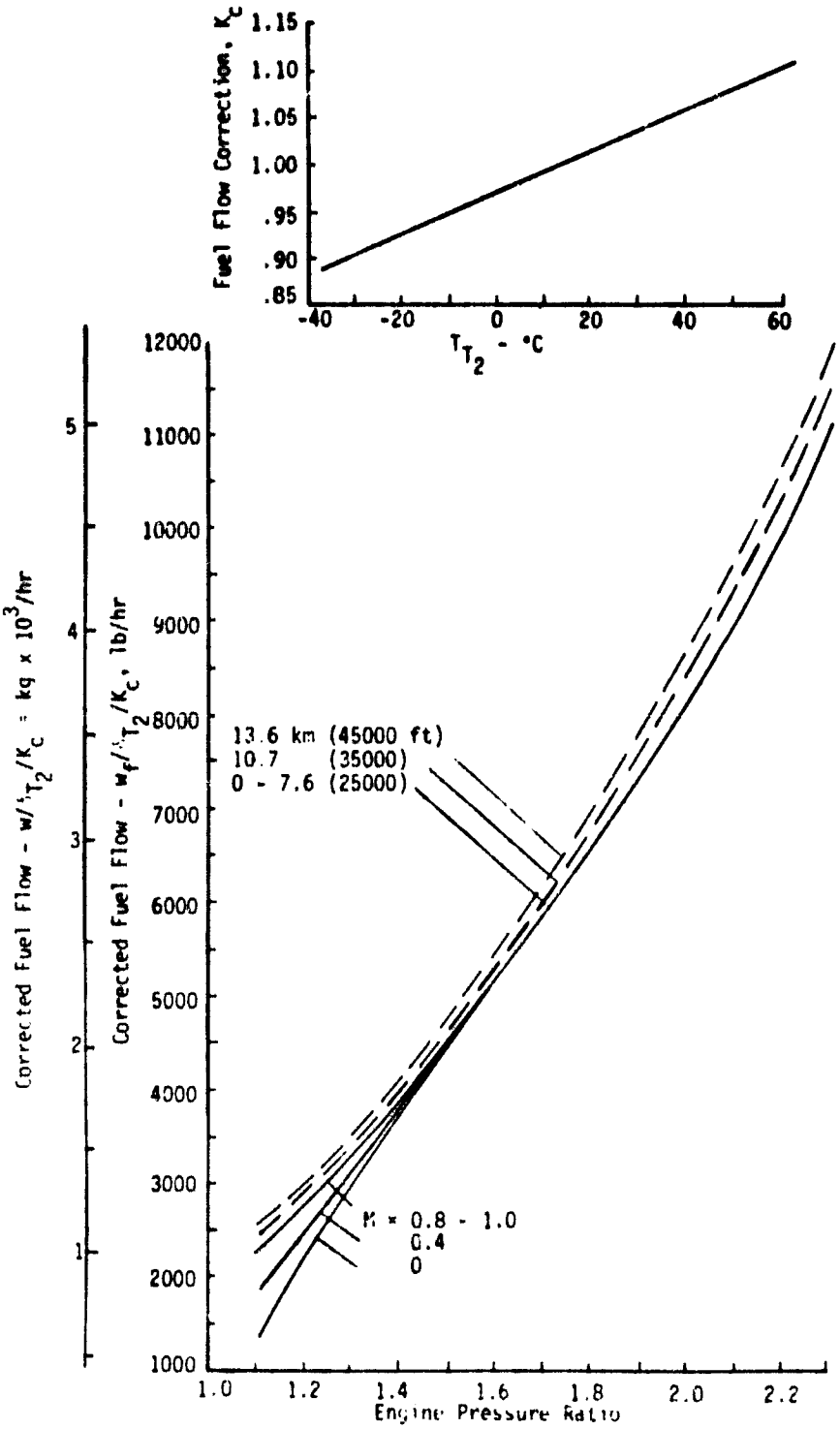

Figure B.10. Corrected Fuel Flow of Engine

factor for fuel flow, K_c, is a simple linear equation developed from the straight line shown on the inset in Fig. B.10. That is,

$$K_c = .0022\ (T_{T2}) + 0.97\ , \tag{B.2}$$

with T_{T2} in degrees centigrade.

APPENDIX C

MODELLING OF THE TWIN-JET AIRCRAFT AERODYNAMICS

Program OPTIM computes the dynamic forces in flight for the complete trajectory - climb, cruise and descent. Thus, aerodynamic models are required to compute lift and drag forces over the complete range of altitude and Mach number in the flight envelope of the aircraft. The following sections outline the twin-jet aerodynamic models now used in OPTIM.

Drag Force

The dimensionless aerodynamic drag force coefficient is separated into its important contributing elements. At a given angle of attack, α,

$$C_D = C_{DBASIC} + \Delta C_{DGEAR} \tag{C.1}$$

where C_{DBASIC} is the basic drag coefficient for the airplane in free air, with the landing gear retracted, no spoilers deflected and not in ground effect. The curves include trim data for level flight.

The low speed drag coefficient is shown in Fig. C.1 as a function of angle-of-attack and flap position. The flaps-up data on this plot are for stall only, where C_L is a function of angle-of-attack. The flaps-up data are shown only for angles-of-attack larger than 8 degrees.

The high speed drag coefficient, showing Mach effects for the flaps-up configuration, is plotted in Fig. C.2 as a function of Mach number and lift coefficient C_L^* (C_L^* is defined later) with gear retracted, no spoilers deflected and out of ground effect. The $M \leq .6$ curve is only to be used for lift coefficients smaller than .757, which agrees with angle-of-attack of 8 degrees or less for a trimmed airplane.

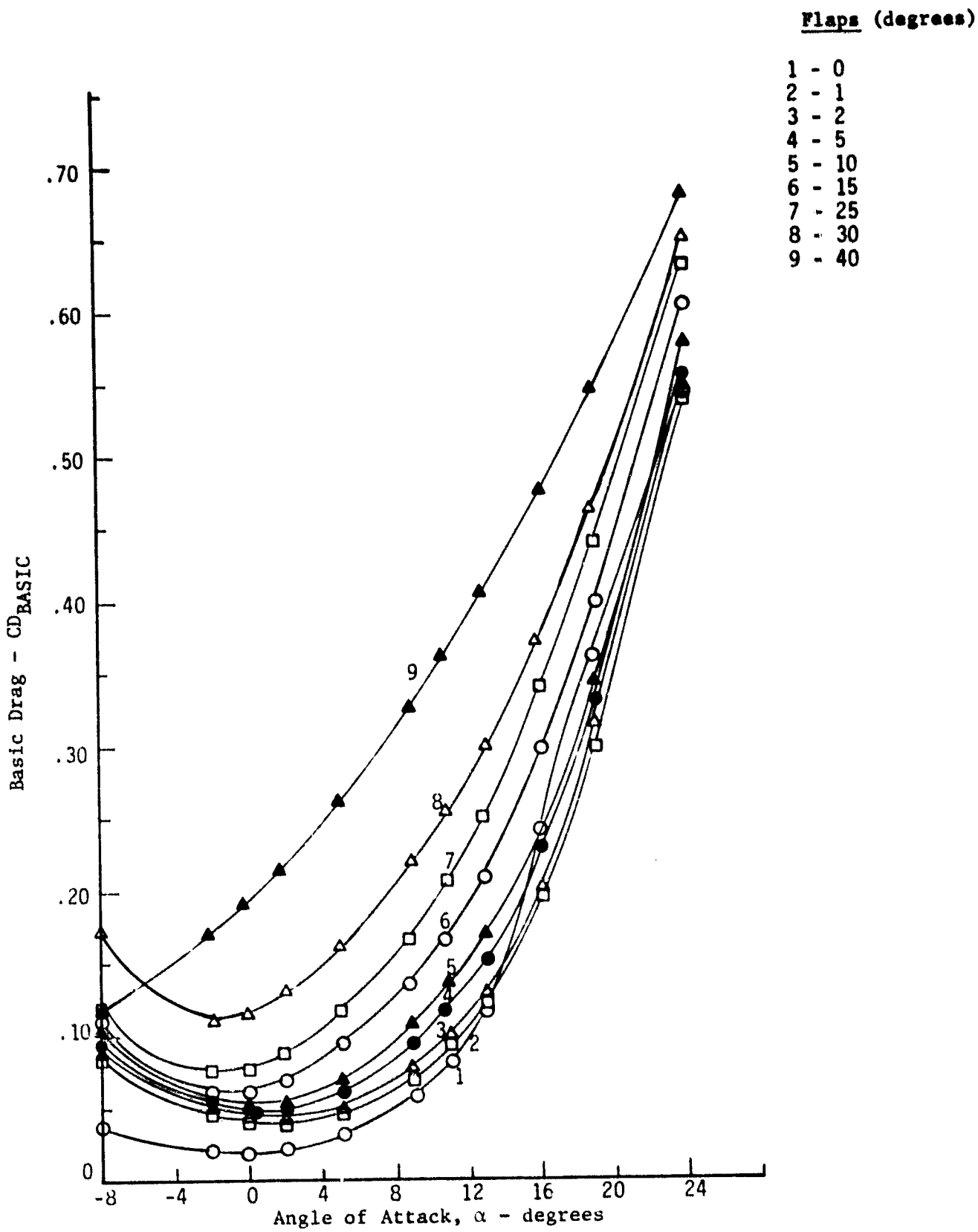

Figure C.1 Basic Low-Speed Drag with Flap Setting

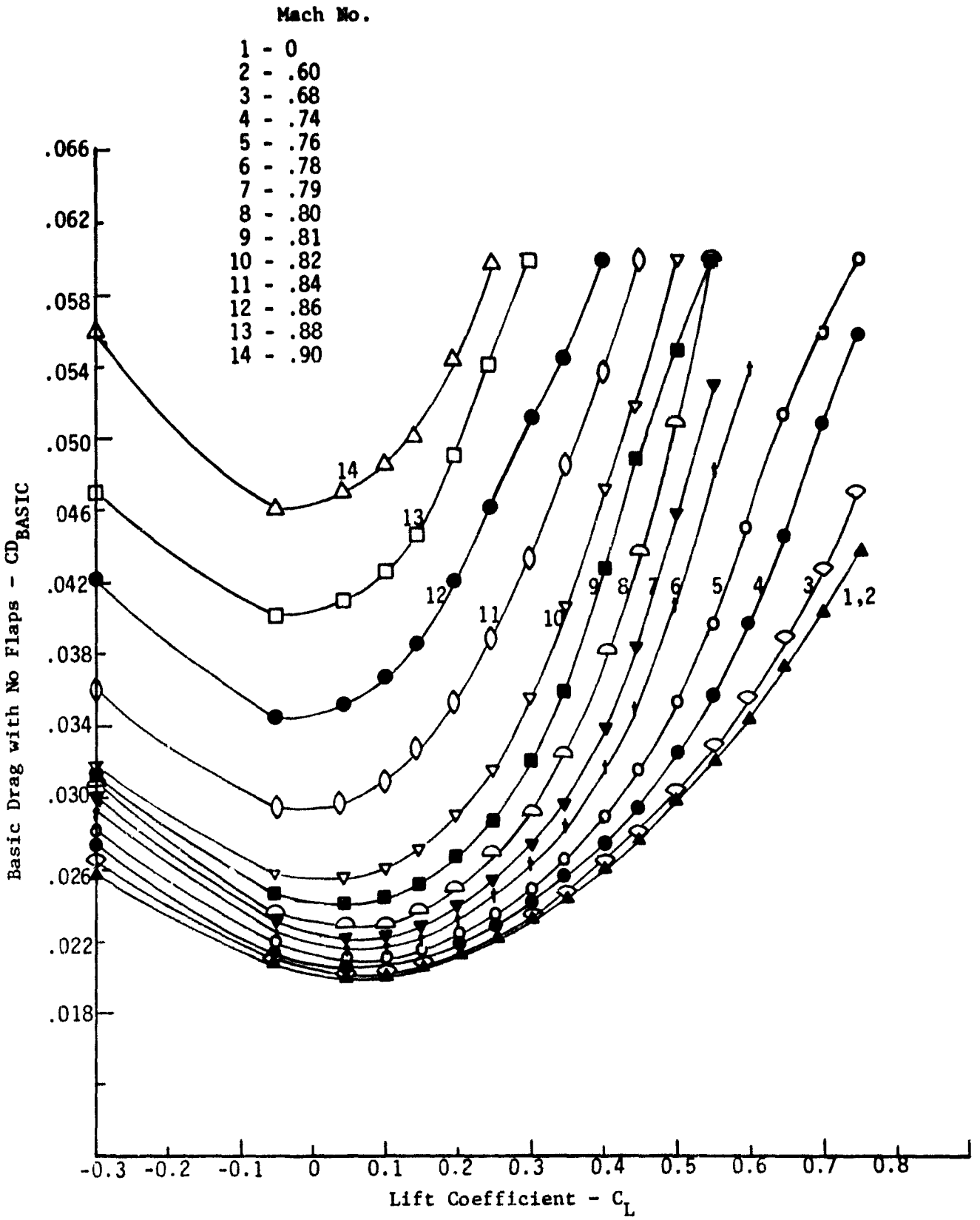

Figure C.2 High-Speed Drag with No Flap Setting

In Eq. (C.1) the coefficient ΔC_{DGEAR} is the increment in basic drag coefficient due to the main and nose landing gear extension given by the following:

$$\Delta C_{DGEAR} = (\Delta C_{DGEAR})_{M=0} \frac{(C_{DGEAR})_M}{(C_{DGEAR})_{M=0}} \quad . \tag{C.2}$$

The low-speed drag increment, $(\Delta C_{DGEAR})_{M=0}$ is plotted in Fig. C.3 as a function of angle-of-attack and flap setting. The flaps-up Mach number factor, $\frac{(C_{DGEAR})_M}{(C_{DGEAR})_{M=0}}$ is plotted in Fig. C.4.

Specific data points are identified in each of Figs. C.1 - C.4 described above. These points are tabulated in subroutine CDRAG3 in Program OPTIM.

Lift Force

The dimensionless aerodynamic lift force coefficient of the airplane is separated into its important contributing elements as

$$C_L^* = C_{L_{BASIC}} + \left[(C_{L_0})_M - (C_{L_0})_{M=0}\right] + \left[\left(\frac{dC_L}{d\alpha}\right)_M - \left(\frac{dC_L}{d\alpha}\right)_{M=0}\right]\alpha \quad . \tag{C.3}$$

Also,

$$C_L = C_L^* + \Delta C_{L_{GEAR}} \tag{C.4}$$

Here, C_L^* is used in the calculation of the basic drag coefficient. $C_{L_{BASIC}}$ is the basic lift coefficient for the rigid airplane at low speed in free air, and with landing gear retracted. The coefficient is plotted as a function of angle-of-attack α, and flap setting in Fig. C.5. Also, the term $\left[(C_{L_0})_M - (C_{L_0})_{M=0}\right]$ is the deviation of the basic airplane flaps-up

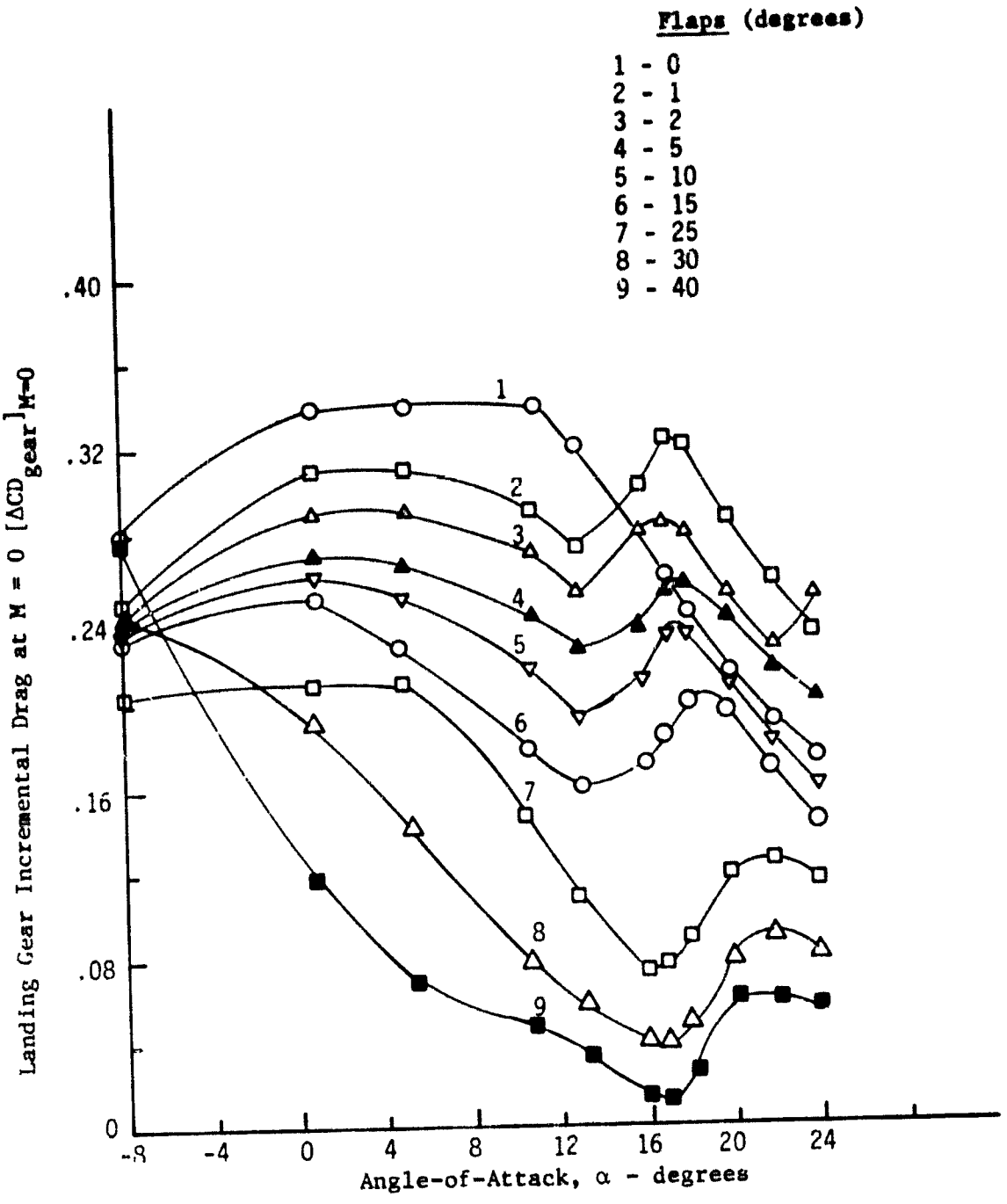

Figure C.3 Increment Drag of the Landing Gear

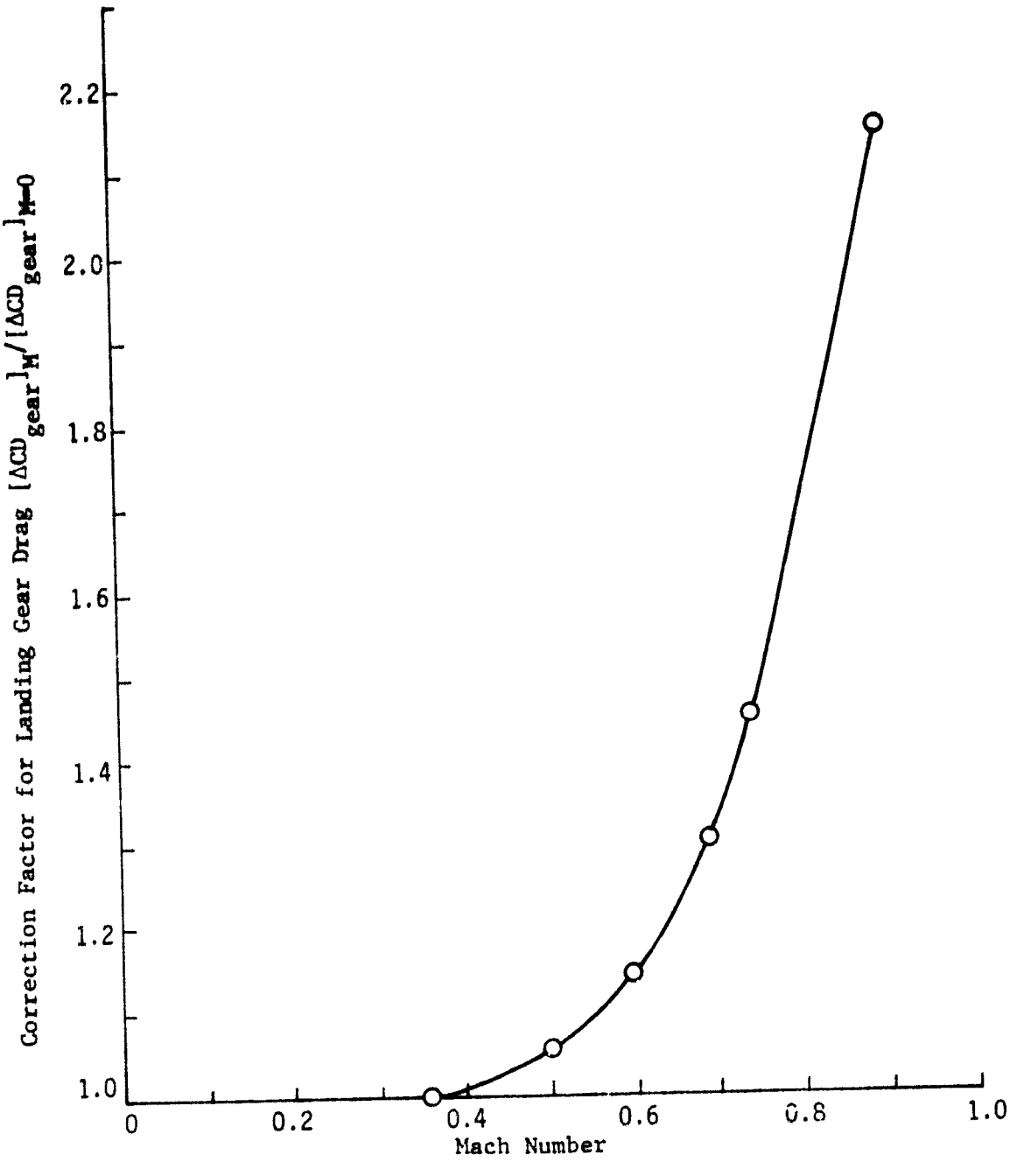

Figure C.4 Landing Gear Drag Correction Factor for a Given Mach Number.

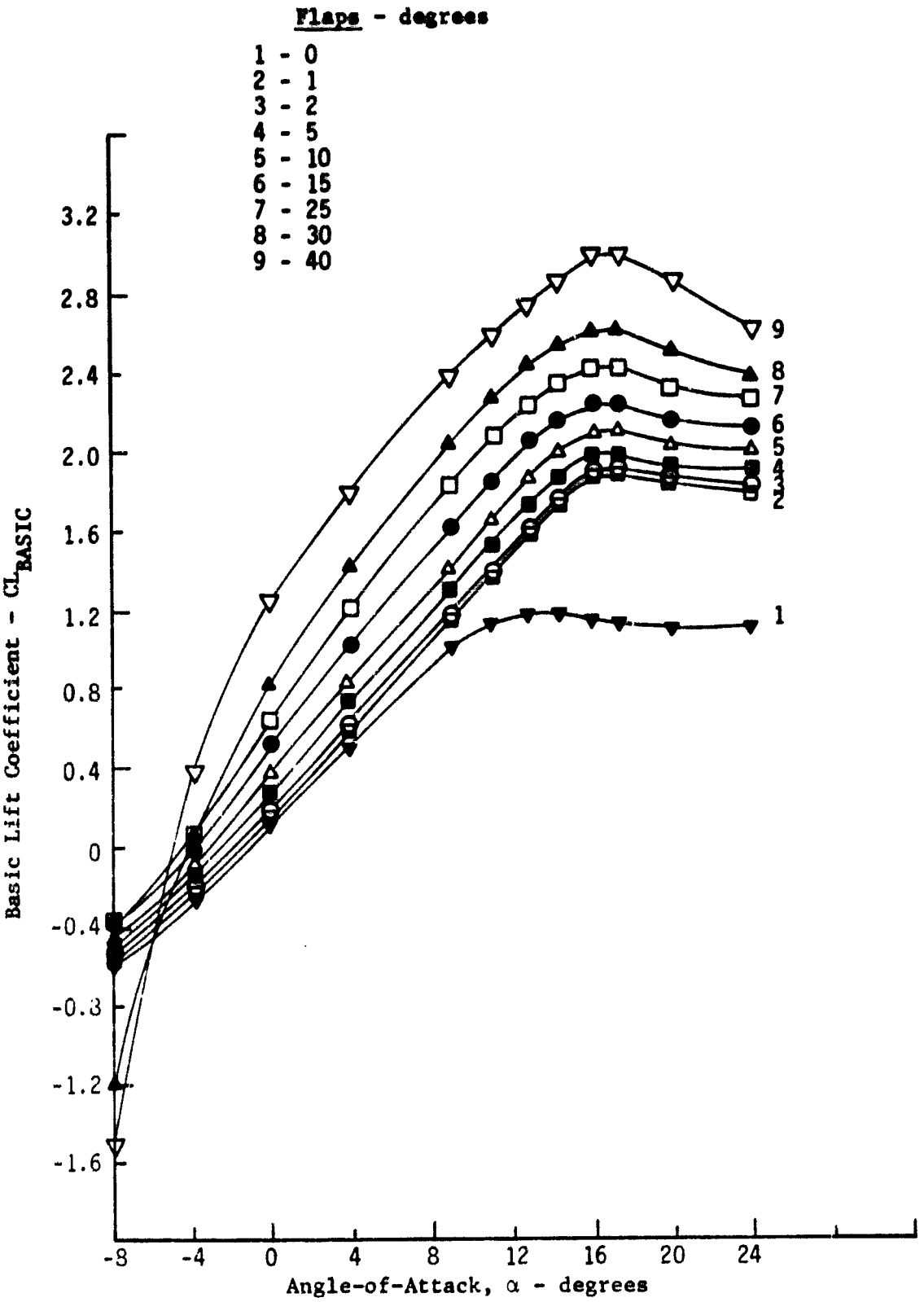

Figure C.5 Lift as a Function of Flap Setting and Angle-of-Attack

lift coefficient at $\alpha = 0°$ with Mach number. The term $\left[(C_{L_0})_M - (C_{L_0})_{M=0}\right]$ is plotted on Fig. C.6.

The term, $\left[\left(\frac{dC_L}{d\alpha}\right)_M - \left(\frac{dC_L}{d\alpha}\right)_{M=0}\right] \alpha$ is the deviation from the basic lift coefficient due to the variation of the lift curve slope at $\alpha = 0°$ with Mach number and altitude. The term $\left[\left(\frac{dC_L}{d\alpha}\right)_M - \left(\frac{dC_L}{d\alpha}\right)_{M=0}\right]$ is plotted in Fig. C.7, and the M=0 value is the slope of the flaps up $C_{L_{BASIC}}$ at $\alpha = 0°$.

As with the drag data in the previous section, specific data points are identified in Fig. C.5 - C.7. These points are tabulated in subroutine CLIFT3 in Program OPTIM.

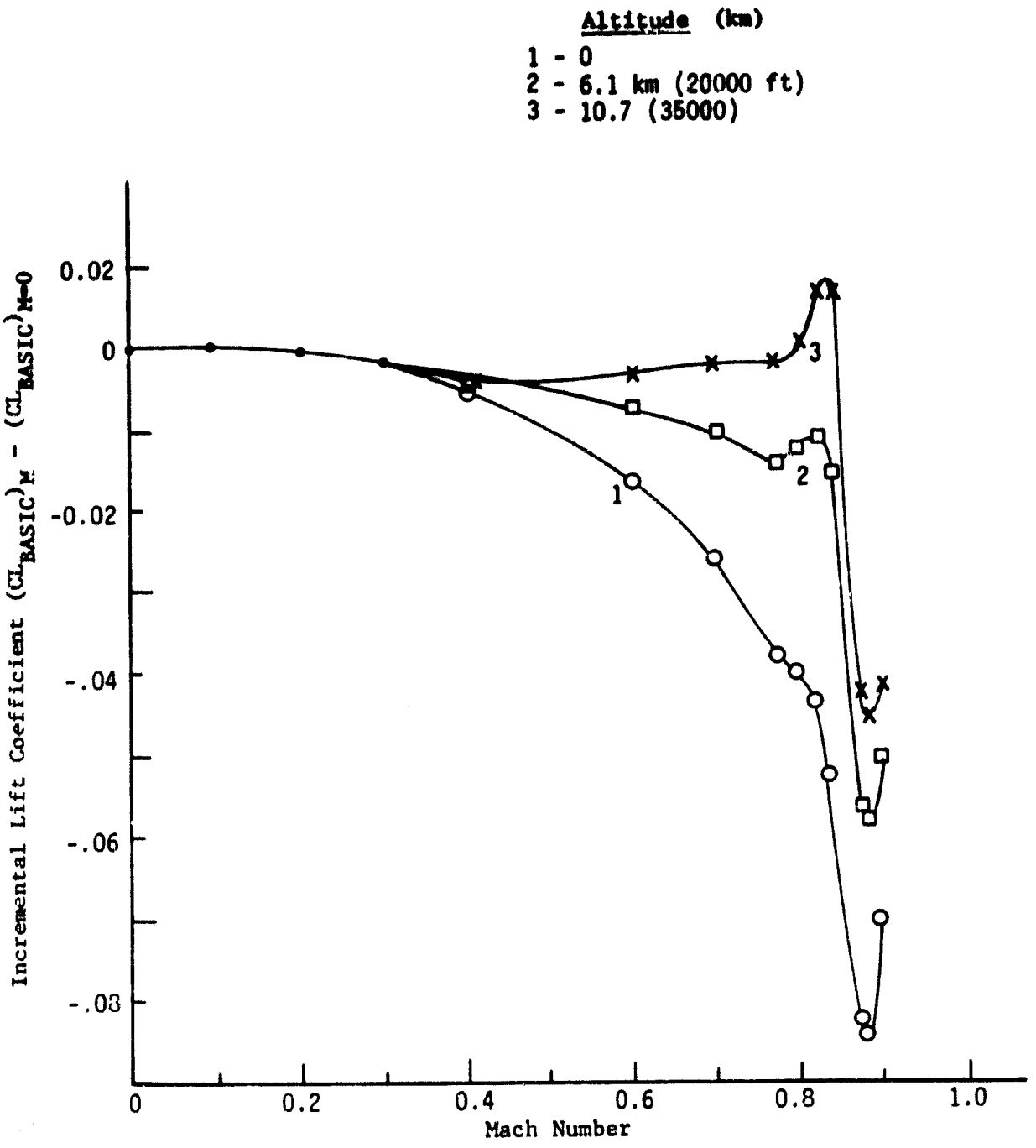

Figure C.6 Incremental Lift Coefficient as a Function of Mach Number and Altitude

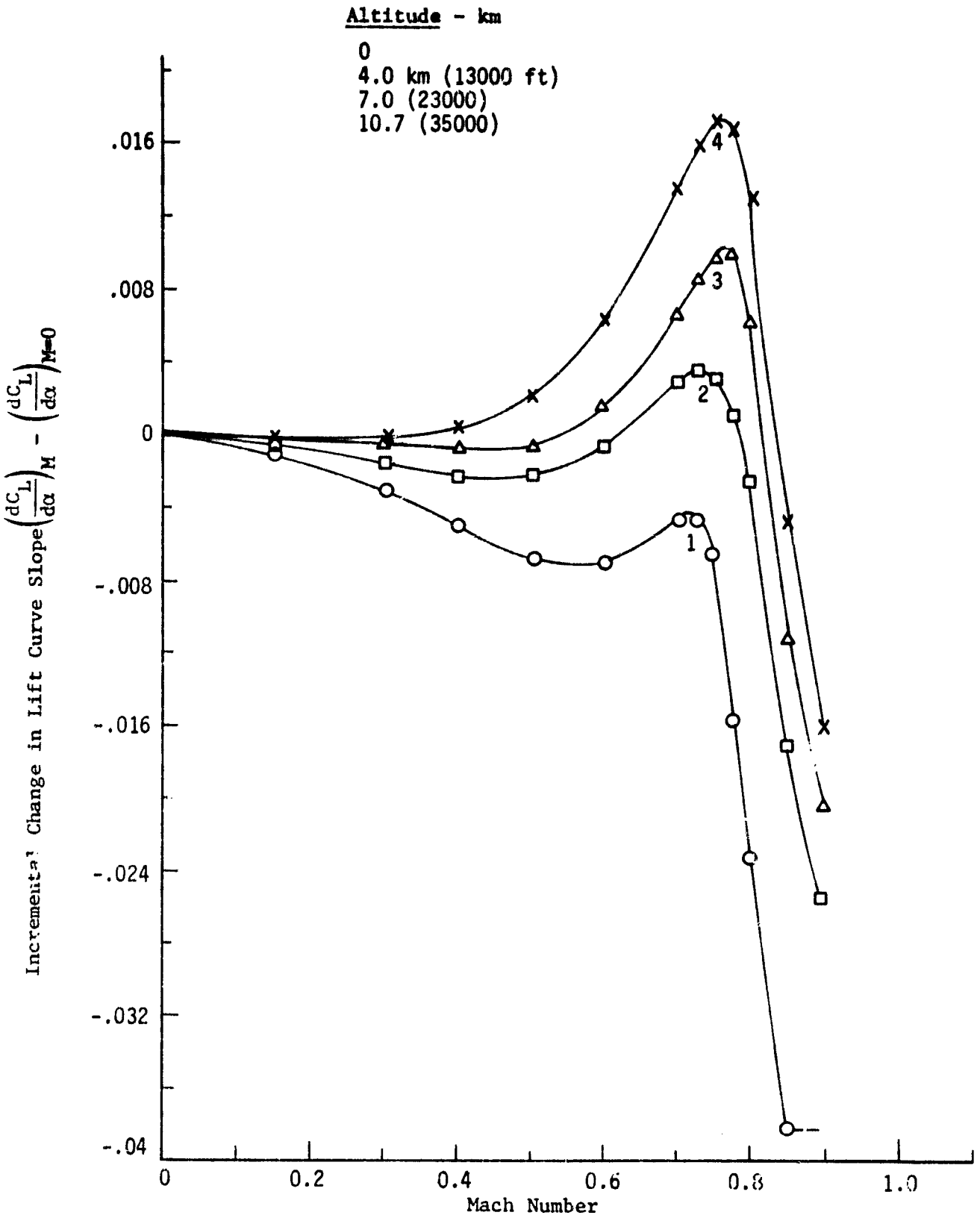

Figure C.7 Incremental Changes in Lift Curve Slope as a Function of Mach Number and Altitude

APPENDIX D

CLIMB FUEL ESTIMATE

Fuel burned during climb is estimated in subroutine FULEST [22] so that the aircraft mass at the beginning of cruise can be determined before actually computing the climb portion of the flight. A new correlation of the climb fuel flow was established using data from OPTIM runs.

Figure D.1 is a plot of the correlation which shows that the fuel fraction of initial mass used in climb is a function of the change in energy state $(E_{ci} - E_{to})$ and the initial gross mass.

The correlation is as follows:

$$W_{fCL}/W_{to} = \text{SLOPE}\ (E_{ci} - E_{to}), \tag{D.1}$$

$$\text{SLOPE} = 2.9 \times 10^{-12}(W_{to}) + .3625 \times 10^{-6}\ , \tag{D.2}$$

where

$$E = \frac{V_a^2}{2g} + h\ . \tag{D.3}$$

Here, for these numerical values, the OPTIM program uses

W_{fCL} = fuel burned in climb, lb,

W_{to} = initial climb mass, lb,

V_a = true airspeed, ft/sec ,

h = altitude, ft ,

g = 32.2 ft/sec^2 .

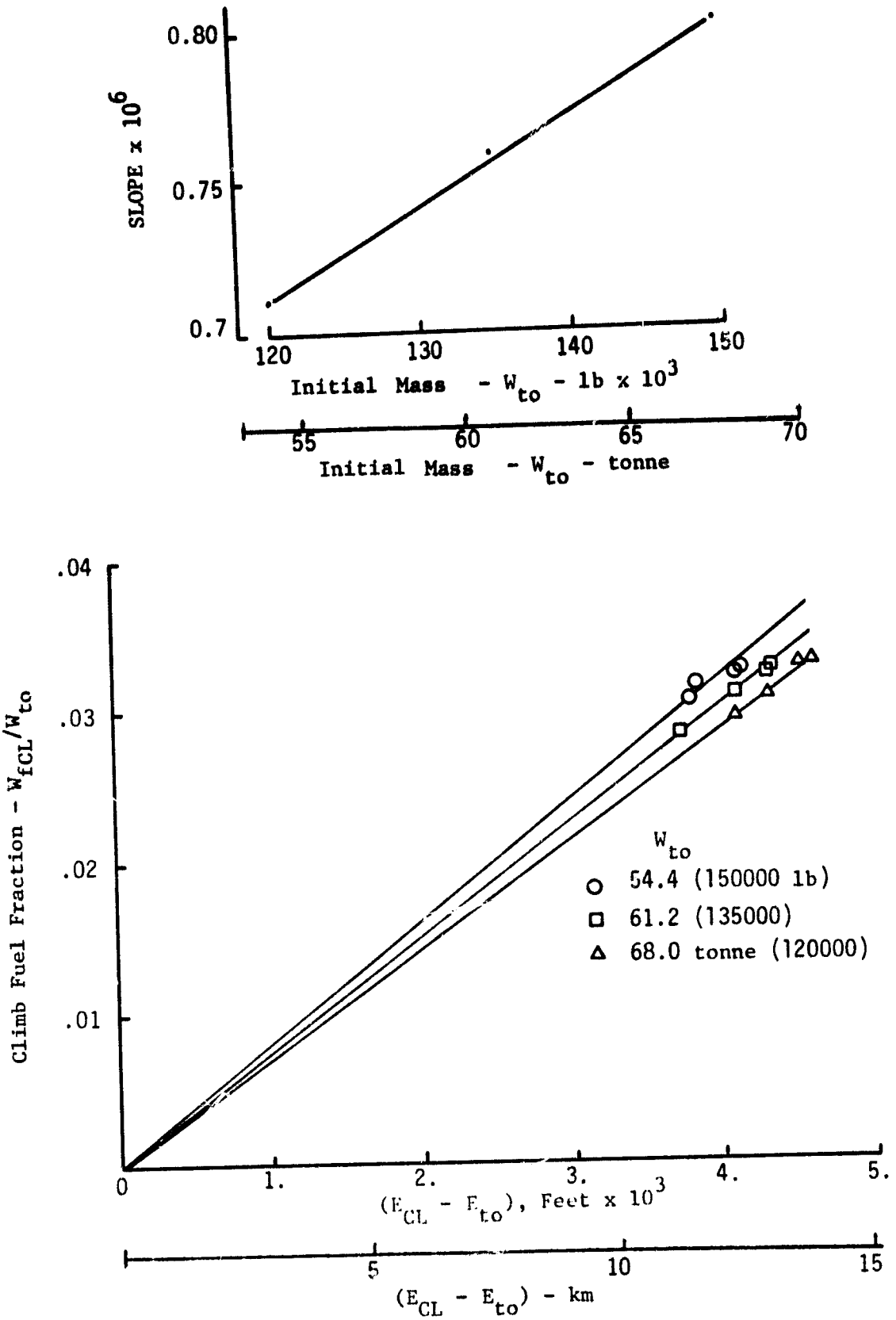

Figure D.1. Correlation for Climb Fuel Fraction Estimate

APPENDIX E

AIRCRAFT EQUATIONS OF MOTION AND AUTOPILOT MODELS

The objective of the TRAGEN program is to simulate a transport aircraft being steered to fly along either an input or computed reference trajectory. This trajectory may either be a climb or descent profile. The simulation must be accurate enough such that the performance of the aircraft (in terms of fuel burned and time required to reach the destination point) is adequately determined, as measured from the output. Adequate accuracy is obtained with a five-state variable longitudinal aircraft model.

The purpose of this appendix is to present the analytical expressions upon which the simulation was developed; this is done in two parts. The first section below defines the overall system and presents the differential equations of motion and fuel burn. The second section describes different methods for generating typical guidance commands and autopilot equations.

Equations of Motion and Fuel Burn

To examine the vertical profile of the aircraft (i.e., altitude and airspeed vs range), the longitudinal equations of motion are of primary importance. The short period equations of motion and the throttle dynamics are ignored. Thus, the control variables in this longitudinal plane are the angle-of-attack α and the magnitude of the thrust vector T. These quantities are shown with respect to aircraft true airspeed V_a, lift L, drag D, mass W, and flight path angle γ in Fig. E.1.

The kinematic equations of motion of the aircraft in the longitudinal plane are

$$\begin{aligned} \dot{x} &= V_a \cos \gamma + V_w , \\ \dot{h} &= V_a \sin \gamma , \end{aligned} \tag{E.1}$$

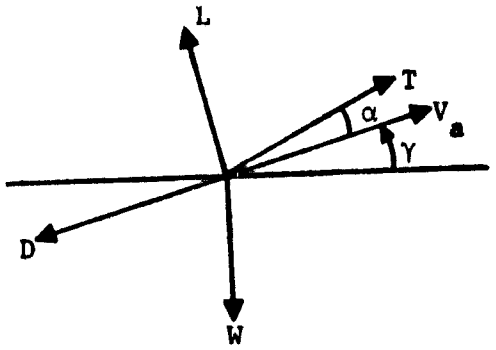

Figure E.1 Vector Diagram of Longitudinal Forces

where

x - distance, or range, measured on the ground,

h - altitude,

V_w - wind speed.

The inertial speed along the true airspeed vector V_a is

$$V_I = V_a + V_w \cos\gamma \tag{E.2}$$

From Fig. E.1, the time rate of change of this vector for constant γ is

$$\dot{V}_I = \dot{V}_a + \dot{V}_w \cos\gamma = \frac{1}{m}(T\cos\alpha - D - W\sin\gamma). \tag{E.3}$$

The time rate of change of the wind speed is

$$\dot{V}_w = \frac{\partial V_w}{\partial h}\dot{h},$$

$$= \frac{\partial V_w}{\partial h} V_a \sin\gamma \quad . \tag{E.4}$$

Substituting Eq. (E.4) into Eq. (E.3) and solving for $\dot{V}_a$ leaves

$$\dot{V}_a = \frac{1}{m}(T\cos\alpha - D - W\sin\gamma) - \frac{\partial V_w}{\partial h} V_a \sin\gamma\cos\gamma \tag{E.5}$$

Also, from Fig. E.1, one can write

$$\ddot{h} = \frac{1}{m} (L \cos \gamma - W + T \sin (\gamma + \alpha) - D \sin \gamma), \qquad (E.6)$$

Equations (E.5) and (E.6) represent the kinetic equations of motion of the aircraft.

The remaining term that must be accounted for is the time-varying mass of the aircraft. Specifying the thrust also specifies the fuel flow $\dot{w}$. Thus, the mass changes at the rate

$$\dot{W} = -\dot{w} . \qquad (E.7)$$

Equations (E.1), (E.5), (E.6), and (E.7) are the five basic equations used to represent the longitudinal dynamics of the aircraft. Lift and drag (L and D) are computed as functions of V_a, h, and α. Fuel flow $\dot{w}$ is a function of V_a, h, and thrust T.

Further refinement could be added to these equations to include the effects of the following:

1). throttle dynamics (including transient fuel flow);

2). relationship between throttle position, EPR setting, and thrust;

3). short period dynamics relating time rate of change of angle-of-attack, pitch rate, and pitch angle to elevator deflection;

4). required turning (lateral) motion for flying over fixed waypoints; and

5). lateral wind and gust effects.

However, these effects are considered to be of second order, and not required for the intent of this simulation. For a more exact autopilot simulation, they would be required.

The flight path angle is defined as

$$\gamma = \sin^{-1} (\dot{h}/V_a) \tag{E.8}$$

By differentating this expression and using Eqs. (E.5) and (E.6), one obtains

$$\dot{\gamma} = \frac{1}{mV_a} (T \sin \alpha - W \cos \gamma + L + m \frac{\partial V_w}{\partial h} V_a \sin^2 \gamma). \tag{E.9}$$

Equation (E.9) can be used in place of Eq. (E.6).

Steering Procedures

The reference trajectories which are given to be followed consist of a sequence of points containing values of time, range, altitude, airspeed, flight path angle, specific energy, mass, and other variables. Any of these quantities which is measurable and monotonically changing can serve as the independent variable. To minimize airborne computer memory requirements, it is important to make the stored data representing the reference trajectory as compact as possible.

In this study, a set of steering equations is used to take points from the reference trajectory, convert these points to reference trajectory commands, and then use these commands to set values of the control variables. This steering process represents a rudimentary form of an autopilot.

The steering process consists of commanding the thrust T and angle-of-attack α values so that the aircraft follows the reference as closely as possible. The system that includes this process is depicted by the block diagram in Fig. E.2. Note that flying along a reference trajectory consists of steering to connect a series of reference points. When a reference point is reached, new steering commands must be issued so that the aircraft will then be guided to the next reference point.

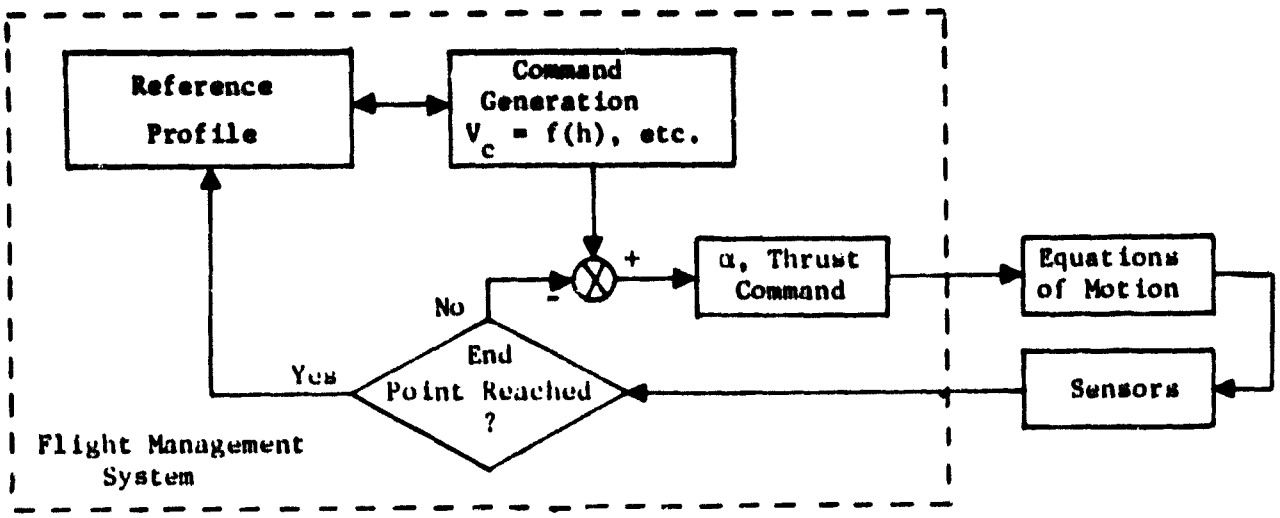

Figure E.2. Elements of the Longitudinal Aircraft Model

To fly along the reference path, an independent variable is first chosen. For this study, two different independent variables were chosen - altitude for climb and range for descent. Then, the remaining variables - primarily airspeed, flight path angle, and altitude (for range as the independent variable) - are stored as tabular functions of the chosen independent variable.

Also, it is possible to fly along a nominal path using two approaches:

1). An open-loop approach where the thrust vector is directed in such a way over the next period that by the end of that period the next reference point is reached.

2). A closed-loop approach where the aircraft is continually steered to a continuously commanded trajectory which connects the reference points.

Both of these approaches were examined for simulation of flying the climb profile. However, good results were only obtained with the closed-loop approach.

A problem with open-loop steering is that it assumes that constant or linearly varying controls will cause the end points of a reference profile to be connected. This assumption does not account for perturbations due to wind, etc. along the way. Although the open-loop methods produce paths which have roughly correct values of airspeed and altitude at given range values, there were large excursions from the reference flight path angle for the climb profiles.

Another problem with the open-loop approaches was that both α and T were varied to achieve fixed values of V_a and h for given range points. For optimum climb, thrust is usually set at the maximum value. Thus, usually only α remains as a valid control variable.

Another consideration for implementing the climb profile is that there is no reason why a particular cruise condition (altitude, airspeed) has to be achieved when a certain range x is reached. Thus, a more logical independent variable is altitude, with range allowed to be a free variable.

For these reasons, a closed-loop steering approach was devised where reference values of flight path angle (with respect to the air mass) and airspeed are obtained as functions of altitude. (This assumes that altitude is monotonically increasing during climb.) A perturbation control law was set up so that variations in α from a reference value α_o were proportional to variations in γ and V_a from their respective command values.

Because γ and V_a tend to change linearly with time, they can be considered as ramp functions. Thus, the closed-loop controller should be considered to be at least a Type 1 system. From Eqs. (E.5) and (E.9), with no wind, the system perturbation equations are

$$m\delta\dot{V}_a = -T\sin\alpha\,\delta\alpha - \frac{\partial D}{\delta\alpha}\,\delta\alpha - \frac{\partial D}{\delta V_a}\,\delta V_a - W\cos\gamma\delta\gamma, \qquad \text{(E.10)}$$

$$m V_a\delta\dot{\gamma} = T\cos\alpha\,\delta\alpha + \frac{\partial L}{\partial\alpha}\,\delta\alpha + \frac{\partial L}{\partial V_a}\,\delta V_a + W\sin\gamma\delta\gamma.$$

The resulting transfer functions between γ, V_a, and α are of the form

$$\frac{\delta\gamma}{\delta\alpha} = \frac{G_B\ (\tau_B\ s + 1)}{(s/\omega)^2 + 2\zeta\ (s/\omega) + 1}\ , \qquad \text{(E.11)}$$

$$\frac{\partial V_a}{\delta\alpha} = \frac{G_c\ (\tau_c\ s + 1)}{(s/\omega)^2 + 2\zeta(s/\omega) + 1}\ ,$$

where the time constants and other parameters are functions of the parameters in Eq. (E.10).

The control problem can now be interpreted as shown in Fig. E.3. To obtain the Type 1 system, the control law has to be of the form

$$\delta\alpha = (K_1 + \frac{K_2}{s})\ \ (V_{a_c} - V_a) + (K_3 + \frac{K_4}{s})\ \ (\gamma_c - \gamma), \qquad \text{(E.12)}$$

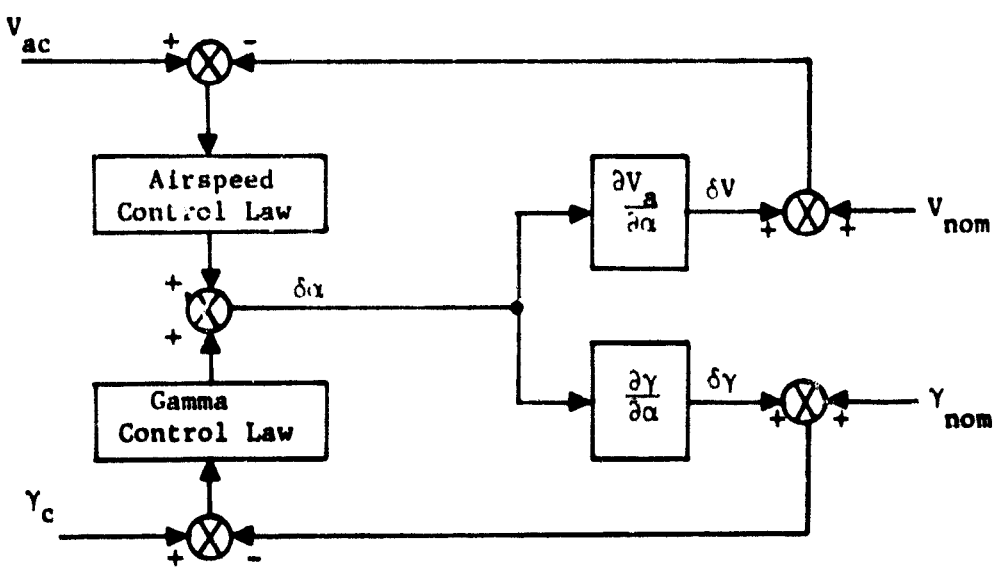

Figure E.3 Control Loops for Perturbation Control of Airspeed and Flight Path Angle.

where V_{a_c} and γ_c are the commanded values of V_a and γ. This is the classical proportional-plus-integral controller. Gains are chosen to produce the desired response for removal of profile errors.

To generate the continuous commands V_{a_c} and γ_c during climb, the computations made at each reference point are

$$\frac{\partial \gamma}{\partial h} = \frac{\gamma_{n+1} - \gamma_n}{h_{n+1} - h_n} \quad , \tag{E.13}$$

$$\frac{\partial V_a}{\partial h} = \frac{V_{a\,n+1} - V_{a_n}}{h_{n+1} - h_n} .$$

Then

$$\gamma_c = \gamma_n + (h - h_n) \frac{\partial \gamma}{\partial h} \quad , \tag{E.14}$$

$$V_{a_c} = V_{a_n} + (h - h_n) \frac{\partial V_a}{\partial h} .$$

When the flight path angle is very small (during the initial period of flight and when the aircraft levels off at 3048m (10000 ft) to gain speed before resuming climb), Eqs. (E.14) do not work well. For these cases, it is more appropriate to set

$$\gamma_c = 0., \tag{E.15}$$

$$V_{a_c} = V_{a\,n+1} ,$$

and use the control law

$$\delta\alpha = (K_3 + \frac{K_4}{s}) (\gamma_c - \gamma). \tag{E.16}$$

The above method worked quite well in causing the simulated profile to closely follow the reference path. Only one set of gain values was sufficient for the entire trajectory.

For decending flight, the thrust again is usually constrained (idle) for optimum performance. Also, for this case, the main concern is to reach a fixed altitude when range-to-go to the destination point is a certain value. Thus, above 3048 m (10000 ft), the airspeed can be allowed to be a free variable. For this case, only inertial flight path γ_{Ic} is required to be controlled.

To generate a continuous command γ_{Ic}, the computation made at each reference point is

$$\gamma_{Ic} = \tan^{-1} \left[(h_{n+1} - h_n) / (x_{n+1} - x_n) \right] . \qquad (E.17)$$

Then, the control law is similar to Eq. (E.16), i.e.

$$\delta\alpha = (K_3 + \frac{K_4}{s}) (\gamma_{Ic} - \gamma_I) , \qquad (E.18)$$

where inertial values of flight path angle are used rather than those with respect to the air mass. Equations (E.17) and (E.18) form the basis for closed-loop control of descending flight. Again, one set of gains is sufficient for the entire descent profile.

REFERENCES

1. Covey, R.R., Mascetti, G.J., and Roessler, W.U., "Examination of Commercial Aviation Energy Conservation Strategies," Report No. ATR-79 (7761)-1, Aerospace Corp., El Segundo, CA. October 1978.

2. Hanks, G.H., "Overview of Technology Advancements for Energy Efficient Transports," AIAA Atmospheric Flight Mechanics Conference, Paper No. 79-1651, Boulder, CO. August 1979.

3. Stengel, R.F., and Marcus, F.J., "Energy Management Techniques for Fuel Conservation in Military Transport Aircraft," AFFDL-TR-75-156, Analytic Sciences Corp., Reading, MA, February 1976.

4. Aggarwal, R., et al., "An Analysis of Fuel Conserving Operational Procedures and Design Modifications for Bomber/Transport Aircraft," AFFDL-TR-78-96, Vol. II, Dynamics Research Corp, Wilmington, MA, July 1978.

5. Yarrington, A.L., and Burghart, J.T., "Terminal Configured Vehicle Fuel Conservation Sensitivity Study," Boeing Commercial Airplane Co., Doc. No. D6-42939, Seattle, WA, July 1976.

6. Collins, B.P., "Estimation of Fuel Consumption of Commercial Jet Aircraft from Path Profile Data," SAE International Air Transportation Meeting, Cincinnati, OH, May 1980.

7. Smith, B.A., "Automated Fuel Management Set for Test," Aviation Week & Space Technology, April 21, 1980. pp. 191-193.

8. Klass, P.J., "Controller Numbers Keyed to Advances," Aviation Week & Space Technology, April 28, 1980, pp. 61-63.

9. Sorensen, J.A. Morello, S.A., and Erzberger, H., "Application of Trajectory Optimization Principles to Minimize Aircraft Operating Costs," Procedings of the 18th IEEE Conference on Decision and Control, Ft. Lauderdale, FL, December 1979, pp 415-421.

10. Sorensen, J.A., "Concepts for Generating Optimum Vertical Flight Profiles," NASA CR 159181, September 1979.

11. Schultz, R.L., and Zagalsky, N.R., "Aircraft Performance Optimization," Journal of Aircraft, Vol. 9, No. 2, January 1972, pp. 108-114.

12. Erwin, R.L., Jr., et al., "Strategic Control Algorithm Development," Boeing Commercial Airplane Co., Contract No. DOT-TSC-538, December 1973.

13. Knox, C.E., and Cannon, D.G., "Development and Flight Test Results of a Flight Management Algorithm for Fuel Conservative Descents in a Time Based Metering Traffic Environment," 18th IEEE Conference on Decision and Control, Ft. Lauderdale, FL, December 1979.

14. Tobias, L., O'Brien, P.J., and Palmer, E.A., "Simulation Study of the Effect of Fuel-Conservative Approaches on ATC Procedures and Terminal Area Capacity," SAE Air Transportation Meeting, Boston, MA, May 1978.

15. Rutowski, E.S., "Energy Approach to the General Aircraft Performance Problem," J. of Aeronautical Sciences, Vol. 21 No. 3, March 1954 pp. 187-195.

16. Bryson, A.E., Desai, M.N., and Hoffman, W.C., "Energy-State Approximation of Supersonic Aircraft," J. of Aircraft, Vol. 6, No. 6, Nov-Dec 1969, pp. 481-488.

17. Erzberger, H., and Lee, H.O., "Characteristics of Constrained Optimum Trajectories with Specified Range," NASA TM 78519, September 1978.

18. Erzberger, H., McLean, J.D., and Barman, J.R., "Fixed-Range Optimum Trajectories for Short Haul Aircraft," NASA TN D-8115, December 1975.

19. Barman, J.E., and Erzberger, H., "Fixed-Range Optimum Trajectories for Short-Haul Aircraft," J. of Aircraft, Vol. 13, No. 10, October 1976, pp. 748-754.

20. Shoaee, H., and Bryson, A.E., "Airplane Minimum Fuel Flight Paths for Fixed Range," SUDAAR No. 499, Stanford University, Stanford CA, March 1976.

21. Lee, H.Q., and Erzberger, H., "Algorithm for Fixed Range Optimal Trajectories," NASA Technical Paper 1565, 1979.

22. Anon., "OPTIM - Computer Program to Generate a Vertical Profile which Minimizes the Aircraft Direct Operating Costs," Revision No. 2, NAS1-15497, Analytical Mechanica Assoc., Inc., Mountain View, CA, October 1980.

23. Anon., "TRAGEN - Computer Program to Simulate an Aircraft Steered to Follow a Specified Vertical Profile," Revision No. 2, NAS1-15497, Analytical Mechanics Assoc., Inc., Mountain View, CA, October 1980.

24. Coykendall, R.E., Curry, J.K., Domke, A.E., and Madsen, S.E., "Study of Cost/Benefit Tradeoffs for Reducing the Energy Consumption of the Commercial Air Transportation System," NASA CR-137891, June 1976.

25. Bryson, A.E., and Ho, Y.C., "Applied Optimal Control," Blaisdell, Waltham, MA, 1969.